ERASMUS MUNDUS MASTER OF MECHANICAL ENGINEERING

MEMOIRE-THESIS

AUTHOR

CUI Yu

TITLE

# Analysis of the rough contact in axisymmetric upsetting

June 20

INSTITUT NATIONAL DES SCIENCES APPLIQUEES DE LYON - FRANCE
ESCOLA TÈCNICA SUPERIOR D'ENGINYERIA INDUSTRIAL DE BARCELONA, UNIVERSITAT POLITÈCNICA DE CATALUNYA - ESPAGNE
THE COLLEGE OF THE HOLY AND UNDIVIDED TRINITY OF QUEEN ELIZABETH NEAR DUBLIN - IRLANDE

# DECLARATION

I declare that the present work has not previously been submitted as an exercise for a degree at any university. It consists entirely of my own work, except where references indicate otherwise.

The library of Trinity College and INSA Lyon may lend or copy this thesis on request.

Yu Cui

June 2006

# ACKNOWLEDGEMENTS

I would like to thank my two supervisors: Prof. Jean-Claude BOYER, Département Génie Mécanique Conception, INSA de Lyon and Prof. Andrew Torrance, Department of Mechanical and Manufacturing Engineering, Trinity College Dublin, for their enthusiasm, encouragement and guidance throughout this project; Technician Sean and Peter of Department of Mechanical and Manufacturing Engineering, Trinity College Dublin, for their help and encouragement on the experiment part; Prof. Henry Rice of Department of Mechanical and Manufacturing Engineering, Trinity College Dublin, for his support and care during my stay in Dublin; The other Erasmus Mundus students and classmates in Ireland and in France; My family and friends in China.

Also I would like to thank Mme Isabelle Véru, Secrétariat des Etudes et Relations Internationales (EMMME), Département GMC, and Mme Esméralda FIGARD, Secrétariat Département GMC for their special effort and attention on the Erasmus Mundus programme.

Finally I would like to thank European Commission for the opportunity of this project and the scholarship.

**Dedicated to**

My parents Cui Zhigang and Jin Lan

My grandparents Cui Baofu, Li Shuzhen

Jin Zhenlie and Qian Yuxiang

# ABSTRACT

Characterization of surface roughness is important in the frictional behavior of two contact surfaces. In general, it has been found that friction increases with average roughness. The prediction of friction and stress/ strain/ deformation is of interest in the friction-sensitive process such as axisymmetric upsetting. However, the classical friction laws, such as Coulomb's law and its extension - Coulomb-Amonton's law, Coulomb-Orowan are found to be coarse and oversimplified especially in the presence of surface complexities.

The first objective of this project is to examine the microscopic evolution of the upsetting process with Finite Element software, with the focus on the interaction between the tool asperity and the plastic wave. The second objective is to evaluate Coulomb's law and Plastic wave theory based on small-scale numerical models. The third objective is to implant the friction laws and prior findings into the experiment-size Finite Element models so that comparison between simulation and expriments could be made.

This project is a contribution to the definition of a new friction test for bulk forming processes.

# RESUME

La caractérisation de la rugosité de surface est très importante pour le frottement de deux surfaces en contact. En général, le frottement augmente avec la rugosité moyenne. La prédiction du frottement et des contraintes et des déformations est à considérer dans les procédés sensibles aux frottements tels que l'écrasement d'un lopin axisymétrique. Cependant, les lois classiques de frottements, telles que la loi de Coulomb et ses extensions - la loi de Coulomb-Amonton ou Coulomb-Orowan sont trop grossières et simplifient trop le problème dès que la surface de contact est très complexe.

Le premier objectif de ce projet est d'examiner l'évolution microscopique de l'interface outil-lopin pendant l'opération d'écrasement avec le logiciel d'Eléments Finis, en étudiant en particulier l'interaction entre les rugosités de l'outil et la vague plastique créée à la surface du lopin. Le deuxième objectif est d'évaluer la loi de Coulomb et la théorie de la vague plastique basée sur des modèles numériques à petite échelle. Le troisième objectif est d'implémenter les lois de frottement et les conclusions précédentes dans les modèles d'Elément Finis à taille réelle pour comparer la simulation avec des essais.

Ce projet est une contribution à la définition d'un nouveau test de frottement pour les procédés de formage.

# CHAPTER 1 Definition of the roughness and the standards

## 1.1 The significance of surface roughness

Characterization of surface roughness is important in applications involving friction, lubrication, and wear. In general, it has been found that friction increases with average roughness. Roughness parameters are, therefore, important in applications such as automobile brake linings, floor surfaces, and tires. Roughness parameters also play a critical role in the metal forming process such as upsetting, free forging and closed die forming.

The effect of roughness on lubrication has also been studied to determine its impact on issues regarding lubrication of sliding surfaces, compliant surfaces, and roller bearing fatigue. In metal forming, where lubrications are sometimes introduced in the process, the understanding of the behavior of the lubricants between the tooling asperities and the workpiece indentations is important.

Furthermore, the influence of surface roughness extends to almost every branch of engineering subjects such as fluid dynamics, thermal or electrical conduction, vibration, bioengineering, etc.

## 1.2 Definition and Parameters

In 1797 Brisson wrote in his *Dictionnaire Raisonné de Physique: "....car ces surfaces, quelques polies qu'elles ne paroissent , ne le sont jamais parfaitement. Ce sont toujours des assemblages de petites éminences et de petites cavités."* In other words, surfaces are never perfectly smooth and flat. The heights and shapes of the summits, or *asperities* of a bearing surface can have a big effect on its performance. Figure 1.1 shows a *profile* of a steel-bearing

surface - a graph of height against distance for a line drawn across it.

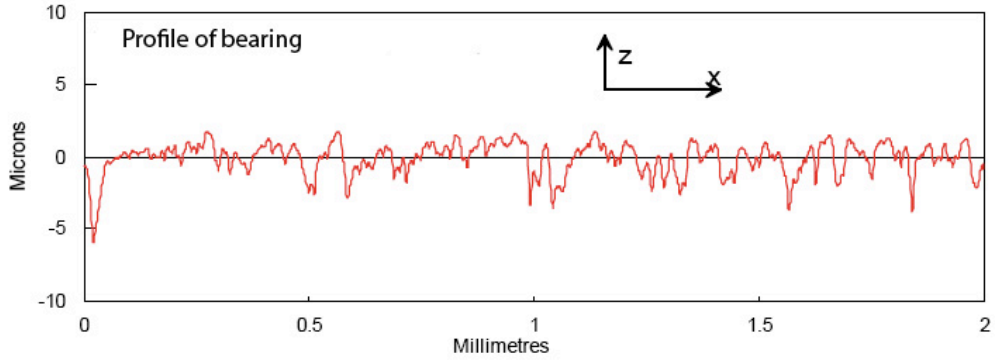


Fig.1.1 asperity of a steel-bearing surface

The ISO (International Standard Organization) 4287-1997 defines the specification about surface filtration, field parameters and feature parameters aiming to reflect genuine properties of a surface. A common one, for example, is the distance between the highest peak and the lowest valley of the unfiltered profile, which was noted as $P_t$. The designation of this parameter was subsequently changed to $R_t$ when electrical filters were incorporated. There are totally ten surface roughness parameters seen in the ISO 4287 document, while in this project, only few parameters are of concern, and are detailed below.

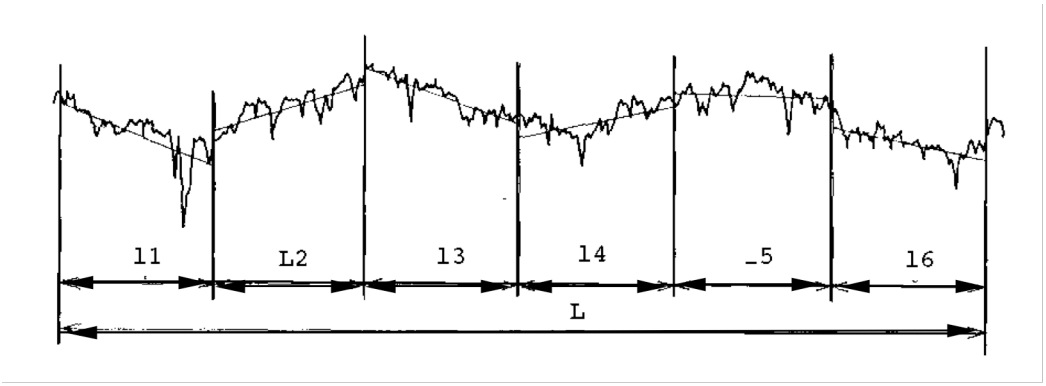


Fig 1.2 length of evaluation L and samples $l_i$

Similar to some surface properties such as hardness, the value of surface roughness depends on the scale of measurement L (length of evaluation). Once L is chosen, it is subdivided into a

number of samples $l_i$ (i=1,…,CN). See Fig.1.2. So the right choice of the concept roughness has statistical implications as it considers factors such as sample size and sampling interval. The next step in the development of roughness parameters was to obtain an average parameter of roughness at the each given sampling interval, and again average it over the total sample length. In US, this was done by connecting an AC voltmeter to measure the root mean square (RMS) average of the electrical signal. Thus, the RMS roughness was defined as follows:

$$R_{q_i} = \sqrt{\frac{1}{l}\int_0^l z^2(x)dx}$$

$$R_q = \frac{1}{CN}\sum_{i=1}^{CN} R_{q_i}$$

where,

$l_i$ = Sample length

z = Height

x = Distance along measurement

CN= Number of samples evaluated

In Europe, the signal of the instrument was passed through a rectifier in order to charge up a capacitor. As a result, the output of the instrument was the center-line average (CLA) roughness:

$$R_{a_i} = \frac{1}{l}\int_0^l |z(x)|dx$$

$$R_a = \frac{1}{CN}\sum_{i=1}^{CN} R_{a_i}$$

$R_a$ and $R_q$ are both included in the ISO roughness definition as a description for surface average roughness. More detailed discussions of these parameters are given in International

Organization for Standardization (ISO) Standard 4287 (ISO 1997).

### 1.3 Surface roughness parameters in the upsetting

To investigate the friction law of metal upsetting process, attention has been paid on the microscopic condition of the contact interface, where surface roughness is an important influential factor. In order to extract the surface feature for the Finite Element modeling in an efficient way, we are particularly interested in the mean height R and mean width AR of the assessed profile.

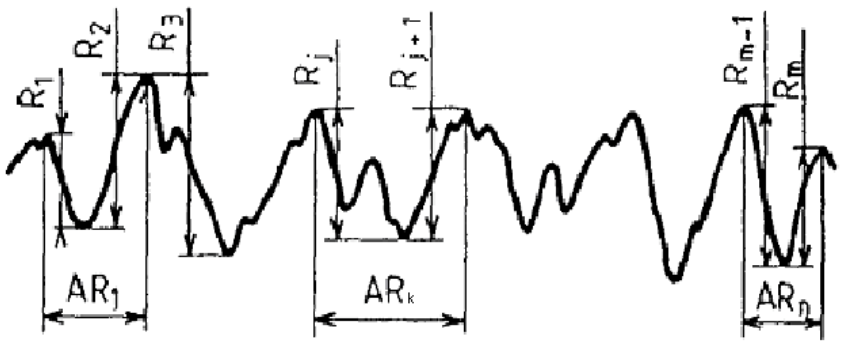


Fig.1.3 the height $R_j$ and width $AR_k$ of the asperity in a sample length

$$R_i = \frac{1}{m}\sum_{j=1}^{m} R_j \,,\; AR_i = \frac{1}{n}\sum_{k=1}^{n} AR_k \;\text{ with }\; m = 2n$$

$$R = \frac{1}{CN}\sum_{i=1}^{CN} R_i \,,\; AR = \frac{1}{CN}\sum_{i=1}^{CN} AR_i$$

The plastic wave theory considers the asperities of the tool as triangles shown in Fig.1.4 below. So the definitions of parameters in this particular case are:

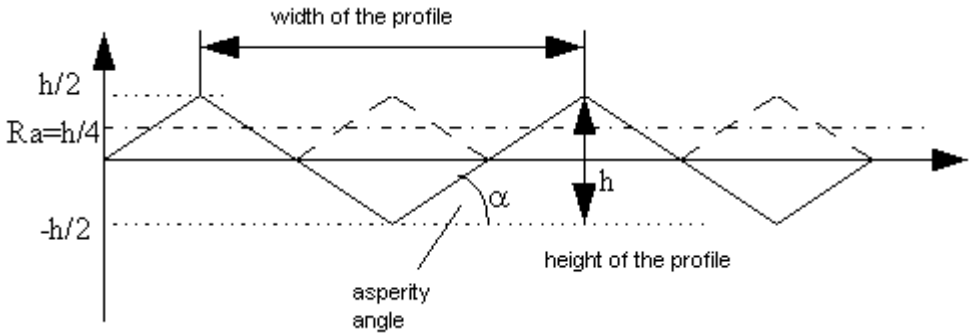


Fig.1.4. Triangle asperity

$$h = 4R_a = R$$

$$p = AR$$

where $$\alpha = \frac{2R}{AR}$$

For the experiment part of this project, the tools surface parameters were measured right after being machined. The parameters of six pairs of conical tools are listed in the table below.

| Pair No. | Cone Angle | R(μm) | AR(μm) | θ(rad) | θ(°) | W(μm) | AW(mm) | Ra(μm) |
|---|---|---|---|---|---|---|---|---|
| 1 | 3° | 2.913 | 120.681 | 0.048 | 2.76 | 0.719 | 1.558 | 0.857 |
| 2 | 5° | 13.842 | 238.970 | 0.11 | 6.61 | 0.954 | 1.505 | 3.608 |
| 3 | 12° | 38.310 | 358.978 | 0.21 | 12.04 | 2.087 | 1.472 | 9.935 |
| 4 | 3° | 9.164 | 240.131 | 0.076 | 4.36 | 0.794 | 1.514 | 2.431 |
| 5 | 7° | 20.985 | 359.060 | 0.11 | 6.67 | 0.577 | 1.294 | 5.576 |
| 6 | 9° | 37.878 | 473.755 | 0.15 | 9.08 | 0.782 | 1.636 | 9.907 |

Table 1.1

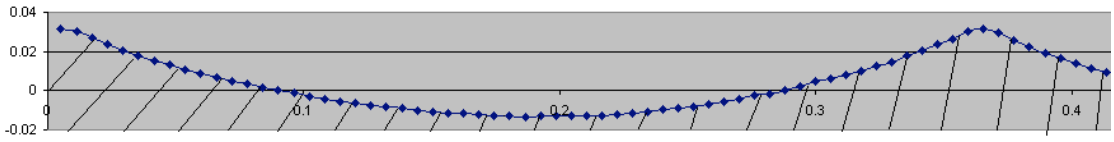


Fig.1.5 The actual asperity of pair 3 (unit: mm, height: width=1:1)

The six pairs of models with different asperity parameters serves as a diverse database source where we can perform different simulations and experiments and see how those parameters affect the frictional behavior in the axisymmetric upsetting.

# CHAPTER 2 The effect of asperity in upsetting

## 2.1 Introduction

Finite element analysis was first termed by R.W. Clough in a paper published in 1960, but the roots of the theory relates back to the Ritz method of numerical analysis, first introduced in 1909. Using the calculus of variations, R. Courant applied the Ritz method to obtain "piecewise approximations" of solutions for problem of equilibrium and vibrations in 1943. Further development of these ideas continued through the 1940's and 50's. By 1953, engineers began to use computers to solve structural problems.

The paper by Turner, Clough, Martin, and Topp, published in 1956 is considered a major turning point in the development of FEA. The paper dealt with the "stiffness and deflection of complex structures" and contributed to increased interest in the method. In 1960 the term "finite element" was first used, and around this time numerical methods began to be widely used in the aerospace industry.

In 1963, finite element analysis was recognized as a specific technique, and a serious academic discipline. This led to much greater research, leading to its application for heat transfer and fluid mechanics problems in addition to structural.

By the early 1970's, finite element analysis had become established as a general numerical technique for the solution of any system of differential equations. The method was still only used at this time on a limited basis, however, because of the availability of powerful computers in industry. The use was primarily in the aerospace, automotive, defense, and nuclear industries.

With the advent of low cost computers (PCs and workstations) in the last two decades, the methods have become more widely used. It is now possible for engineers in virtually every industry to take advantage of this powerful tool.

As a numerical method, Finite Element Analysis (FEA) serves as a powerful complement to the experiment. In this specific project, FEA is indispensable to the experimental findings. With FEA, a slow motion of the upsetting process is allowed, so that the phenomenon of interest could be examined carefully and repeatedly, without additional cost. As roughness is a very important factor in upsetting process, the knowledge of the microscopic interaction between the tool asperity and the workpiece material is crucial in understanding the whole process. FEA facilitates the microscopic observation at each step of the process, which is very difficult to obtain through experiment. Furthermore, a good number of FEA models, varying in roughness parameters or friction coefficient, were executed in the project to help better understand what affects the contact behaviour of the upsetting interface. Last but not the least, the combination of FEA and experiment makes it possible to test the friction law-plastic wave theory, as well as its pros and cons in comparison with classical Coulomb friction law.

**2.2 Finite Element Modeling**

Since surface roughness plays an important role in the processes involving friction, two group of numerical models were set up – one group with roughness (asperity model) and the other without (flat model) – to see how actually surface roughness affects the friction as well as the upsetting force, the pressure distribution at the interface, the strain/ stress distribution and the deformation of the workpiece.

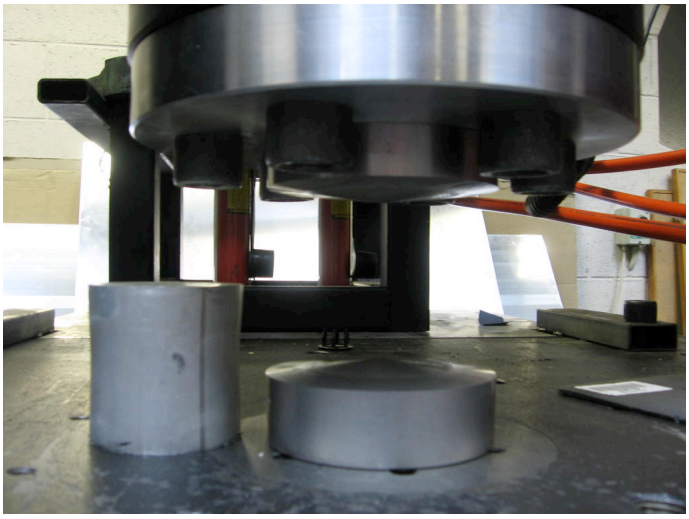

Fig.2.1 Experimental setting

Fig.2.1 is the experimental setting of the upsetting process. In ABAQUS, a group of preliminary axisymmetric models with tool as 2-D analytic rigid shell and workpiece as 2-D shell planar were exercised. No problem in finding converging solutions for the flat models under such condition. However, for the models with asperities, the calculation time was generally longer, with some convergence problems at the top right point of the workpiece. A plot of contact pressure CPRESS in Fig.2.2 clearly shows the convergence problem. The pressure grows to an obviously unrealistic high value. So are the other values at the same point.

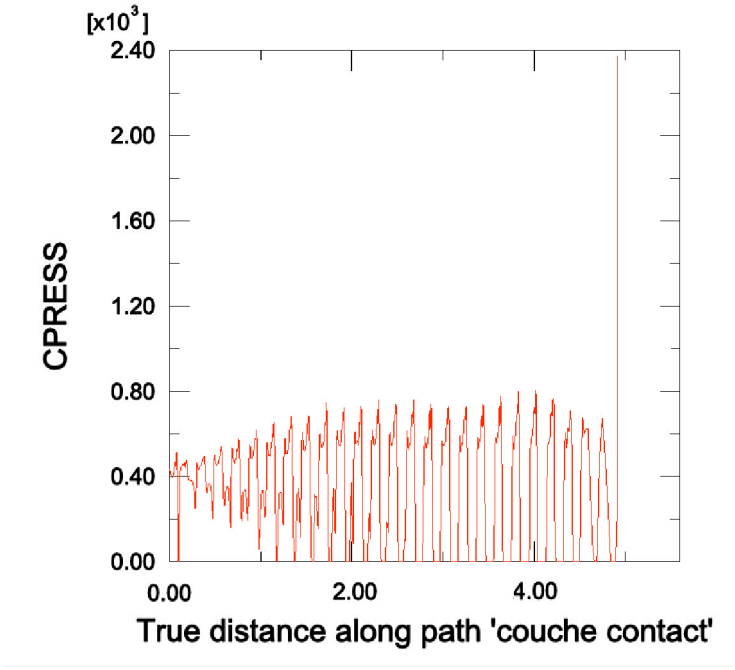


Fig.2.2 Interface contact pressure against off-axis distance

To tackle with the numerical divergence, an improved model was set up with deformable tool material being hard steel rather than rigid body. The material is closer to reality, and the small deformation of the tools provides the workpiece with a less rigid boundary, hence the phenomenon of stress concentration at sharp angles could be alleviated. It is proved that the improved model, even with the most aggressive surface asperity (very sharp asperity angle), is robust enough to overcome the convergence difficulty.

| Model description | |
|---|---|
| Size of workpiece (height × width) | Refer to F.2.3 (a) |
| Asperity parameters | R=21um AR=360um |
| Tool material | Hard steel |
| Workpiece material | Aluminum, rigid plastic |

| | |
|---|---|
| Stroke course | 1mm |
| Contact properties | frictionless |
| Element type | Implicit, CAX4R (4-node bilinear axisymmetric quadrilateral, reduced integration, hourglass control) |
| Element size (height × width): | 0.030 × 0.015mm |
| Number of elements | 5805 |
| Total number of variables | 16934 |
| Solver | ABAQUS Standard (Implicit) |

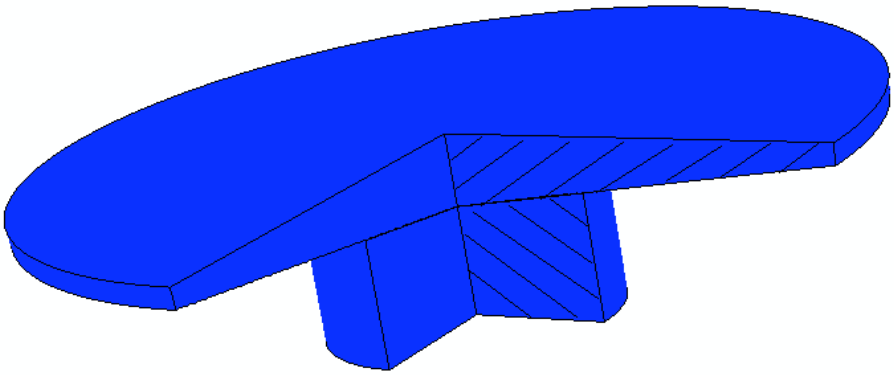

(a)

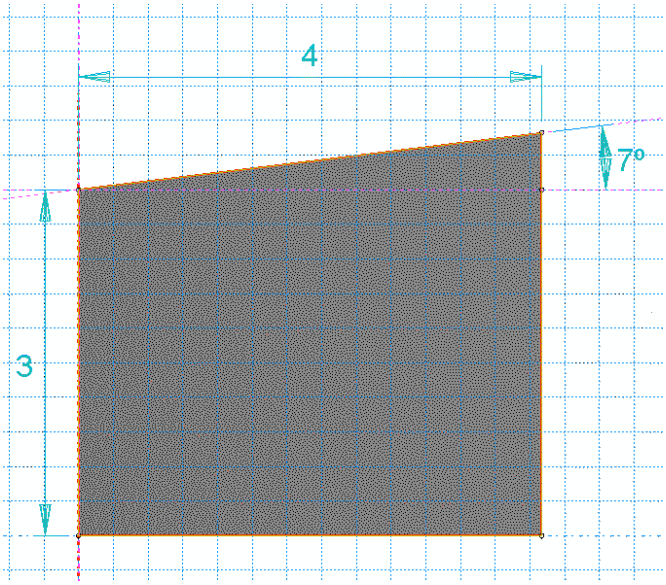

(b)

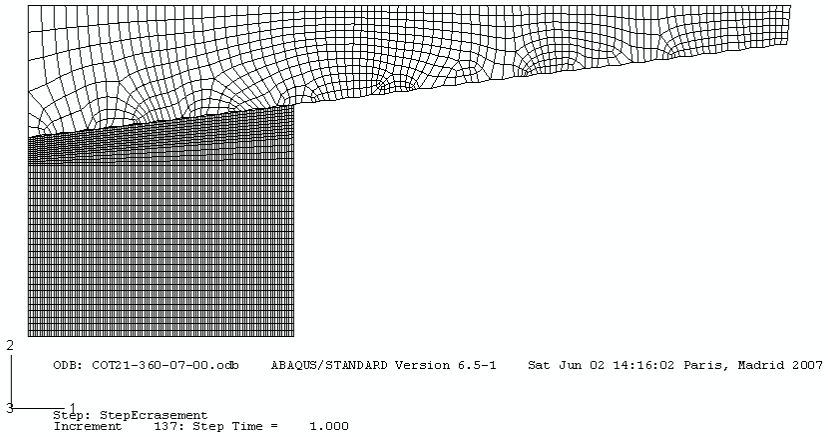


(c)

Fig.2.3 (a) The 3-D illustration (b)2-D axisymmetric model of workpiece (c) 2-D axisymmetric model of tool and workpiece (with mesh)

## 2.3 Results comparison and discussion

### 2.3.1 The local material outflow and the corresponding experimental observation

With the same stroke course (1mm) applied, the asperity model is found to have a bigger displacement value in the top right outgoing point than the flat model. This phenomenon is identified as local volume outflow of the workpiece material. It is illustrated in Fig.2.4. The relatively softer workpiece material is squeezed outwards along the radius direction under the 'intrusion' of tool asperities. The material flow accumulates at its furthest end, the outer edge of the workpiece, where the burr takes form. This phenomenon is later proved to exist in every asperity model where sliding is significant, no matter what value the cone angle is. However, as the simulation indicates, this phenomenon has a local feature as the thickness of the flowing layer is on the same order with the width of a single tool asperity, which is around 200 $\mu m$ depending on different asperity parameters.

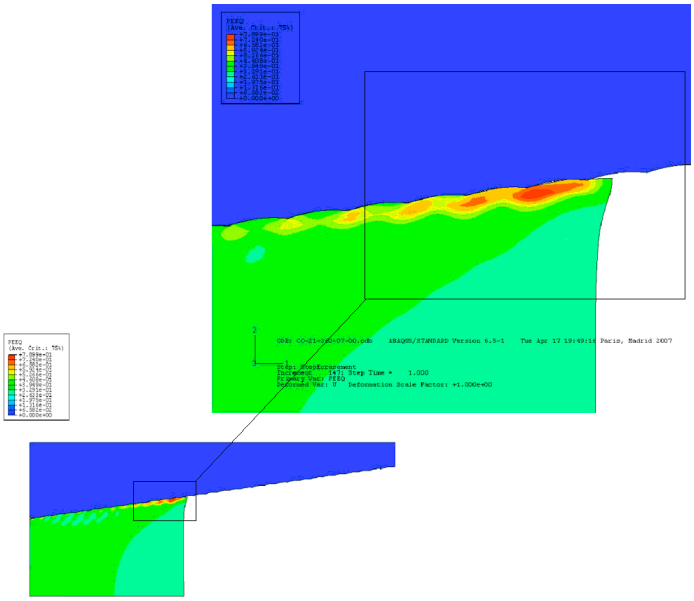

Fig.2.4 the local volume outflow results in a maximum plastic strain at the furthest end

The local material outflow is confirmed by experimental findings. Fig. 2.5(a), (b) shows the edge of two deformed workpieces with the same tool (Pair 1, refer to table 1.1) observed from a microscope. Grease was applied to the surface of one piece to simulate a frictionless contact while the other piece remains unlubricated. The outflow of the frictionless one, as shown in Fig.2.5 (a), is more prominent than the dry-friction one in Fig.2.5 (b). When friction exists, the material cannot 'flow' freely but being held back by the opposite friction force. If the friction coefficient is big enough, the material will stick to the tool asperity without slipping. Fig.2.5 (c) shows the deformed surface of the workpiece, where indentation was formed under the corresponding tool asperity.

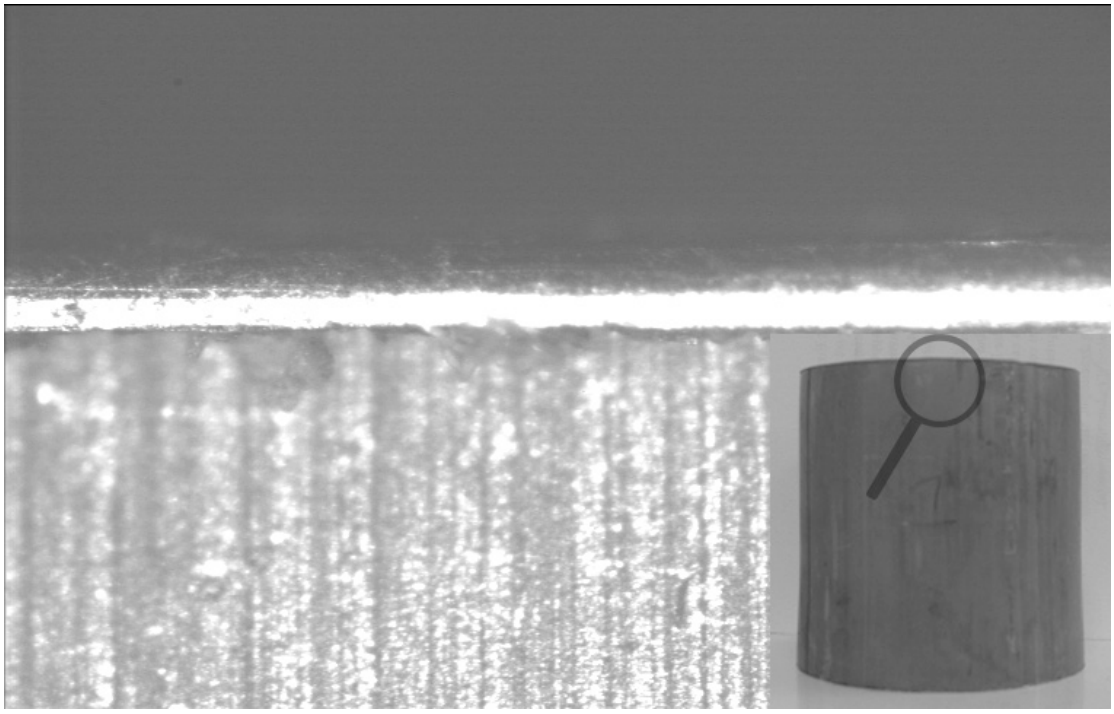

(a) Layer thickness = 0.08mm

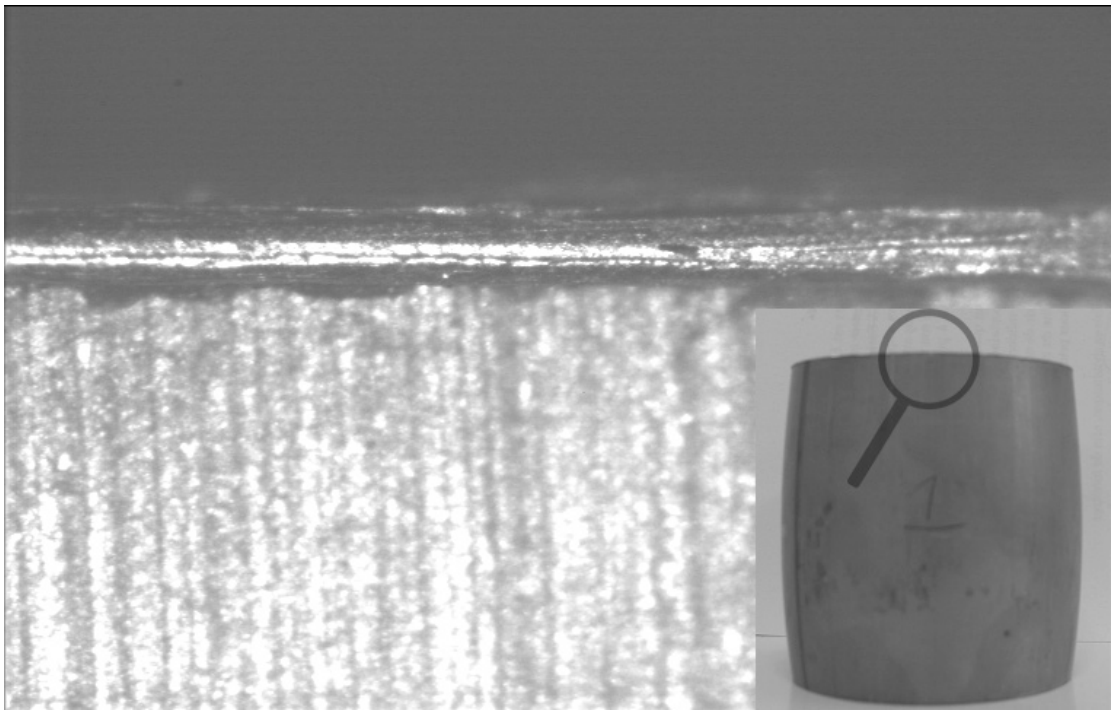

(b) Layer thickness = 0.07mm

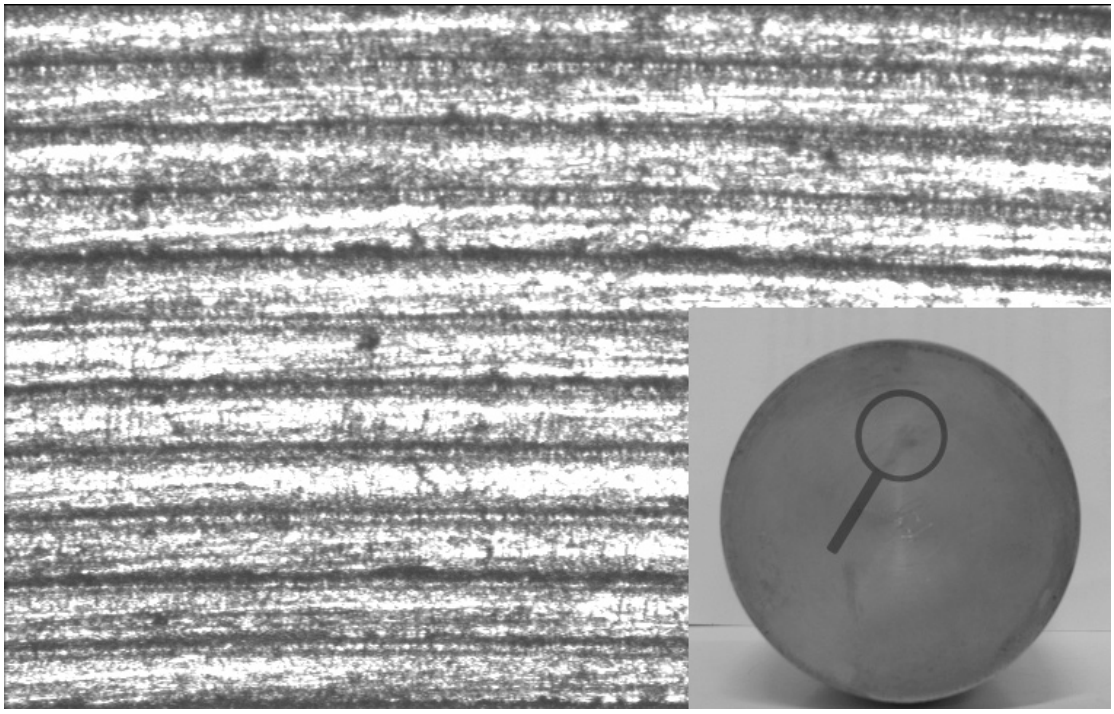

(c) Plastic wave, wave length= 0.1mm

Fig.2.5 Pair 1, the outflow layer under microscope ( $10 \times 5$ )

(a) Upsetting with grease - frictionless (b) upsetting without grease – dry friction (c) the deformed surface of workpiece

On the other hand, no local volume flow exists in the flat model. The deficiency of the flat model and the classical friction law based on it urges a closer look on their validity.

### 2.3.2 The Reaction Force of the two models

| Model | RF | RF1 | RF2 |
|---|---|---|---|
| Asperity | 138775 | 9884.64 | 138442 |
| Flat | 136315 | 6773.48 | 136147 |

* The data is taken at the last increment. RF is short for Reaction Force given by the workpiece. RF1 and RF2 are in the horizontal and vertical directions respectively.

Table 2

While RF2 of the two models stays almost the same, the difference in RF1, the horizontal Reaction Force, is immediately noticed. This is also due to the phenomenon of local material

outflow. The added reaction force RF1 is to balance the pressure from the opposite side of the asperity during the outflow.

### 2.3.3 The evolution of outflow and contact behaviour

The initial state (T=0) of the tool and the workpiece are as in Fig. 2.6, only the tool asperity vertex touch the workpiece.

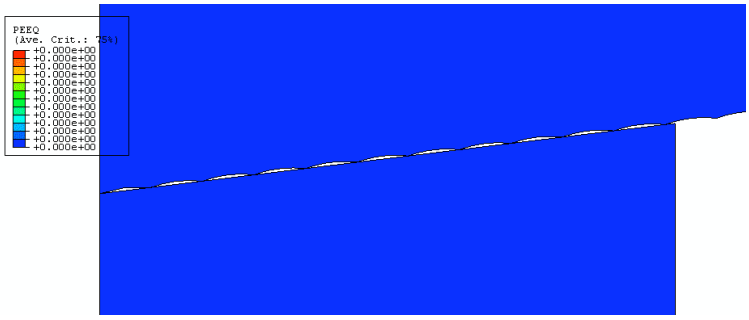


Fig.2.6 Initial state

At T=2.36E-2 in Fig.2.7, the relative softer workpiece material begins to settle in the caves of tool asperity. Plastic strain is seen at the parts in contact with the tool asperity vertex.

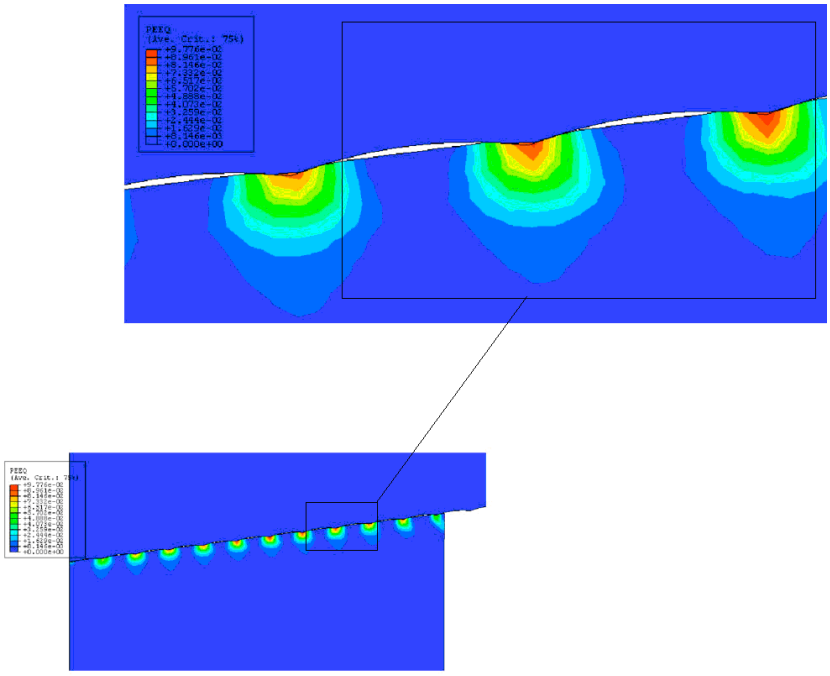

Fig.2.7 Asperity sets in

From T=0.1, the workpiece material largely fulfils the asperity cavity and begins to flow outwards. It encounters the opposite side of the asperity, which is an obstacle for its expansion. However, the expansion cannot be stopped since the tool continues to descend. So the workpiece material follows a boundary condition of tool asperity as it flows out. The added reaction force RF1 is to balance the pressure from the opposite side of the asperity.

When observe carefully, a vacancy at the left side of each asperity could be noticed in Fig.2.8 (the white part). A plot of contact pressure CPRESS along the surface of the workpiece confirms this: at R < 2mm the contact pressure exists at either side of the asperity, though the magnitude varies. This means only at the region near the axis the workpiece material is in full contact with the asperity cavity. At R >2mm oscillation of the contact pressure amplifies with the pressure of certain points dropping at zero, which means no contact. Those points correspond to the vacancy area at the left side of the asperity. This fact indicates that at the region further from the axis, part of the left side of the asperity is not in contact with the workpiece during the whole process.

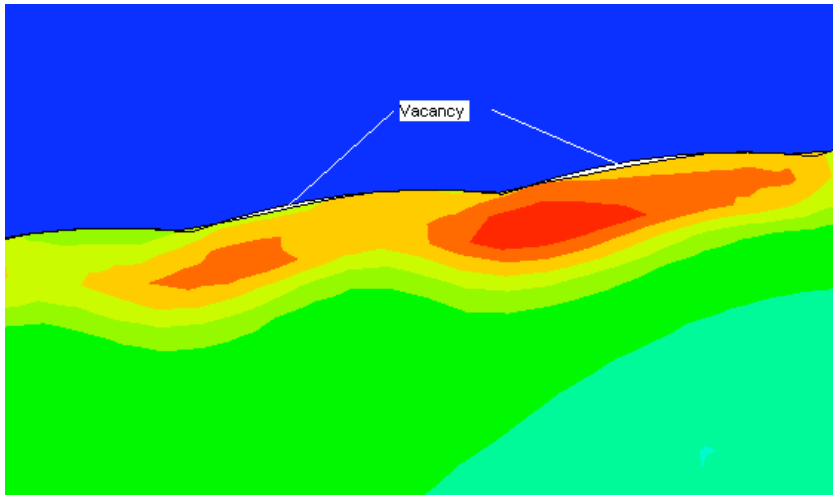


Fig.2.8 The vacancy in the PEEQ contour

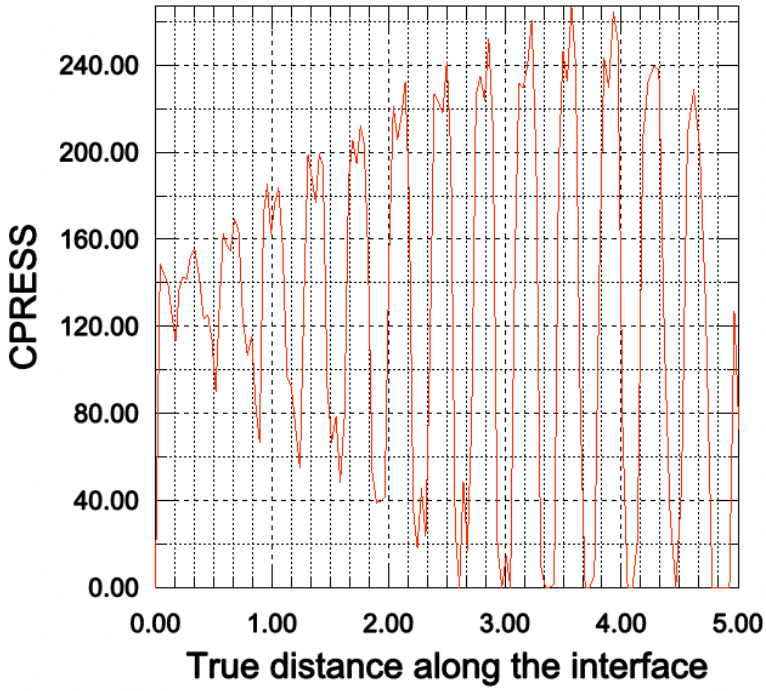


Fig.2.9 Contact pressure against interface distance

### 2.3.4 Contact opening

In ABAQUS contact opening indicates the clearance value between two contact surfaces. A positive contact opening indicates the distance between the two surfaces that are out of contact, while a negative contact opening means overclosure. Zero or infinitesimal contact opening means in contact.

In our case, the contact opening could be plot against the distance along the interface, in Fig.2.10, thus a more intuitive understanding of the overall contact condition is provided. It's worth noticing that in the frictionless model, the largest contact opening occurs at the edge (top right point). It is because the edge bit is already shaped by previous asperities in a way that it is parallel to the right side of the asperity. Taking that form, the edge bit barely touches the tool asperity. On the other hand, the frictional model sees an overall smaller contact opening, with its maximum contact opening at 2/3R, but not the edge. The maximum contact opening of the frictional model is only 1/7 of the frictionless model.

The introduction of friction seems to make the two surfaces adhere to each other, without leaving too much contact opening. This could also be explained in the point of view of the local outflow. Friction counters the outflow, making the material more difficult to slip. Microscopically, the material is more likely to get stuck inside the asperity rather than flowing outwards. This allows material continue to fill in the asperity cave before it overcomes the critical friction and begins to slip.

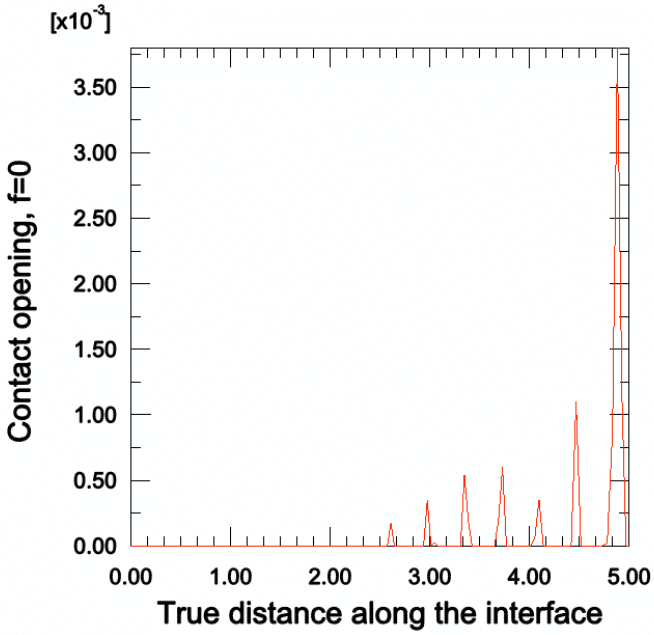

(a)

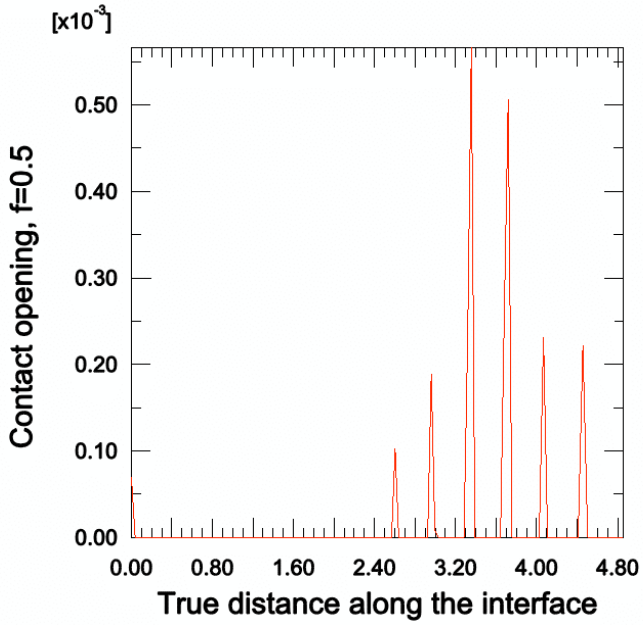


(b)

Fig.2.10 Pair No.5, the contact opening along the interface (a) frictionless model (b) friction coefficient=0.05

Fig.2.11 illustrates the microscopic prints of Pair No.2 under the microscope observation. As it is predicted in the simulation, the piece subjected to dry friction has a smaller contact opening and the material fills up most of the tool asperity. Under microscope the prints could be clearly seen. On the contrary, the piece subjected to grease lubrication has a large contact opening because the lubricant fluid is trapped inside the asperity cavity, which actually hinders the development of plastic wave.

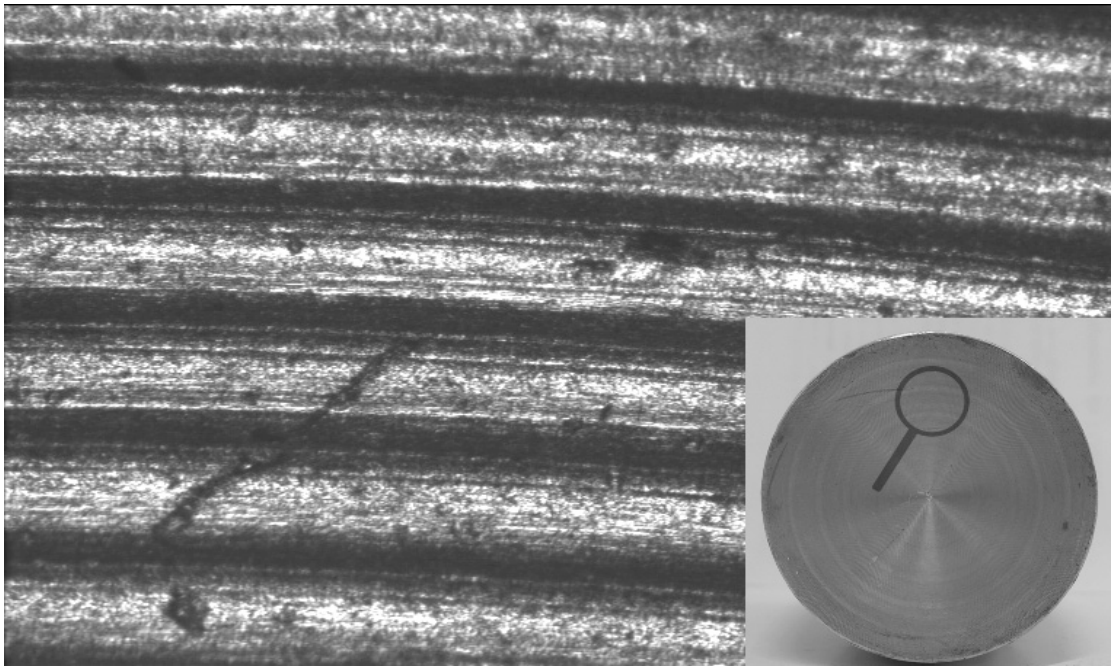

(a)

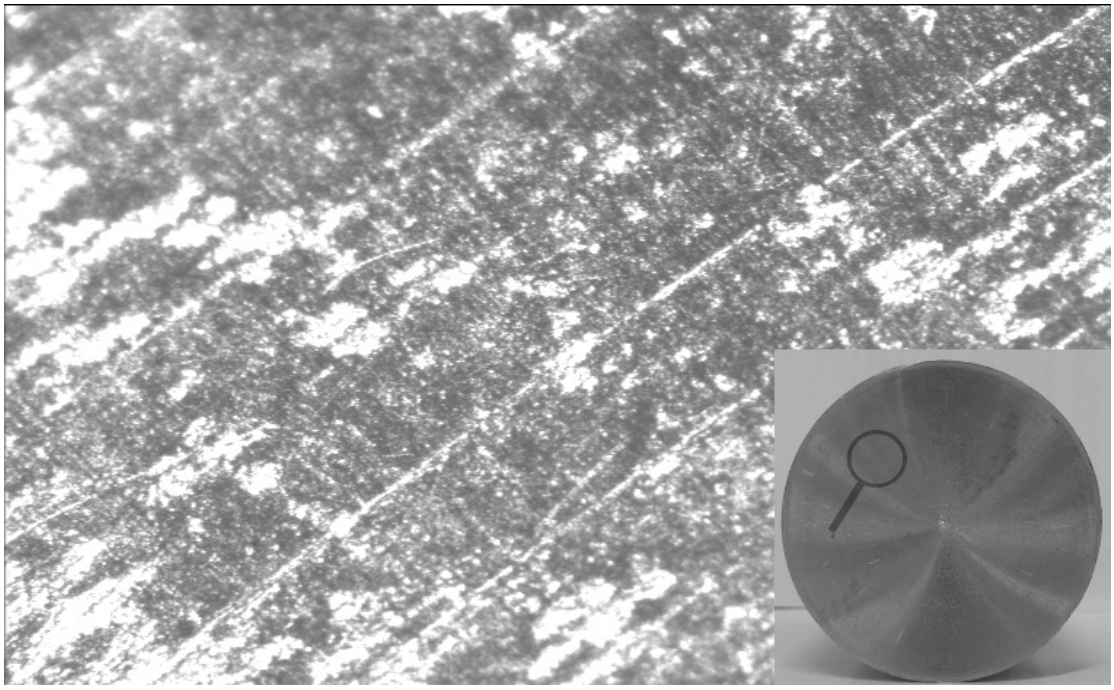

(b)

Fig.2.11 Pair No.2 the microscopic prints on the material surface by microscope ( $10 \times 5$ ) (a) dry friction (b) with grease

While having six models (refer to Table 1.1) available at hand, three specific models with frictionless tangential behaviour are chosen to see how much the workpiece material fills up the tool asperity in each case.

In Fig.2.12 (a) (b) (c), it is noticed that the contact opening increases with the cone angle. For example, in Fig.2.12 (a) the average contact opening is about 1×10E-3 unit with the asperity height and width being 9.2×10E-3 and 240×E-3 respectively (when talking about the average opening, the free edge point is not counted in because its value is usually large and not typical for the common points). The average opening is about 4×10E-3 in Fig2.12 (b) and 13×E-3 in Fig.2.12(c).

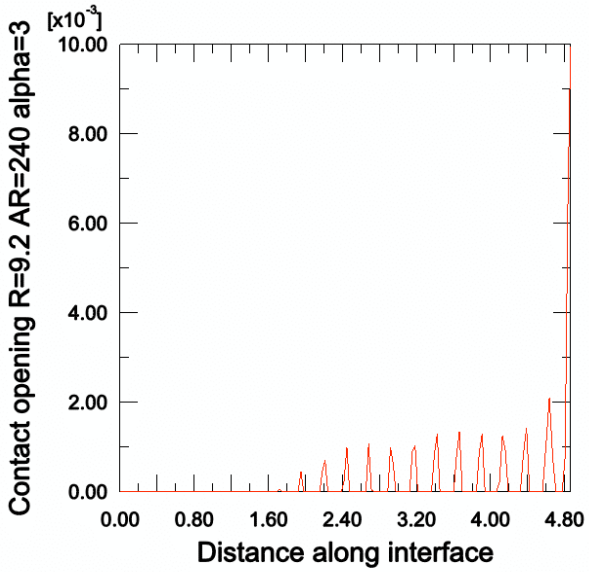


(a)

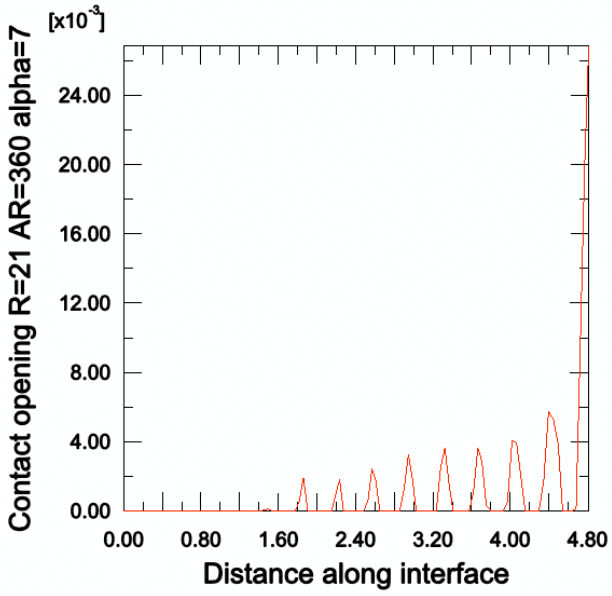


(b)

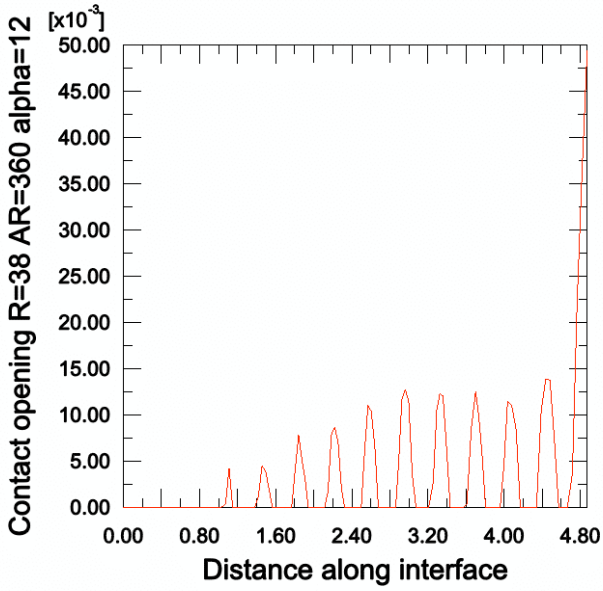


(c)

Fig.2.12 the contact opening of three models at the end of the upsetting (a) Pair No.4 (b) Pair No. 5 (c) Pair No. 3

When tracing the evolution of the contact opening of Pair No.3, a very interesting phenomenon is noticed: contrary to the intuition, the contact opening between the tool

asperity and the material doesn't only diminish when the material is squeezed. Rather, at some part of the interface, the contact opening increases over time. See Fig 2.12 (a) and Fig 2.12(b). For the workpiece, at the region where R>2, the contact opening increases over time while at the region where R<2, the contact opening decreases over time. This fact is due to the local plastic flow of the material. If there were no material flow (for example if the sticking friction dominates), the contact opening would only decrease over time.

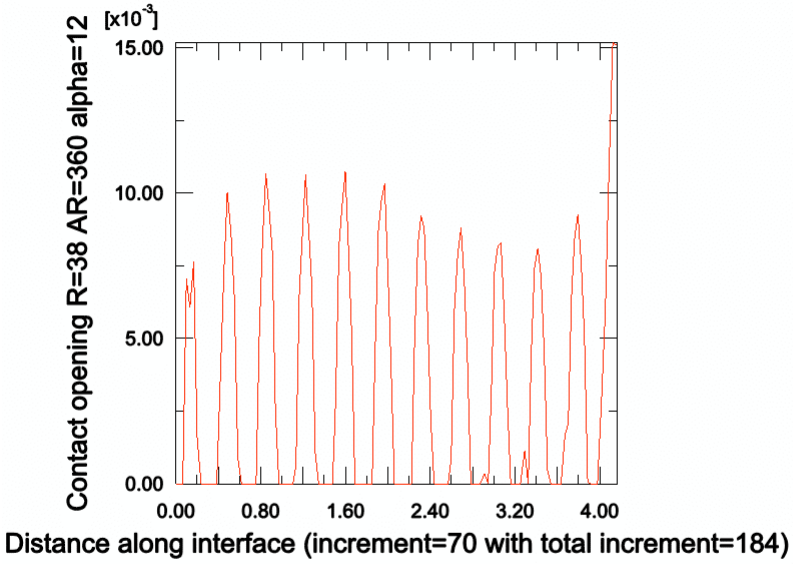


(a)

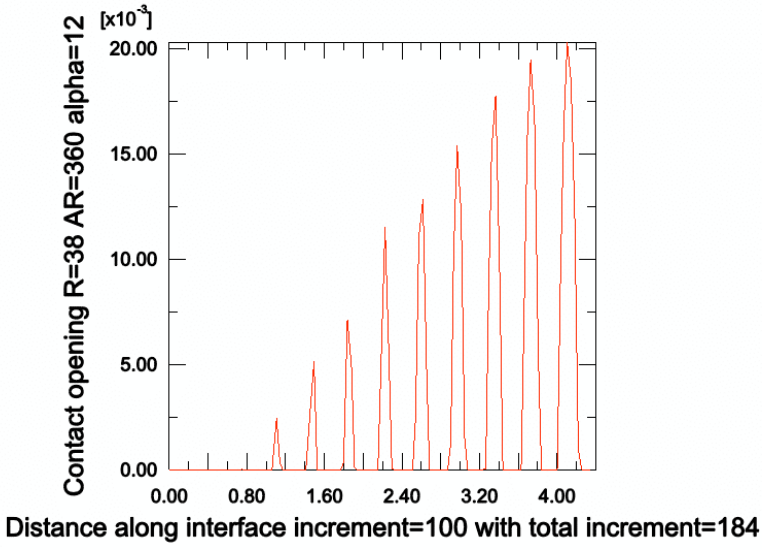


(b)

Fig.2.12 Pair No.3, the increase in contact opening at R>2 (a) increment=70 (b) increment=100

When taking a close look at the interface itself, as in Fig.2.14, it is found out that the local plastic outflow only begins when the tool asperity cavities is largely filled. That is to say, when the contact area at the interface is small, the squeezing force is not enough to make the material flow because of the lack of contact area. So the workpiece material continues to come in the tool asperity hence the contact area is increased. Notice that the major outflow hasn't taken place, so the workpiece material comes from both sides of the asperity (rather than from only one side as is described in plastic wave theory), and there is usually a small vacancy at the topmost of each asperity if the asperity shape is sharp enough. Then the critical point is reached, where the interface accumulates up enough contact area so the contact force could make the material flow. Until this instant the tool only descends at a distance on the same order with the asperity height – actually just a few μm more than the height, depending on the specific case. There is no globally squeezing taking place yet, everything happens within a local layer whose thickness is around the same value of the asperity height and the rest part is nearly unaffected. However, as the tool continues to descend, the local flow takes form and the rest part of the body begins to 'feel' the squeezing.

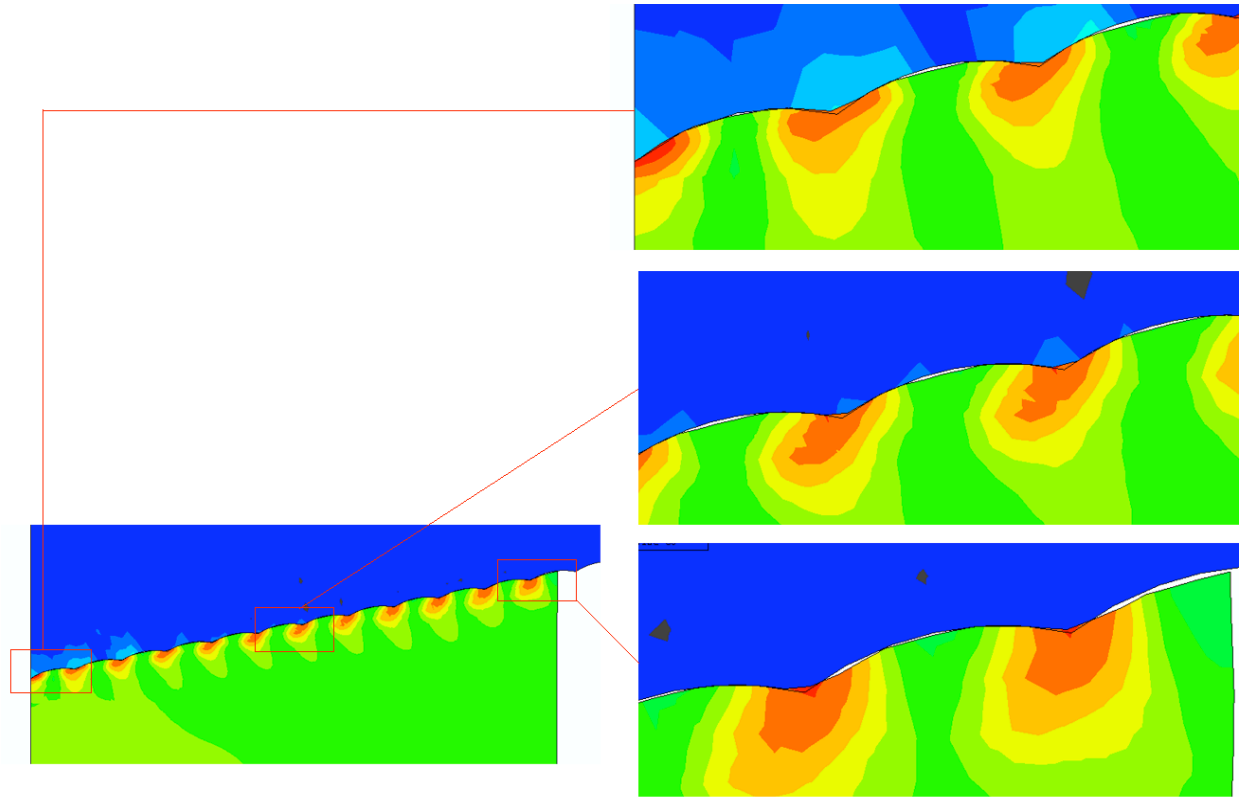

(a)

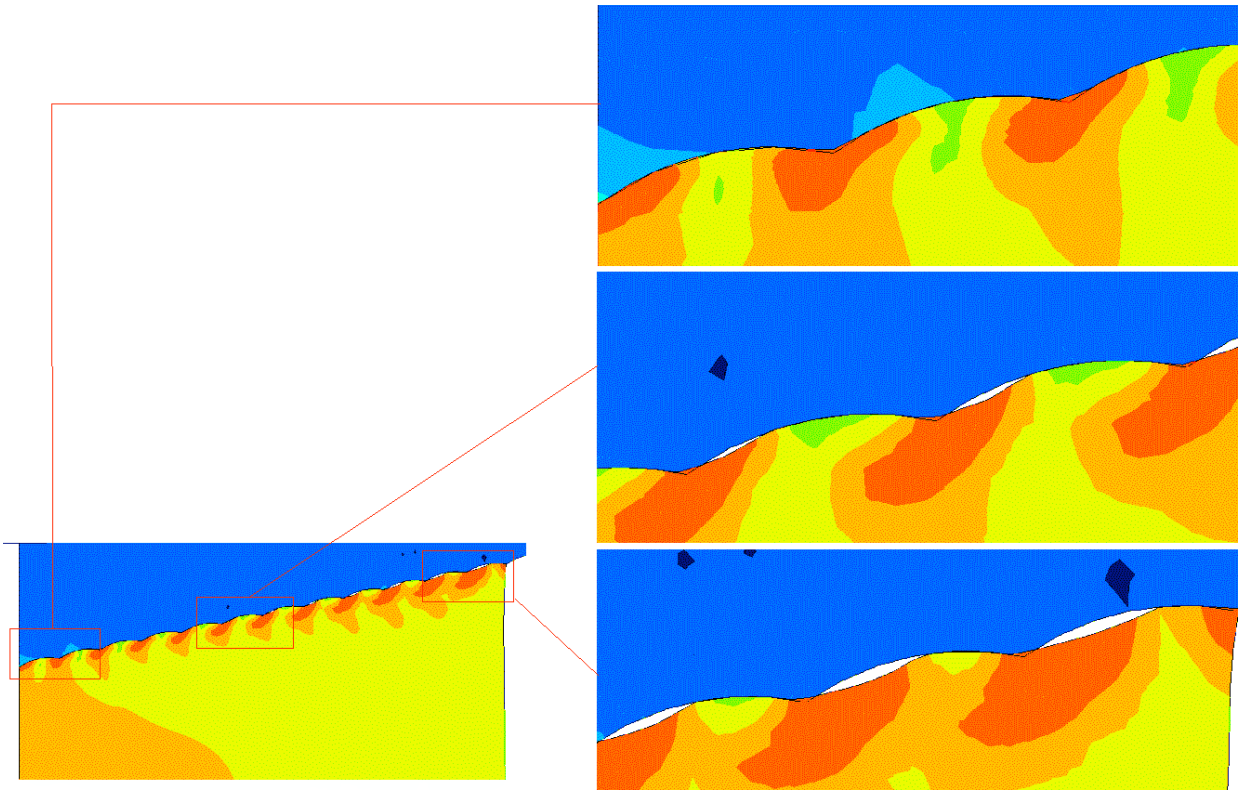

(b)

Fig.2.14 the contact opening at three different regions in Mises contour plot (a) increment=70 (b) increment=100

The trending is that at the region near the axis, the friction is sticking dominant, while at the region far from the axis, the friction is slipping dominant. Fig.2.15 illustrates the evolution of the plastic wave at the slipping dominant region. In (b) the vacancy is formed by the asperity vertex (marked by the cross) and it still holds the shape of the asperity as it moves right. In (c) the vacancy grows to its maximum value and the local outflow stalls for a moment because of the lack of contact area. In (d) the vacancy area begins to shrink in order to gather enough contact area so the outflow could take place again.

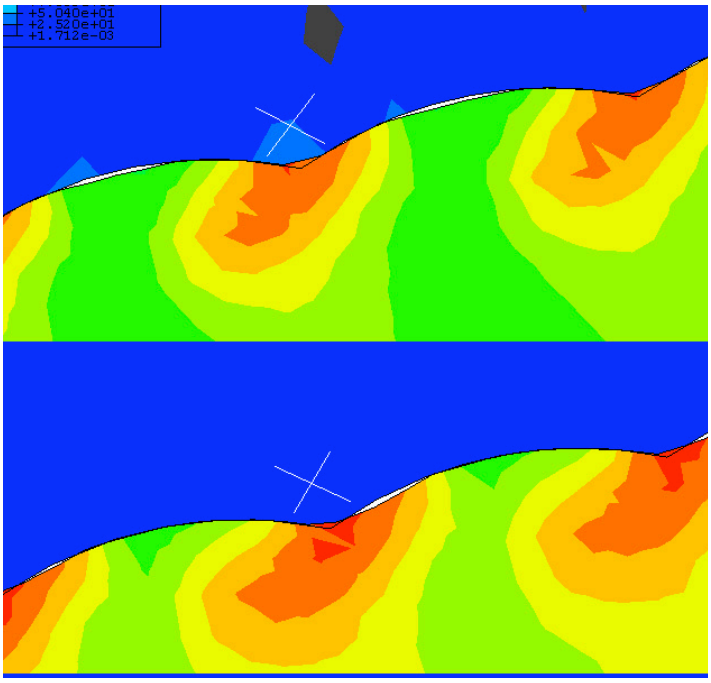

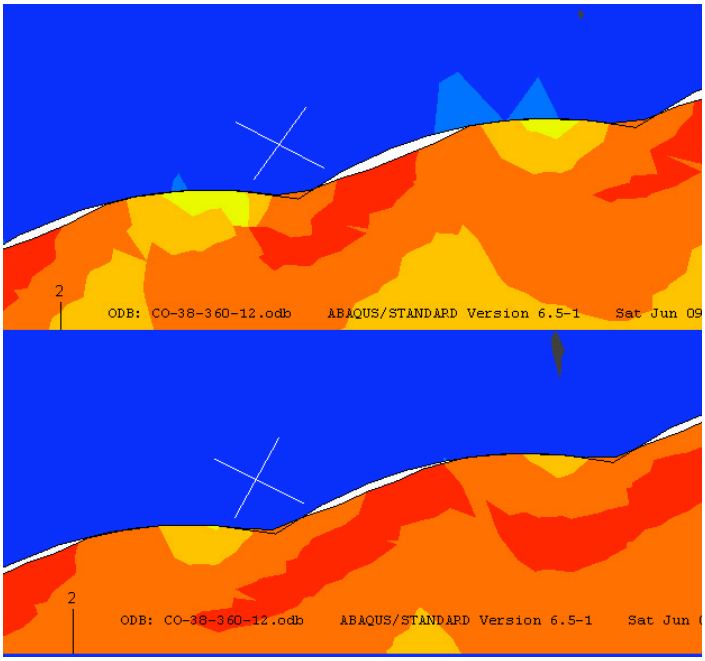


Fig.2.15 the evolution of plastic wave at R=4.5 in Mises contour plot

### 2.3.5 Analysis of single asperity

One asperity is singled out in both the frictionless and frictional model to observe the contact pressure and plastic strain distribution along its width.

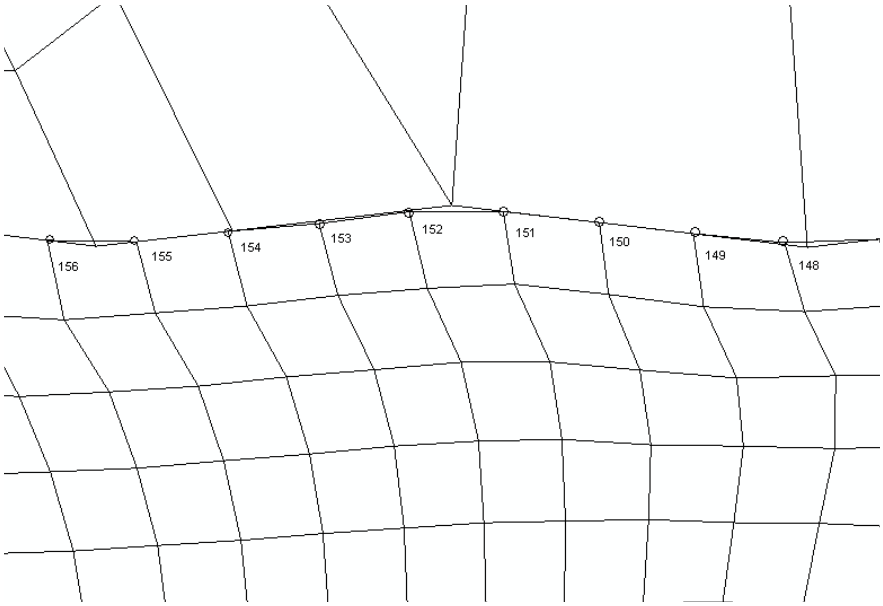


Above: frictionless

(a)

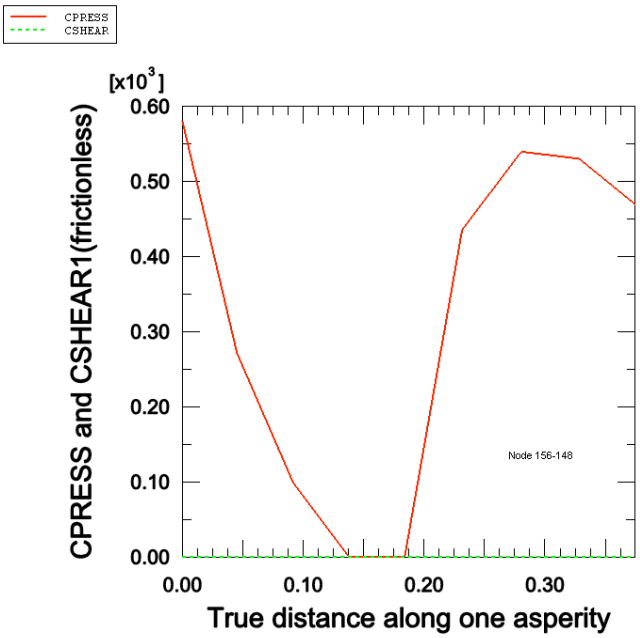


(b)

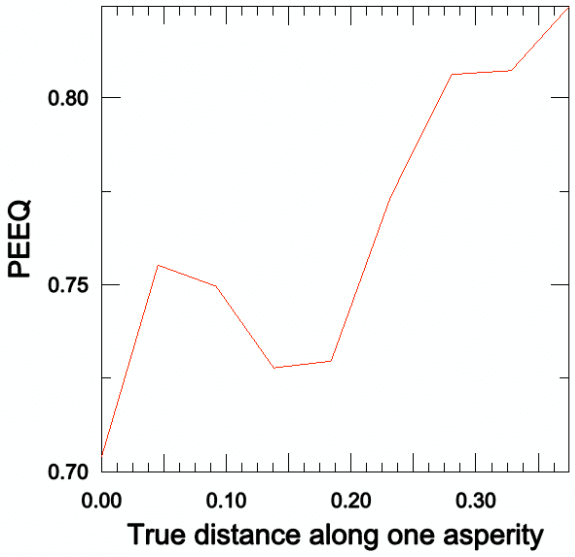


(c)

Fig.2.16 one asperity in frictionless model (a) nodes selected (b) contact pressure and friction distribution along the asperity (c) Plastic strain distribution along the asperity

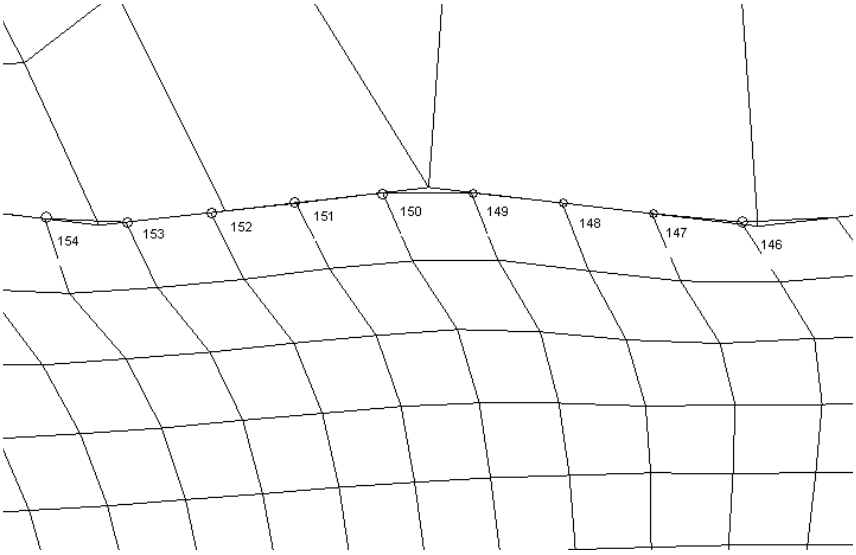
154
153
152
151
150
149
148
147
146

(a)

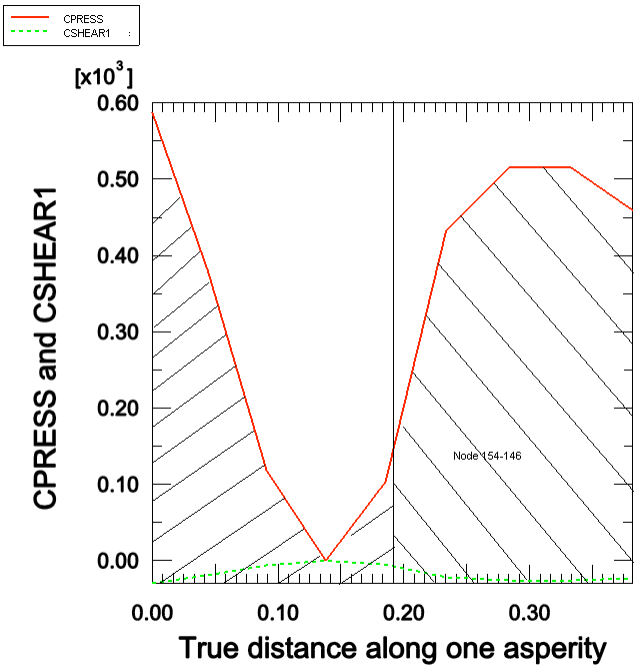
CPRESS
CSHEAR1
[x10^3]
0.60
0.50
0.40
0.30
0.20
0.10
0.00
CPRESS and CSHEAR1
Node 154-146
0.00
0.10
0.20
0.30
True distance along one asperity

(b)

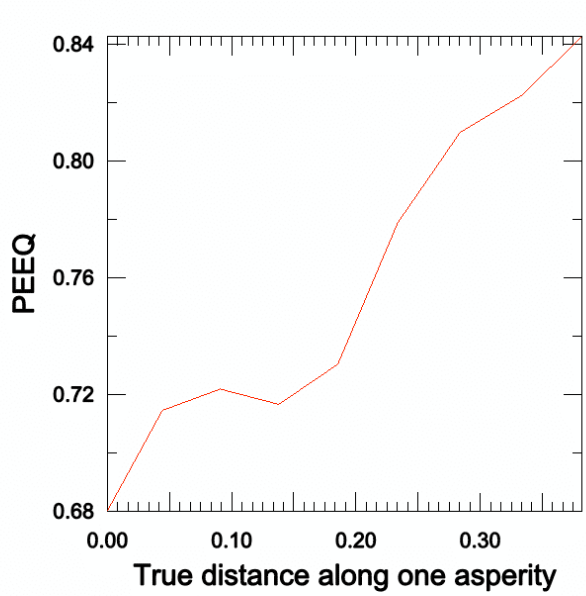


(c)

Fig.2.17 one asperity in frictional model f=0.05 (a) nodes selected (b) contact pressure and friction distribution along the asperity, and the total pressure force on each side (indicated by area)

(c) Plastic strain distribution along the asperity

| CONTACT NODE | OUTPUT STATUS | CPRESS | CSHEAR1 | COPEN | CSLIP1 (E-3) |
|---|---|---|---|---|---|
| 146 | SL | 459.175 | -22.9588 | 105.723E-15 | -761.769 |
| 147 | SL | 515.119 | -25.7559 | 20.1589E-15 | -738.321 |
| 148 | SL | 515.475 | -25.7738 | 5.29255E-15 | 710.496 |
| 149 | SL | 432.697 | -21.6349 | -170.235E-15 | -682.909 |
| 150 | SL | 103.326 | -5.16632 | -12.5567E-15 | -632.054 |
| 151 | OP | 0. | 0. | 221.782E-06 | -590.31 |
| 152 | SL | 118.387 | -5.91935 | -52.2283E-15 | -588.265 |
| 153 | SL | 379.232 | -18.9616 | 83.958E-15 | -558.286 |
| 154 | SL | 586.898 | -29.3449 | 312.546E-15 | -615.465 |

*SL= Slip, OP= Open

Table 3 output contact variables

For the single asperity, the total pressure on the right side of the asperity is greater than that on the left side. This could be seen from Fig.2.16 (b) and Fig 2.17(b), the pressure curve enclosed a greater area in the right side of the asperity than the left side. Furthermore, the right side has seen a higher plastic strain, according to Fig.2.16 (c) and Fig.2.17(c).

The summation of the imbalance of the pressure at each asperity will serve as a macroscopic force that hinders the expansion of the material at the interface, even in the frictionless case.

### 2.3.5 The tracing down of three particular points

It might be interesting to trace the movement of some particular points at the workpiece surface. Fig below shows the time evolution of contact pressure and tangential shear stress of three particular points at around 1/3R, 2/3R and R of the workpiece surface. The pressure varies through time, and zero contact pressure means the point comes into the vacancy of one asperity. So it's clear that those three particular points have all travelled some distance in the whole process – point 1 with a distance of two asperities and a little bit more, point 2 with a distance of six asperities while point 3, at the edge, travelled up to 10 asperities, the furthest.

This is what we call the local outflow of the material. It is the logical consequence of an upsetting process: the correlation of the slipping distance and the location of the point is generally inverse proportional.

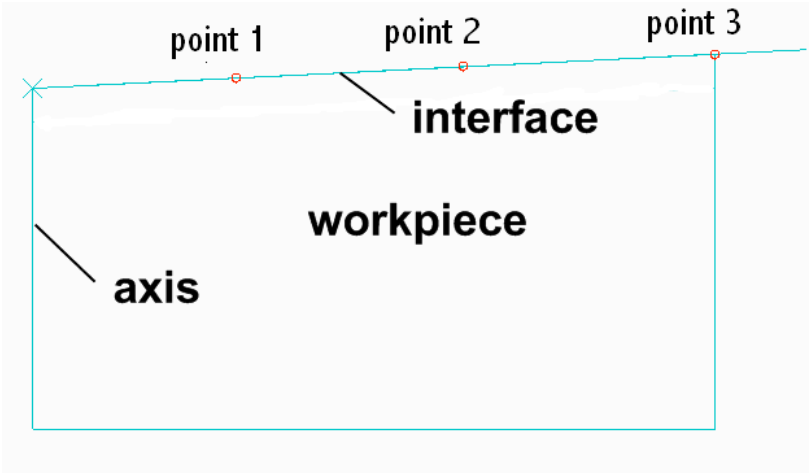
point 1
point 2
point 3
interface
workpiece
axis

(a)

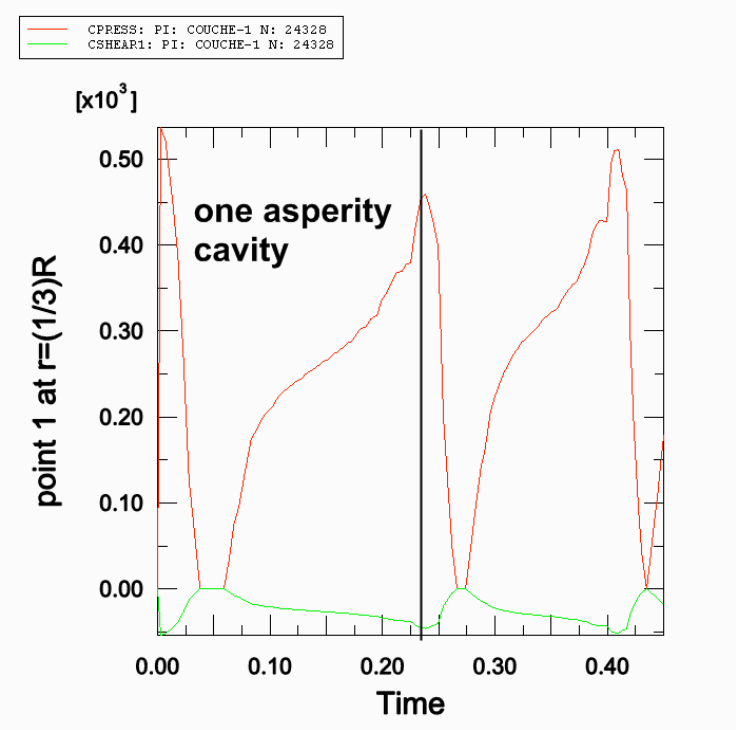
CPRESS: PI: COUCHE-1 N: 24328
CSHEAR1: PI: COUCHE-1 N: 24328
[x10^3]
point 1 at r=(1/3)R
one asperity
cavity
0.50
0.40
0.30
0.20
0.10
0.00
0.00
0.10
0.20
0.30
0.40
Time

(b)

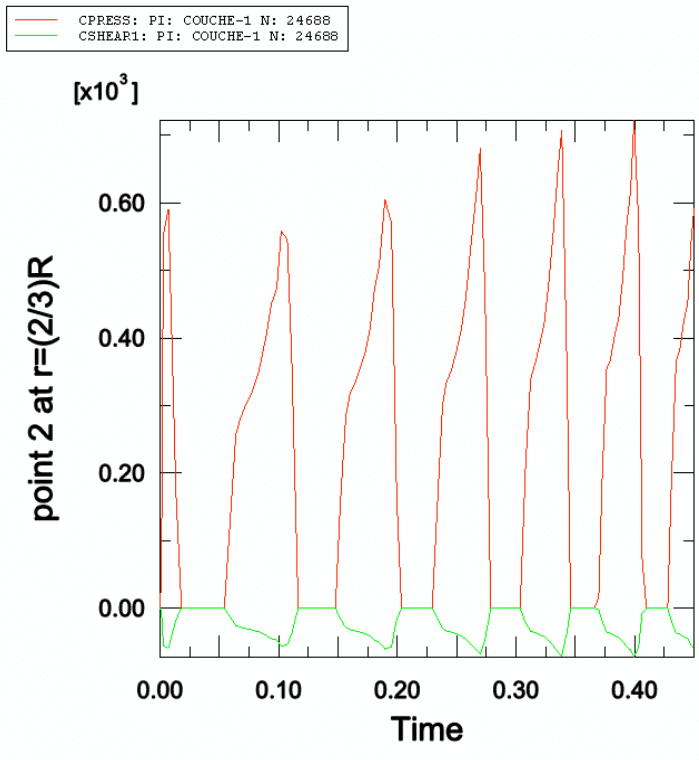


(c)

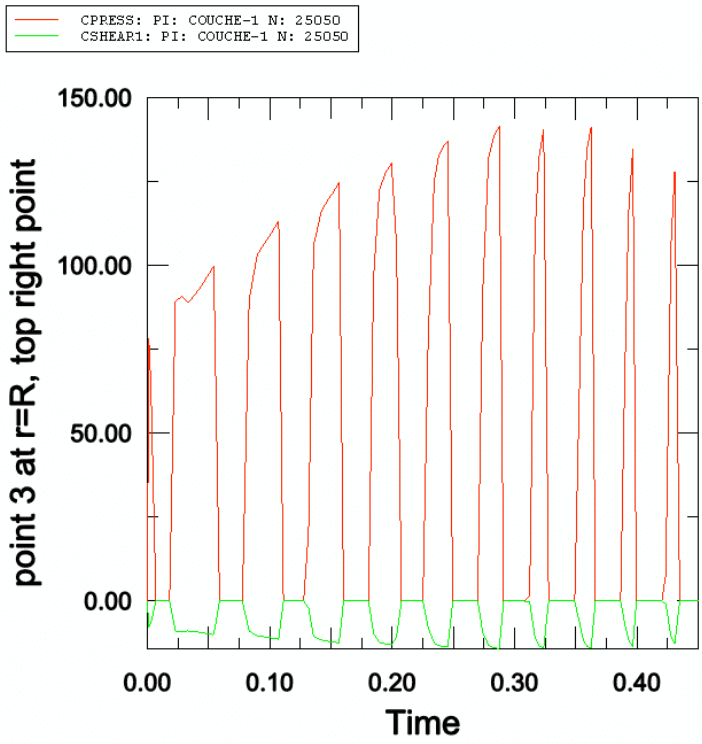


(d)

Fig. 2.18 the evolution of contact pressure and tangential shear stress of three particular point (a) the location of the 3 points (b) point 1 (c) point 2 (d) point 3

# CHAPTER 3 Equivalent Roughness

## 3.1 the necessity of Equivalent Roughness

In the previous chapter the local material outflow due to the indentation of the tool asperity is discussed. In order to improve the conventional Coulomb friction law so that the local material outflow could be taken into account, it is necessary to model the tool asperities microscopically. The tools are machined with a turning insert so real asperity cavity takes the form of an arch. See Fig. 3.1.

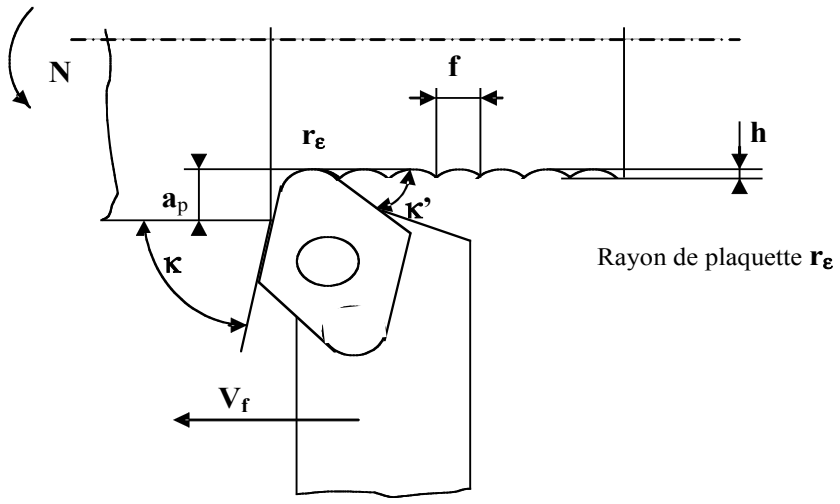


Fig.3.1 Machining of the tool asperity

However, the theory of plastic wave, which sums up the wave shape formation of the workpiece material under the tool asperity in three steps, is based on the assumption of triangular tool asperity. Taking into consideration of the local material outflow, this theory makes possible to correlate the normal force and the friction force at the upsetting interface in a more reasonable way. To compare the pros and cons of this theory with Coulomb friction law, numerical models should be set up with triangular asperity to comply with the plastic wave theory.

Considering both sides of the problem: arch asperity in reality but triangular asperity in the theory, it is necessary to find out the equivalent triangular asperity to the arch asperity, so that the plastic wave theory could be employed as a friction law.

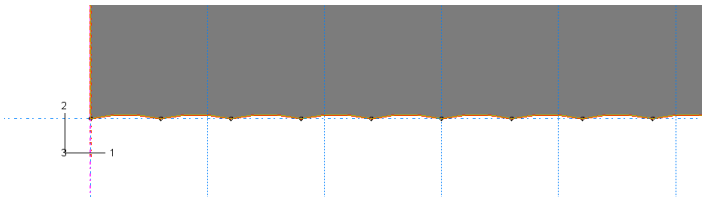

(a)

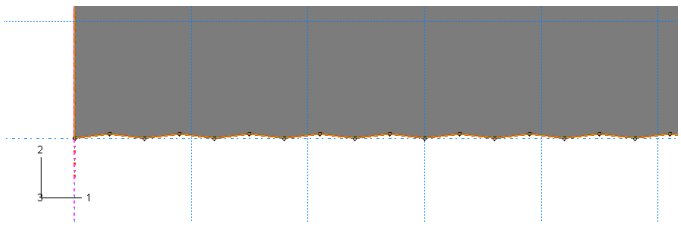

(b)

Fig.3.2 (a) real asperity (b) triangular asperity

Two different triangular geometries were proposed attempting to approach as close as possible the real arch asperity. In Fig.3.3 (a), the triangles remain the same width and height with the arch asperity, so we name it same height model, and in Fig.3.3 (b) the triangles have the same width and surface area with the arch asperity so we name it same area model.

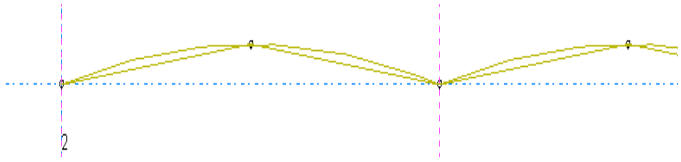

(a)Same height model

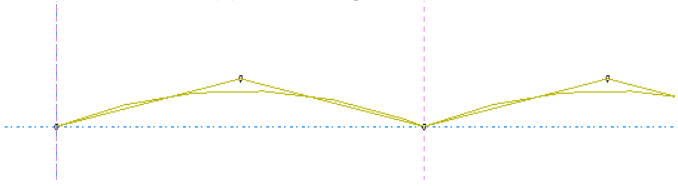

(b)Same area model

Fig.3.3 (a) Same height model (b) Same area model

### 3.2 numerical results and discussion

A number of simulations varying in roughness parameters and cone angles were executed, with the arch asperity as reference, the two triangular candidates being examined against the displacement and plastic strain criteria.

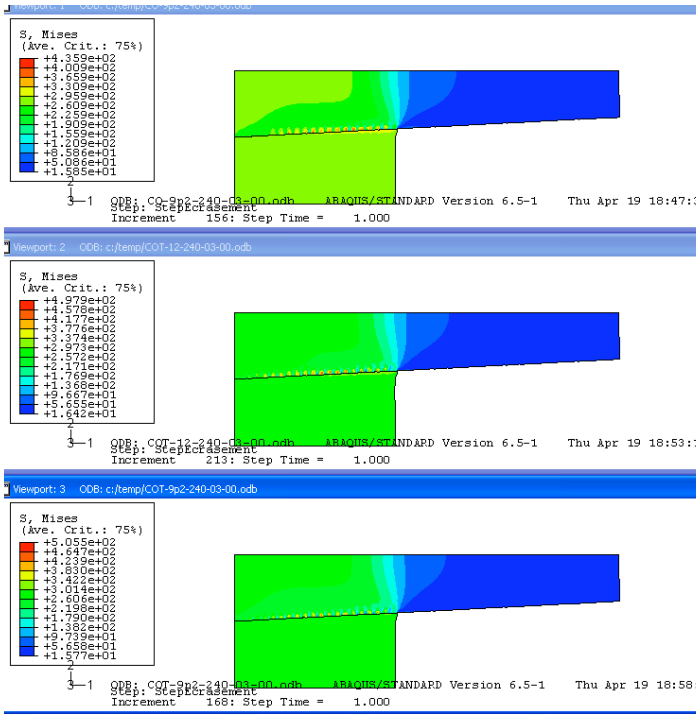


Fig 3.4 Arch asperity and two triangular models

Below are five groups of results of the numerical experiment. The title of each group follows a pattern to indicate the asperity parameters and cone angle: 'R'-'AR'-'Cone Angle'. For example, 21-360-07 means the average asperity height, width and the cone angle are 21μm, 360μm and 7 degree respectively. CO means arch asperity (reference), COT means triangle asperity, and COT-21-360-07 is the same height model of CO-21-360-07, while COT-28-360-07 is the same area model.

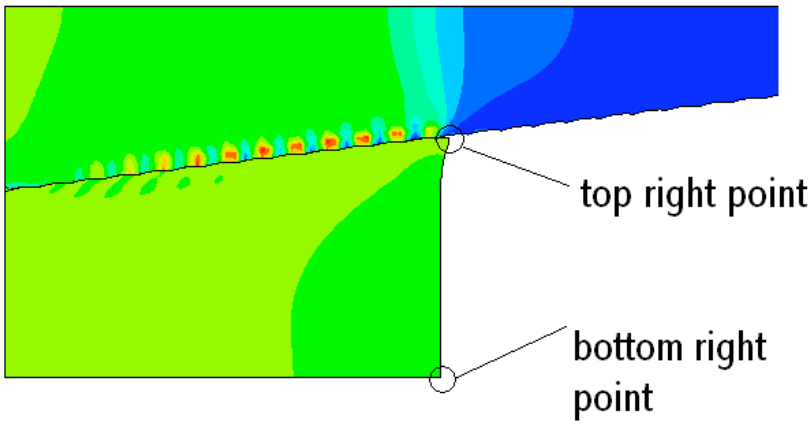


Fig.3.5 The location of the points in focus

21-360-00

| Point displacement | CO-21-360-00 | COT-21-360-00 | COT-28-360-00 |
|---|---|---|---|
| Top right U | 1.32471 | 1.33579 | 1.30251 |
| Top right U1 | 0.896305 | 0.904569 | 0.880135 |
| Bottom right | 0.895346 | 0.898229 | 0.906096 |

21-360-07

| Point displacement | CO-21-360-07 | COT-21-360-07 | COT-28-360-07 |
|---|---|---|---|
| Top right U | 1.20736 | 1.20375 | 1.19688 |
| Top right U1 | 0.79530 | 0.79234 | 0.779510 |
| Bottom right | 0.701723 | 0.699483 | 0.71079 |

9.2-240-00

| Point displacement | CO-9.2-240-00 | COT-12-240-00 | COT-9.2-240-00 |
|---|---|---|---|
| Top right U1 | 0.939441 | 0.929095 | 0.927767 |
| Top right U | 1.37059 | 1.36378 | 1.36144 |
| Bottom right | 0.897231 | 0.904222 | 0.8983 |

9.2-240-03

| Point displacement | CO-9.2-240-03 | COT-12-240-03 | COT-9.2-240-03 |
|---|---|---|---|
| Top right U1 | 0.873853 | 0.868015 | 0.868915 |
| Top right U | 1.29462 | 1.29137 | 1.29106 |
| Bottom right | 0.800531 | 0.807651 | 0.801406 |

38-474-09

| Point displacement | CO-38-474-09 | COT-51-474-09-00 | COT-38-474-09-00 |
|---|---|---|---|
| Top right U1 | 0,745955 | 0.715432 | 0,746882 |
| Top right U | 1,16032 | 1.14049 | 1,16018 |
| Bottom right | 0,665454 | 0.67710 | 0,661008 |

In terms of the Finite Element Analysis, the displacements of both models are satisfactory as the errors are within 5%. The better one, according to all the results, is the same height model. This coincides with the theory that the friction is dependent on the average asperity angle. In the 'same height' model, the angle is closer to the average asperity angle of the arch, while in the 'same area' model, the angle is equal to the maximum asperity angle of the arch. So the 'same area' model tends to over-predict the friction at the interface. This results in a slight underestimate of the displacement at the end of the interface – the top right point (edge point).

In terms of plastic strain and Mises stress, the same height model also gives out a closer value to the reference one. The 'same area' model, over-predicts the level of Mises stress because of its unrealistic sharp asperity angle.

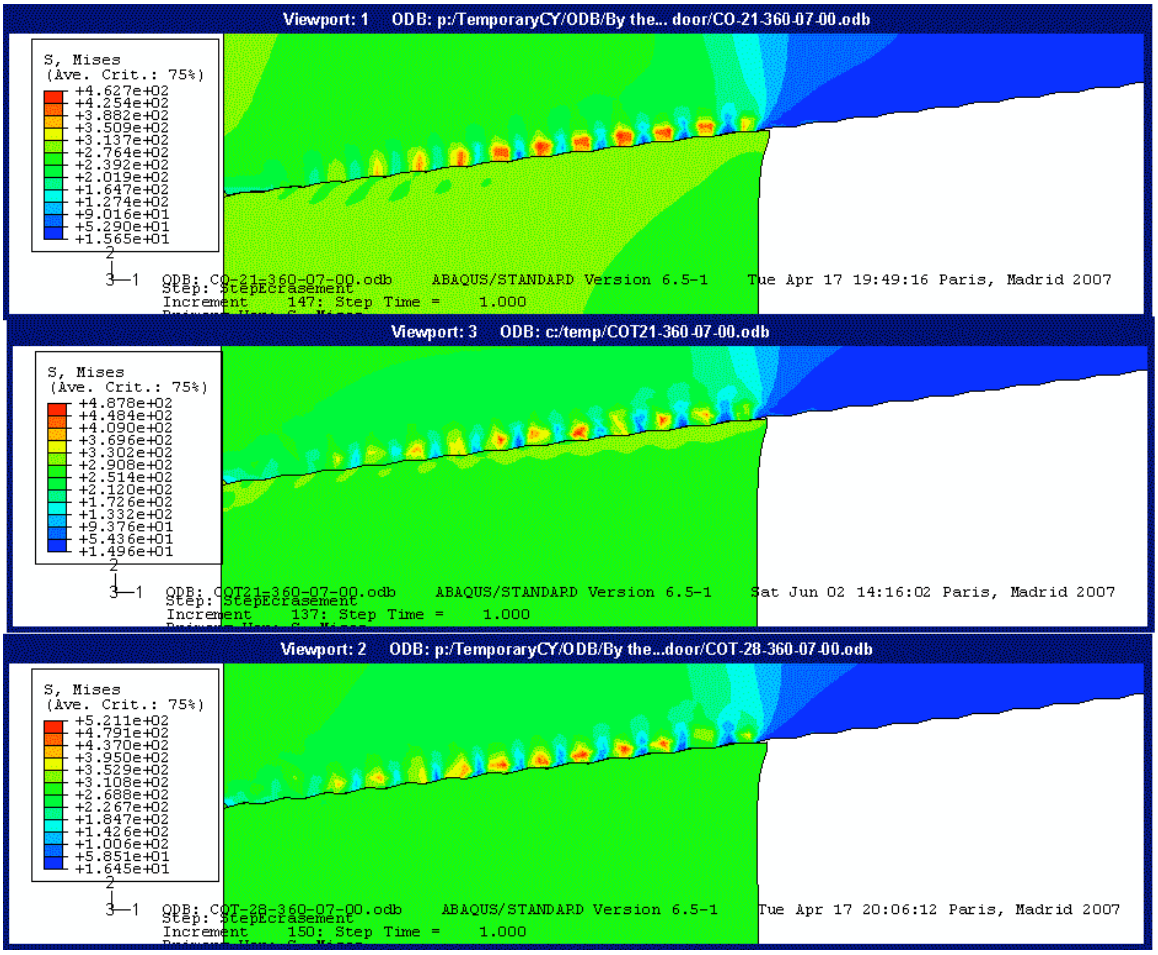


Fig. 3.6 The Mises stress – top: arch asperity (reference); middle: same height; bottom: same area

All the numerical trials prove that the ‘same height’ model is a good replacement for the real arch asperity, and with the ‘same height’ model, it is possible to implement further numerical simulations to validate the plastic wave theory.

# CHAPTER 4 Comparison of Coulomb friction law and plastic wave theory in simulation

## 4.1 The two theories

### 4.1.1 Coulomb model

*Coulomb friction* is a common friction model used to describe the interaction of contacting surfaces. The model characterizes the frictional behaviour between the surfaces using a coefficient of friction, $\mu$.

The tangential motion is zero until the surface traction reaches a critical shear stress value, which depends on the normal contact pressure, according to the following equation:

$$\tau_{crit} = \mu p$$

where $\mu$ is the coefficient of friction and $p$ is the contact pressure between the two surfaces. This equation gives the limiting frictional shear stress for the contacting surfaces. The contacting surfaces will not slip until the shear stress across their interface equals the limiting frictional shear stress, $\mu p$. In ABAQUS Coulomb friction can be defined with $\mu$. There is zero relative motion/slip of the surfaces when they are sticking.

#### 4.1.2.1 Plastic wave model

In 2.3.3 the evolution of outflow and contact behaviour, the forming of the plastic wave is discussed microscopically from the results of simulation. In this section the whole evolution is more carefully examined and classified into three stages, based on the plastic wave theory. Each stage is characterised by the distinct mechanical significance in terms of strain-stress correlation.

The plastic wave model was proposed by J.M.CHALLEN, J.M.LEAN and P.L.B.OXLEY. In the model the tool is assumed to be perfectly rigid and the analytical correlation between normal stress and frictional stress in the asperity cave is derived from 'slip line field' theory. The object of the microscopic study of the plastic wave development under tool asperity, was to obtain a macroscopic friction law that determines the shear stress at each point of the interface according to the contact normal stress, the shear yield strength of the workpiece, the angle of asperity and the local friction coefficient of Tresca.

Plastic wave model assumes triangular asperity. From the simplified geometry of roughness profile, the contact on a microscopic scale can be broken down to the three following stages:

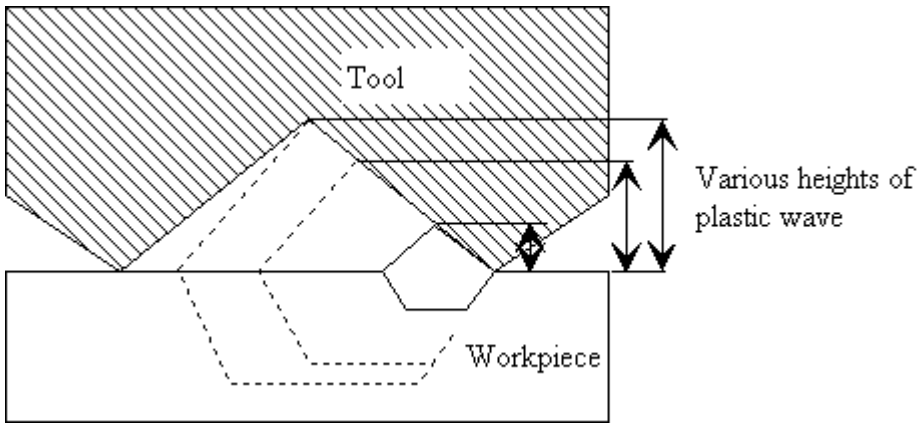


Fig.4.1 First stage

The normal load on the interface makes 'prints' on the workpiece, which means that it gives rise to a local thin layer of plastic waves under the tool asperity by relative movement (see Fig.4.1). The height of the plastic waves can be calculated from the 'slip line' theory by supposing a TRESCA friction as tangential behaviour. This assumption is coherent with the formation of the plastic wave model, which requires the local normal stress higher than the yield strength of the workpiece material, and $m_o$ is the local Tresca friction coefficient.

This step leads to a correlation of tangential stress $\tau$ varying linearly with the normal stress $\sigma_n$, and the corresponding slope depends primarily on the angle of asperity $\alpha$. It also depends on the Tresca local friction coefficient $m_o$, but in a less significant way.

The end of this stage is when the height of wave equals to the height of asperity, and the normal stress reaches a value ranging between 0.8 and 1.2 times of the workpiece material yield strength.

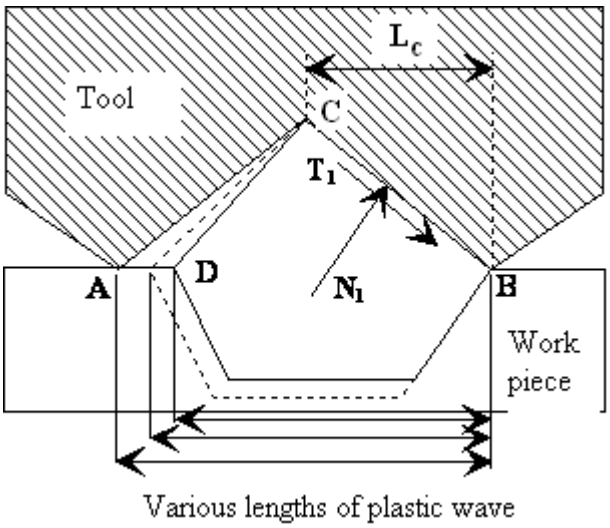


Fig.4.2 Second stage

When the top of the plastic wave reaches the height of the tool asperity and cannot increase its height any more, it begins to expand its width until it fully fills the asperity cavity. In this process some part of the workpiece material gets in contact with the left side of the tool asperity. See Fig.4.2.

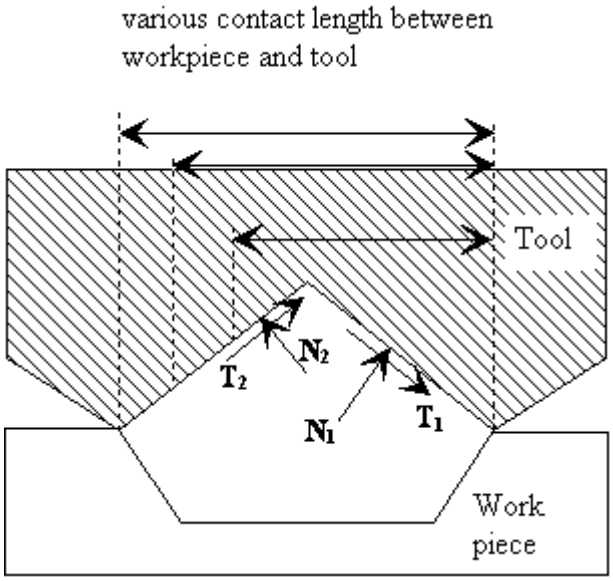


Fig.4.3. The third stage

When the wave fills up the tool asperity, the total tangential stress begins to increase because the local friction acts on an increasingly larger surface, see Fig.4.3.

The local plastic flow during this stage and the previous one can be analyzed by upper bound method that provides the evolution of the friction force at strong contact pressure. The results show an asymptotic behaviour for a contact normal force 5 to 6 times higher than the yield strength.

To sum up the normal-tangential stress correlation, the plastic wave model has seen a preliminary linear curve and then an asymptotic curve between normal stress and tangential stress. The two curves are connected at a transitional point. See Fig.4.4 in the next section.

### 4.1.3 The implantation of the plastic wave theory in FEA model

For the finite element simulation, the normal-tangential stress curve obtained from plastic wave model is approached by a linear function for the first stage and an arctangent function

for the second and third stage. From the equations of 'slip line field' theory, the frictional stress of the three stages can be acquired in function of shear yield strength, asperity angle $\alpha$ and local Tresca friction coefficient $m_0$.

The transition point between the linear law and the asymptotic law corresponding to normal stress and tangential stress is defined as:

$$\sigma_{nt} = \frac{\sigma_0}{2\sqrt{3}\cos\alpha}\left[\left\{1+2(\frac{\pi}{4}+\Phi-\eta)\right\}\cos\alpha+\sin(\alpha+2\Phi)\right]$$
$$\tau_t = \frac{\sigma_0}{2\sqrt{3}\cos\alpha}\left[\left\{1+2(\frac{\pi}{4}+\Phi-\eta)\right\}\sin\alpha+\cos(\alpha+2\Phi)\right]$$

where

$$\begin{cases}\Phi = 0.5 arc\cos(m_0)-\alpha \\ \eta = arrc\sin\left\{(1-m_0)^{-0.5}\sin\alpha\right\}\end{cases}$$

The linear correlation below the transitional point is defined by:

$$\tau = \frac{\tau_t}{\sigma_{nt}}\cdot\sigma_n$$

In the regime of high contact pressure, the arctangent function is determined by the shear yield strength $\tau_{\lim}$, which is obtained with the slip line theory and the upper bound method applied to the plastic flow of the workpiece surface under the tool asperities.

For every couple of $(\alpha, m_0)$, the value of $\tau_{\lim}$ is interpolated as:

$$\begin{aligned}\tau_{\lim} = {} & (3.32\times10^{-4}\alpha^2 - 1.88\times10^{-2} + 5.54\times10^{-2})m_0^2 \\ & + (-2.54\times10^{-4}\alpha^2 - 1.85\times10^{-3}\alpha + 0.53)m_0 \\ & + (-2.78\times10^{-4}\alpha^2 - 2.51\times10^{-2}\alpha + 4.08\times10^{-3})\end{aligned}$$

So the friction stress in function of normal stress is put into simulation in the following form:

$$\tau = \frac{\tau_t}{\sigma_{nt}}\cdot\sigma_n \quad \text{for } \sigma_n < \sigma_{nt}$$

$$\tau = \frac{2 \cdot \tau_{\lim}}{\pi} \arctan\left( \frac{\sigma_n \tan\left( \frac{\pi \tau_t}{2\tau_{\lim}} \right)}{\sigma_{nt}} \right) \quad \text{for} \quad \sigma_n > \sigma_{nt}$$

The above formula is illustrated by the curve in Fig.4.4.

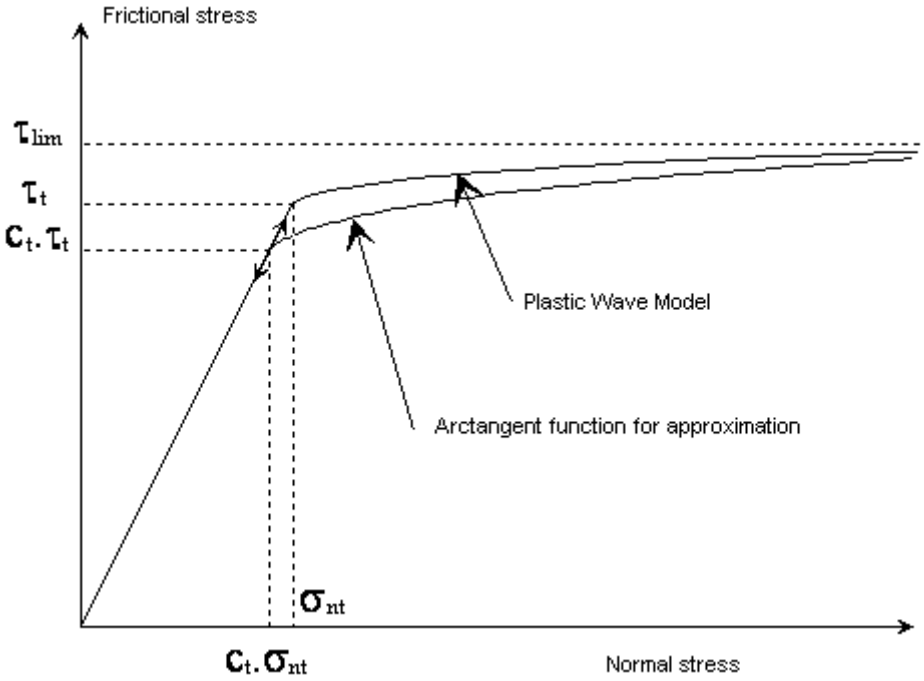


Fig.4.4. Plastic wave model and its approximation

## 4.2 Simulation with the two theories

### 4.2.1 Simulation models

The physical models are the same – only the governing friction law differs in order to highlight the difference of the two theories. The next step is to integrate the two theories as contact frictional behavior in the simulation. Coulomb friction law is the default friction law in ABAQUS, and using it is no more than a few clicks away. However, when the Coulomb model and its extended versions provided in ABAQUS are too restrictive, and a more complex definition for frictional behavior between two surfaces, such as plastic wave theory, is needed, the user subroutine FRIC has to be called. This is done by linking a user subroutine

file, which contains the normal-tangential stress relationship according to the plastic wave theory, with the contact tangential behavior in ABAQUS.

In the item 'Interaction Properties' of ABAQUS, the User-defined contact formulation should be chosen as tangential contact behavior. Three parameters, designating the asperity angle, local Tresca friction coefficient and shear yield strength are supposed to be passed in as 'Friction Properties' to the User subroutine file during the simulation.

Three numerical models were exercised in order to compare the plastic wave model and Coulomb friction model (refer to Fig.4.6). Notice that the Reference model and the Coulomb model both follow Coulomb friction law, the only difference is that the reference model has physical asperity at the interface aiming to simulate the real condition of the contact surfaces, while the Coulomb model's interface is flat, so is the Plastic Wave model. *The point is to compare how the Coulomb's law and plastic wave theory manage to integrate the factor of surface roughness on a macroscopic scale.* The related information of each model is listed in Table 4.1.

Common values:

**2-D Dimension Height×Width:** 3×4mm

**Stroke course along height:** 1mm

| **Model Name** | **Interface physical properties** | **Roughness Characteristics** | **Frictional law** |
|---|---|---|---|
| Reference | Roughness: Triangle asperity | R=21, AR=360 μm<br>Asperity angle=7<br>And Coulomb's friction | Coulomb |

| | | | |
|---|---|---|---|
| | | coefficient | |
| Coulomb | No physical roughness | Coulomb's friction coefficient | Coulomb |
| Plastic wave | No physical roughness | Asperity angle = $7^0$<br>Local Tresca friction coefficient | Plastic wave |

Table 4.1 The reference, Coulomb model and plastic wave model

Notice that Coulomb's law reflects all the possible surface roughness into one parameter: Coulomb's friction coefficient. The plastic wave theory relies on two roughness parameters: the asperity angle and the local Tresca friction coefficient.

### 4.2.2 Results of the frictionless simulation

The frictionless simulation is a special case for all the three models. To simulate the frictionless condition, the Coulomb friction coefficient is set to be zero for the Reference model and the Coulomb model. For the plastic wave model, the local Tresca friction coefficient also has to be zero – but it has another non-zero variable to reflect the characteristic of surface roughness: the asperity angle, which is $7^0$ in this case.

#### 4.2.2.1 Displacement

| Frictionless Model | Nodes | Undeformed(x,y) | Deformed(x,y) | Error(%) |
|---|---|---|---|---|
| Reference (Triangle asperity) | TR | 4, 3 | 4.978, 2.000 | N/A |
| | BR | 4, 0 | 4.890, 0.000 | N/A |
| Coulomb | TR | 4, 3 | 4.896, 2.001 | 1.651 |
| | BR | 4, 0 | 4.896, 0.000 | 0.123 |
| Plastic wave | TR | 4, 3 | 4.727, 2.000 | 5.042 |
| | BR | 4, 0 | 4.979, 0.000 | 1.820 |

Table 4.2 the deformed and undeformed coordinates of two points in frictionless model

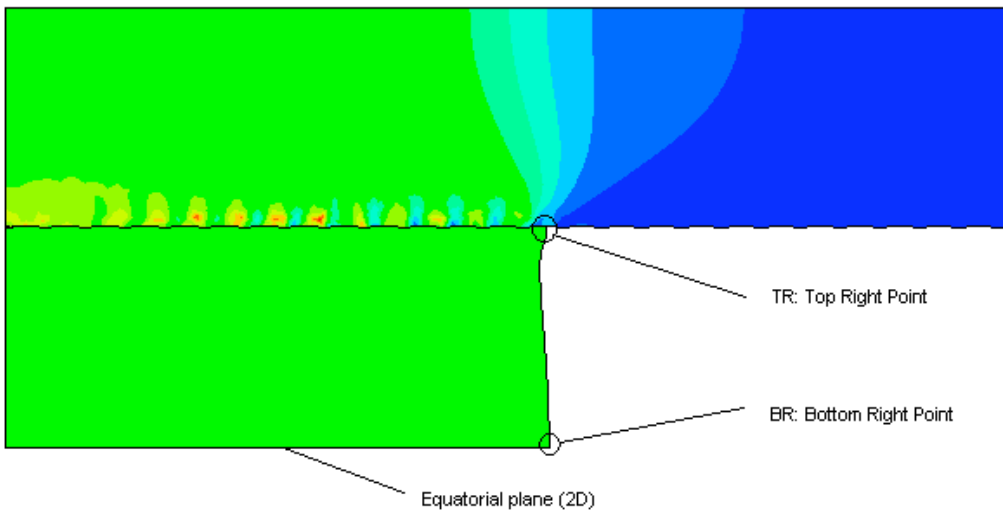


Fig.4.5. The location of TR and BR in the model

The numbers in Table 4.2 indicate that Coulomb's model excels in predicting the displacement at two characteristic points. However, the displacement U1 contour (Fig4.6 (b)) is obviously wrong. Notice that in the frictionless model there is actually no governing friction law at the interface for the reference model and the Coulomb model (refer to Fig 4.6(a) and Fig 4.6 (b)), because the Coulomb friction coefficient equals to zero. It is the physical properties of the interface that is counted for the different deformations. If there were no asperities in the reference model, the U1 distribution of the reference model (Fig 4.6(a))

would be exactly the same as in Fig.4.6 (b) - a homogenous expansion. The existence of asperities affects the displacement at the interface as well as the region far from it. Only the region near the equatorial plane is not disturbed by the asperity, because the equatorial plane locates furthest from the asperities at the interface. As seen in Fig 4.6(a), the tangential vector of the U1 gradient remains vertical near the equatorial plane. However, if the height of the workpiece is relatively small or the stroke course is deep enough, the influence of the asperity would be able to reach the equatorial plane.

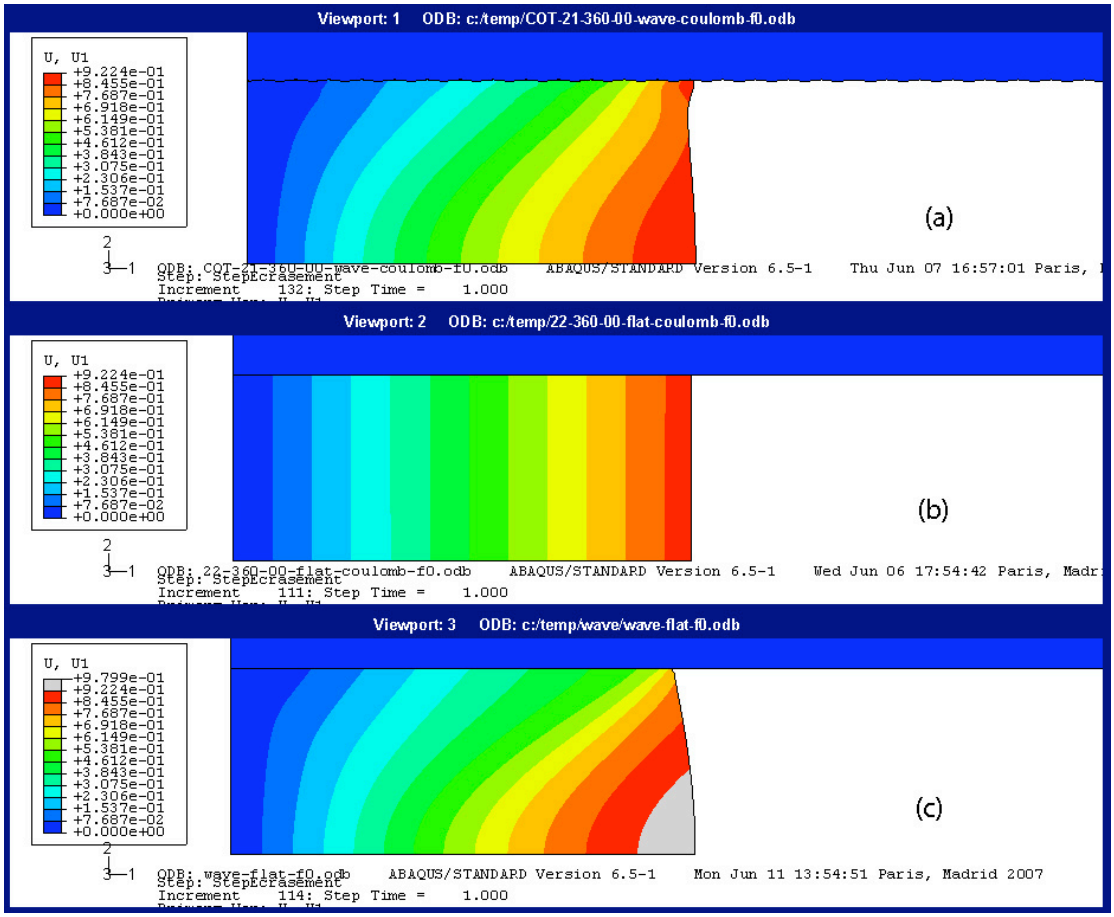


Fig.4.6 U1 contour plot of frictionless model: (a) Reference model. (b) Coulomb model. (c) Plastic Wave model

At the interface of the Reference model illustrated in Fig 4.7, the asperity geometry actually hinders the material flow near the interface even when the contact is frictionless. This could be seen both from the U1 contour and the distortion trending of the mesh. It is only at the

edge bit the workpiece catches up the expanding movement with rest of the body and exceeds its vertical vicinity.

Now disregard the edge bit and see the major part of the model: it is as if there were friction acting on the interface even though no actual friction exists at each microscopic point. This 'virtual' friction comes purely from the microscopic geometry of the asperity and has a noticeable influence on the macroscopic scale. Specifically, the 'virtual' friction is the summation of the contact pressure force imbalance at both sides of one single asperity (refer to chapter 2.3.3 and 2.3.4). Now look back at our Coulomb's model and Plastic wave model. The frictionless case is the 'worst scenario' for Coulomb's model because the only available surface roughness parameter: the Coulomb friction coefficient has to be zero. It is incapable of capturing the surface roughness details, so to speak. While in plastic wave model, although the Tresca local friction coefficient is zero as well, the other parameter – the asperity angle, reflects what kind of surface the law is acting on. So in Fig. 4.6 (c) the U1 contour is closer to the reference.

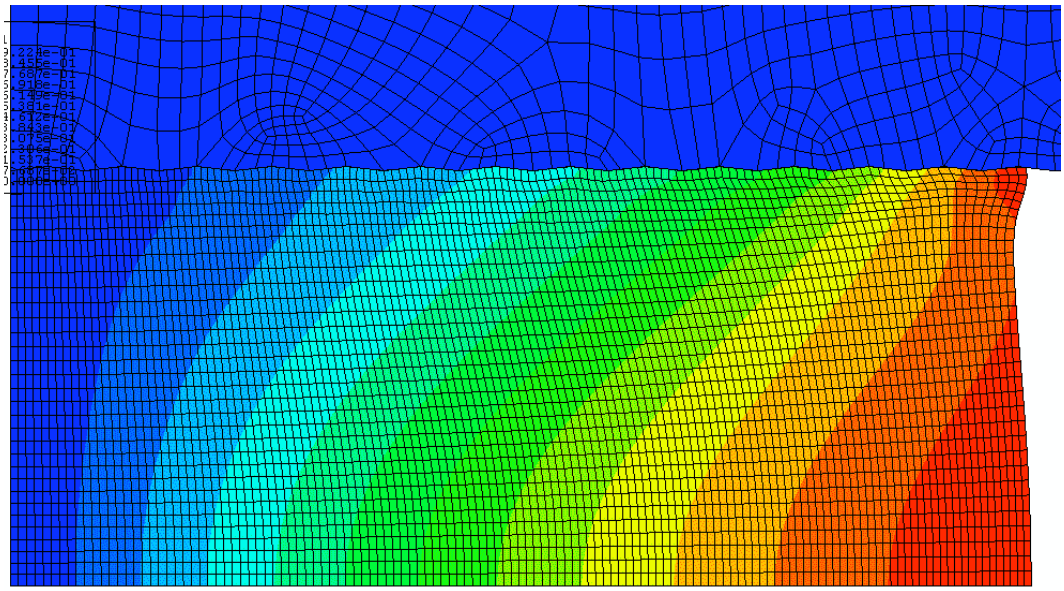

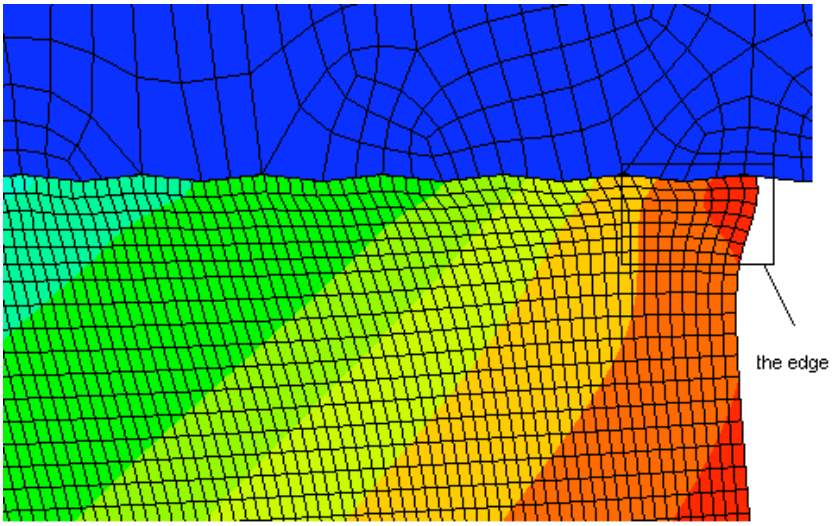


Fig.4.7 the U1 contour plot of Reference model (with mesh)

### 4.2.2.2 Stress and strain

In terms of stress and strain, the plastic wave model matches the Reference model better than Coulomb's model in the frictionless case. See Fig 4.8

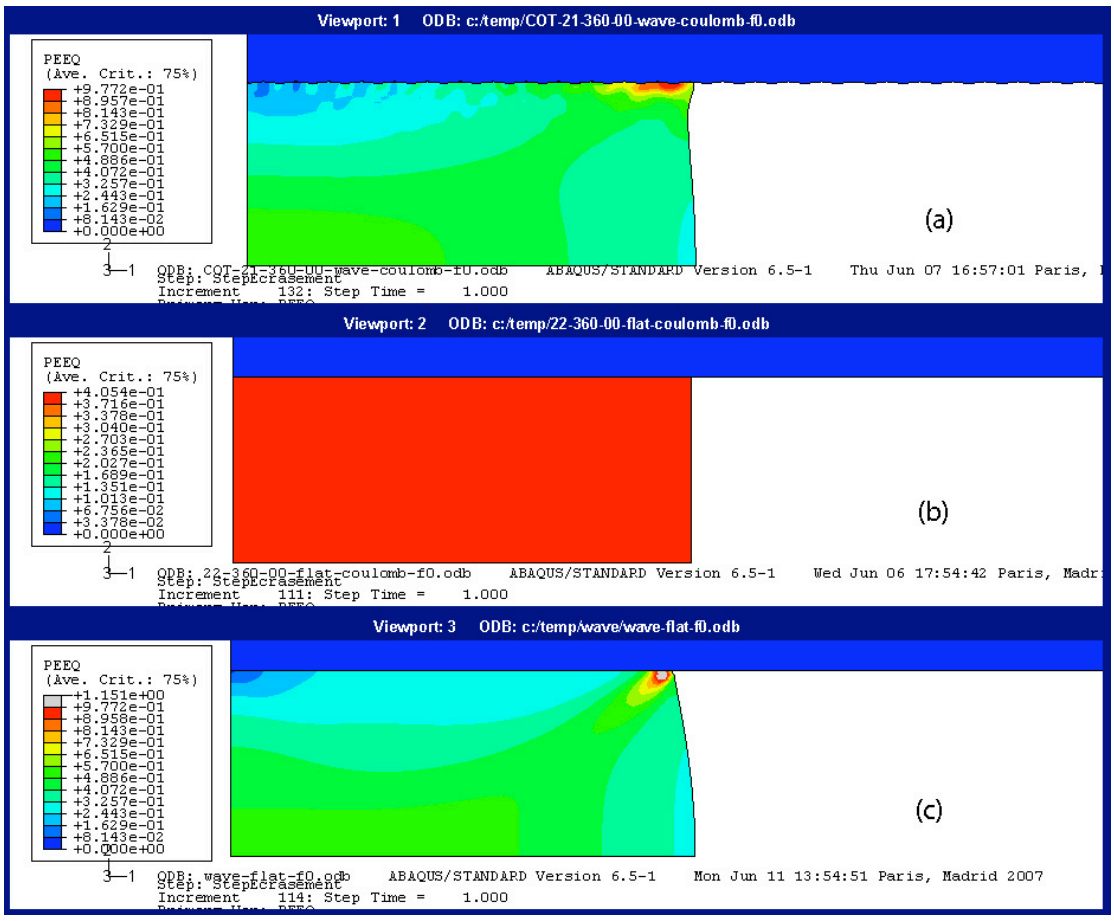

Fig.4.8 PEEQ (Equivalent plastic strain at integration points) contour plot of frictionless model: (a) Reference model. (b) Coulomb model. (c) Plastic Wave model

### 4.2.3 Frictional model

| Frictional Model<br>f=0.05 | Nodes | Undeformed(x ,y) | Deformed(x,y) | Error(%) |
|---|---|---|---|---|
| Reference<br>(triangle asperity) | TR | 4, 3 | 4.895, 2.018 | N/A |
| | BR | 4, 0 | 4.922, 0.000 | N/A |
| Coulomb | TR | 4, 3 | 4.816, 2.001 | 1.614 |
| | BR | 4, 0 | 4.935, 0.000 | 0.264 |
| Plastic wave | TR | 4, 3 | 4.701, 2.001 | 3.963 |
| | BR | 4, 0 | 4.985, 0.000 | 1.280 |

Table 4.3 the deformed and undeformed coordinates of two points in frictional model :friction coefficient f=0.05

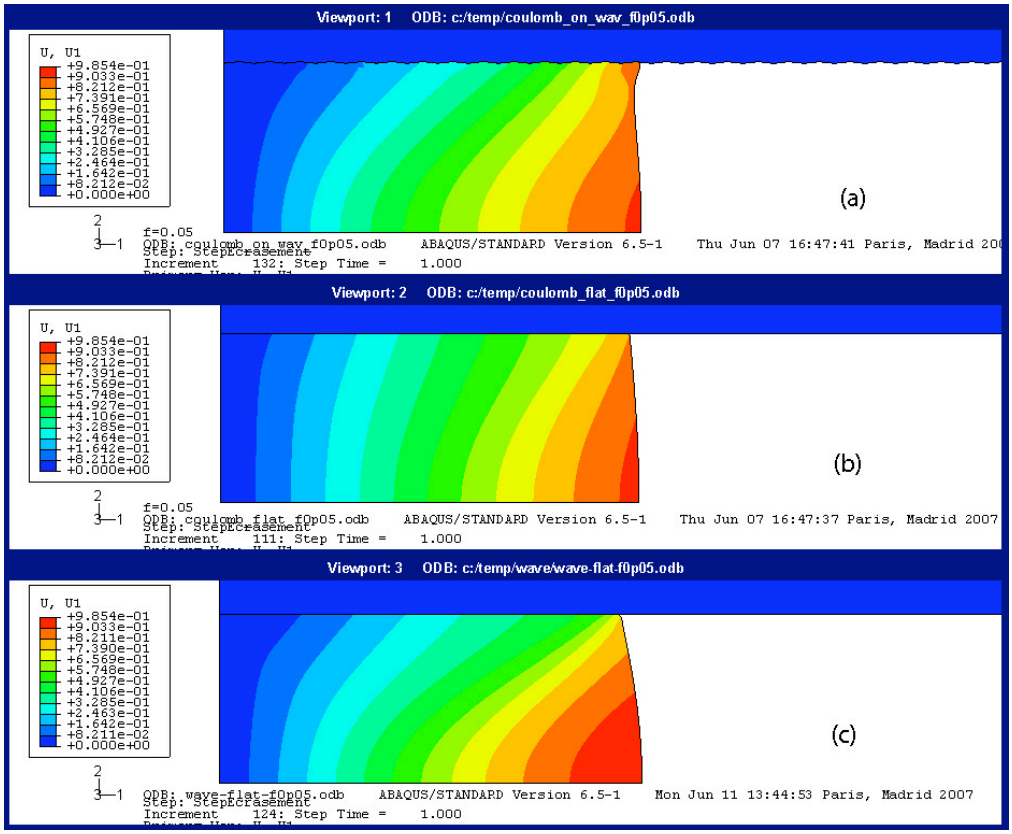

Fig.4.9 U1 contour plot of frictional model: (a) Reference model. (b)Coulomb model. (c) Plastic Wave model

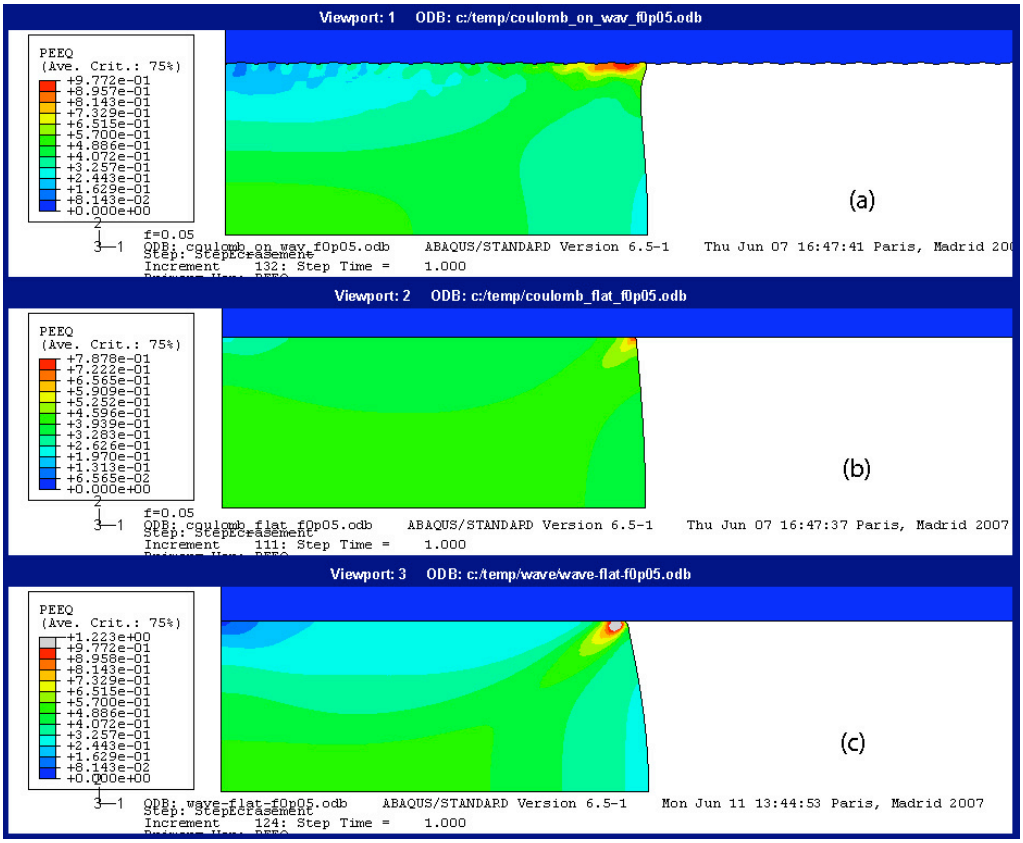


Fig.4.10 PEEQ(Equivalent plastic strain at integration points) contour plot of frictional model: (a) Reference model. (b)Coulomb model. (c) Plastic Wave model

The Coulomb model has seen a good performance against all the displacement criteria. It is concise and practical – it sums up all the roughness information in a single parameter – the Coulomb's frictional coefficient, thus it is very easy to use.

However, when it comes to stress and strain prediction, the Coulomb's model tends to underestimate those values, as shown in Fig.4.10 (b). On the other hand, the plastic wave model (Fig.4.10(c)) overestimates the stress and strain by 20%, but the stress/strain distribution is closer to the Reference. In the metal forming process such as upsetting, the

stress prediction is a very important task in order that no material failure takes place in the process. In material science, a conservative law is always preferential. The plastic wave model has seen its strength over Coulomb's model in stress/strain prediction.

### 4.3 The plastic wave model with improved boundary condition

POLLUX is a special-purpose axisymmetric program for the numerical simulation of thermo-mechanical forming processes. It was developed by INSA-Lyon in 1980s. In order to improve the displacement performance of the plastic wave model, the virtual boundary condition at the interface of the tool and workpiece should be introduced. The accessibility of POLLUX's code makes this possible.

The improved plastic wave model in Fig 4.13 shows some improvement in terms of displacement over the standard plastic wave model in Fig 4.12. This improvement is due to the artificial introduction of physical boundary condition, which forces the points in contact to follow the

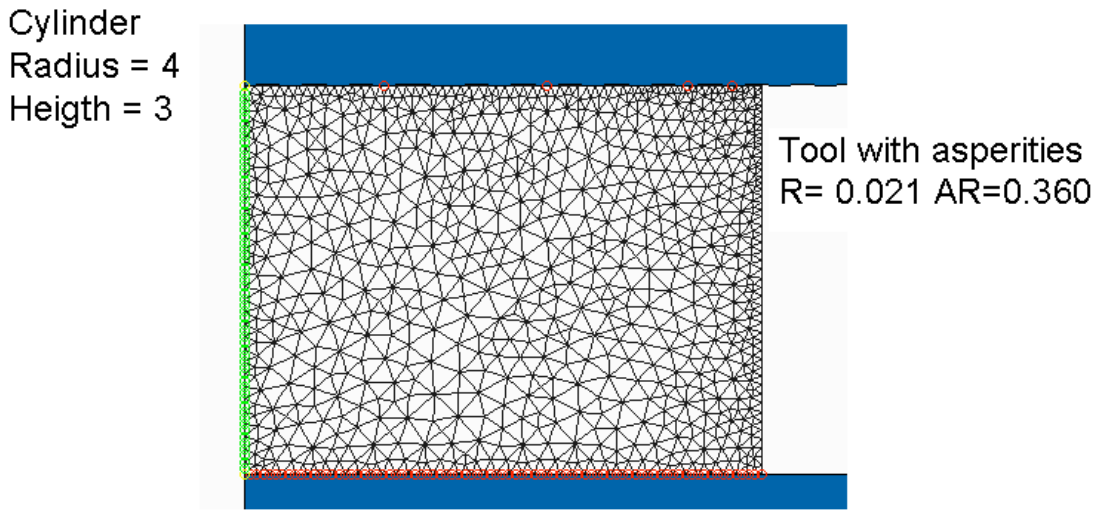


Fig 4.11 the numerical model in POLLUX

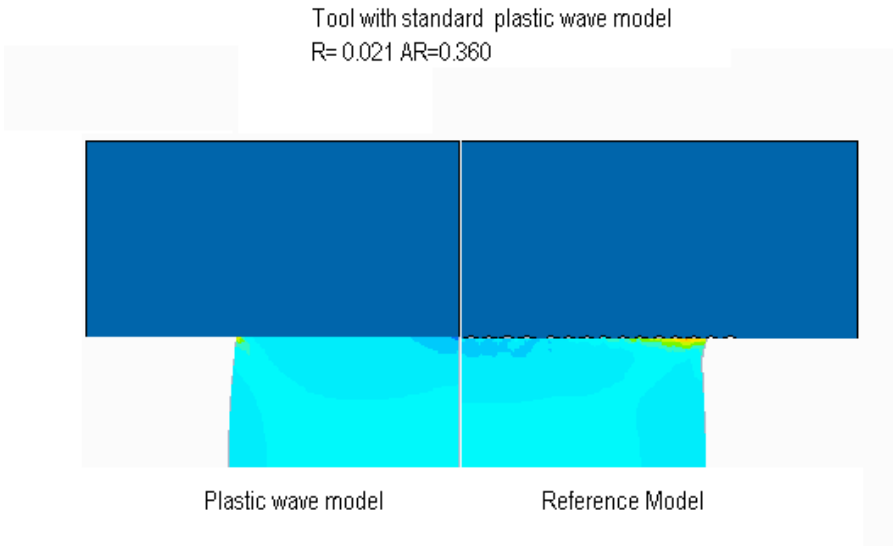


Fig.4.12 The PEEQ with POLLUX (left half: plastic wave model; right half: reference model)

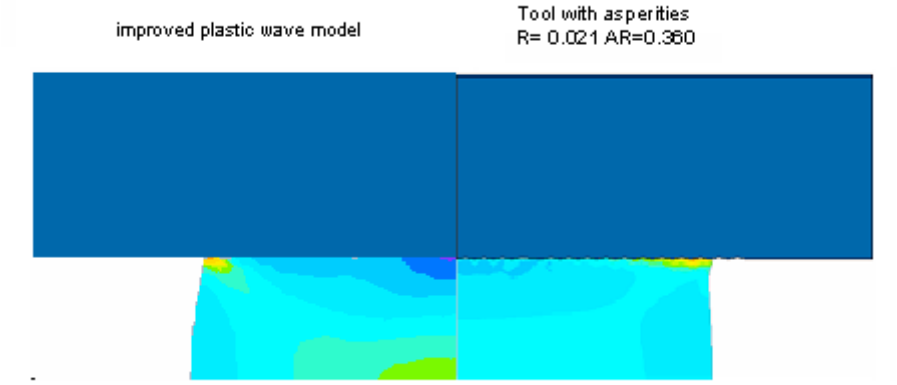


Fig.4.13 The PEEQ with POLLUX (left half: improved plastic wave model; right half: reference model)

# CHAPTER 5 Comparison of experiments and FEA model

## 5.1 Experiment

### 5.1.1 stress-strain correlation

The preliminary step is to determine the stress-strain correlation so that the data can be put into the material property of the simulation. At the same time, it gives a general idea of how far the tool can descend under certain load in the upsetting.

The material of the workpiece is suggested to be a non-hardening material as pure aluminium, in order to comply with the plastic wave theory. Specimens of the workpiece material were made and tensile tests were carried out to determine the material property.

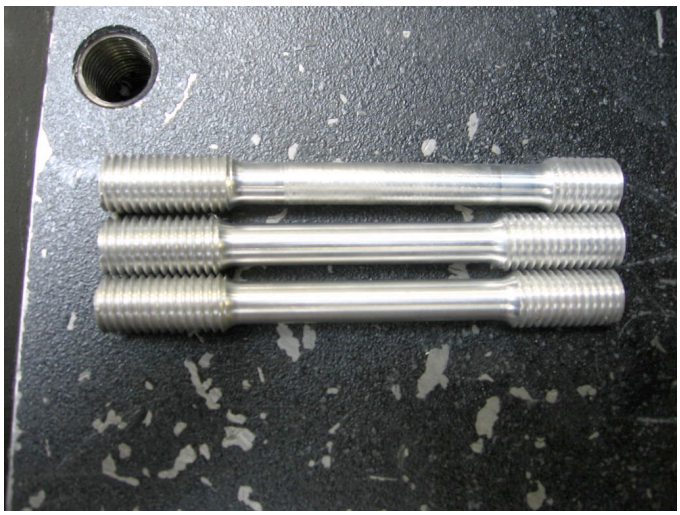

Fig.5.1 tensile test specimen

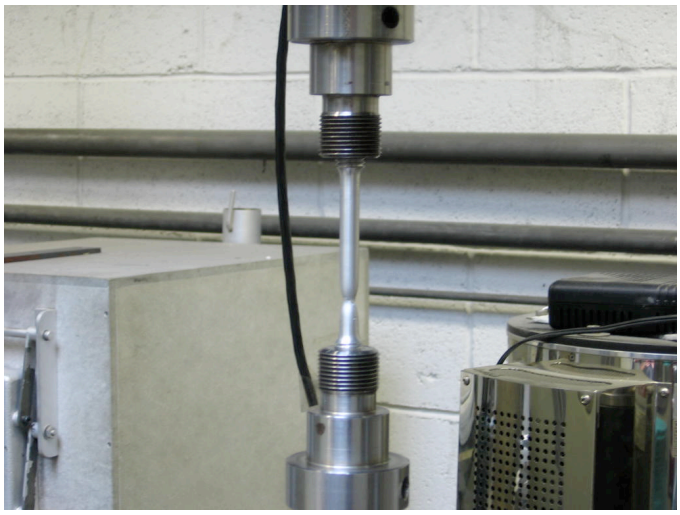

Fig.5.2 tensile test

A curve of nominal stress versus nominal strain is shown in Fig.5.3. They are converted to real stress and real strain by the following formula, and the new curve is overlay plot in the same figure.

$$\sigma = \sigma_n(1+\varepsilon_n)$$
$$\varepsilon = \ln(1+\varepsilon_n)$$

Where $\varepsilon_n$ and $\sigma_n$ are the nominal value of strain and stress, and $\varepsilon$ , $\sigma$ the real value.

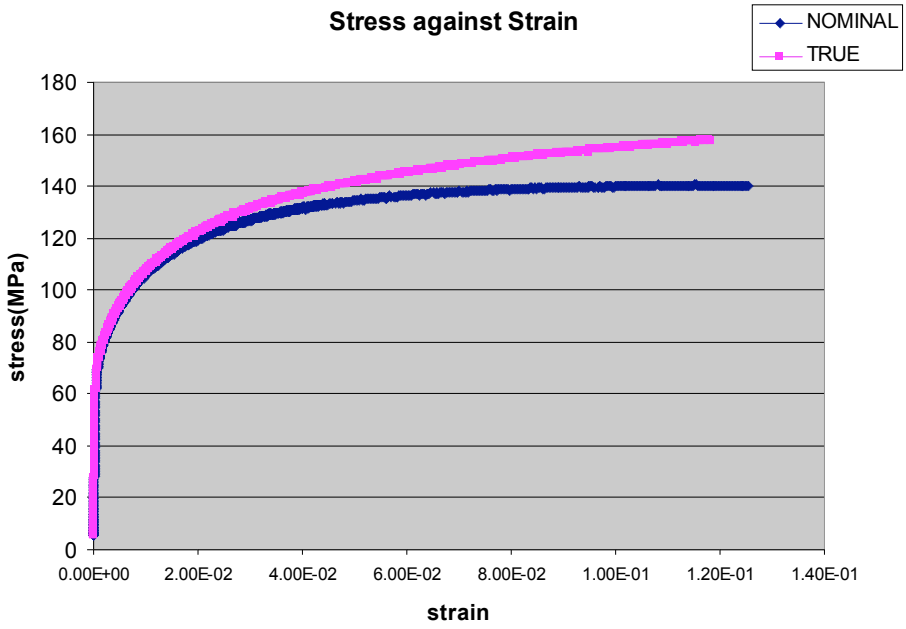


Fig.5.3 stress against strain

The analysis of the rough model suggests a maximum strain up to 0.40. It is necessary to do a curve fit in order to extend the range of the strain. A logarithmic trend line was seen as the best fit other than a power fit or polynomial fit. The data of stress versus strain is finally put into the plastic property of material in the simulation.

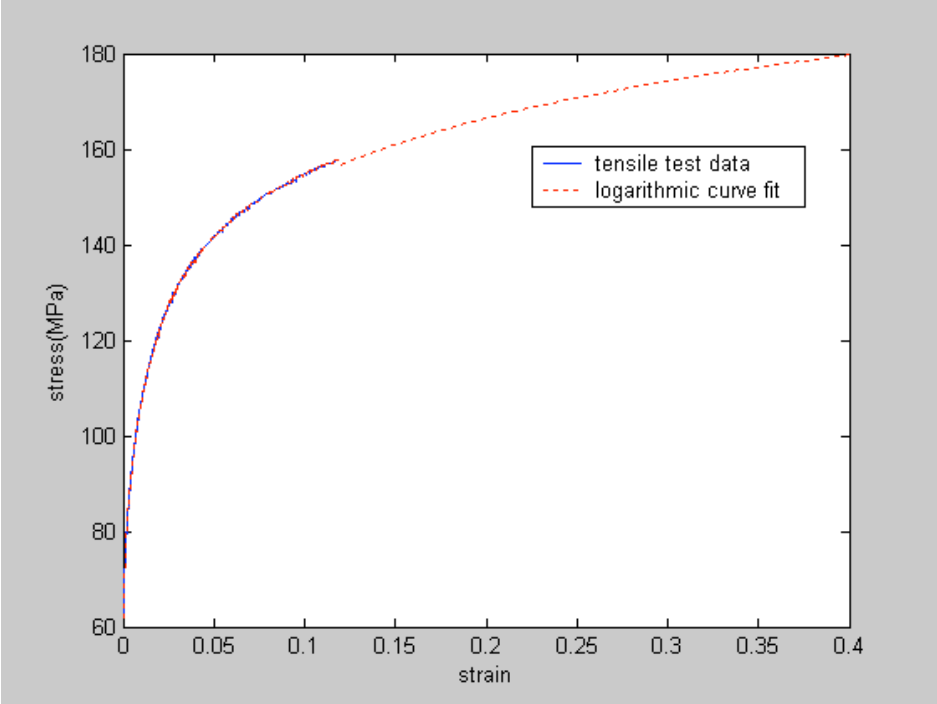


Fig.5.4 The curve fit of extended stress-strain correlation with Matlab for work hardening material
*Apart from the work hardening material, certain simulations also use rigid plastic material.

In order to eliminate the work-hardening effect, and to centralize the workpiece to make the axis of tooling and the workpiece coaxial, the two ends of the workpiece is machined in a conical shape that matches the tool.

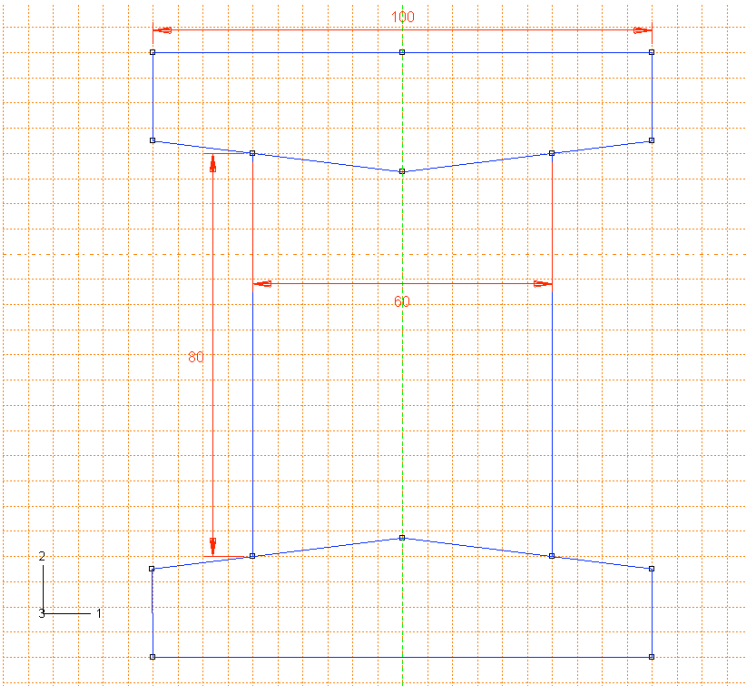

Fig.5.5 The vertical slice of the components and their dimensions.

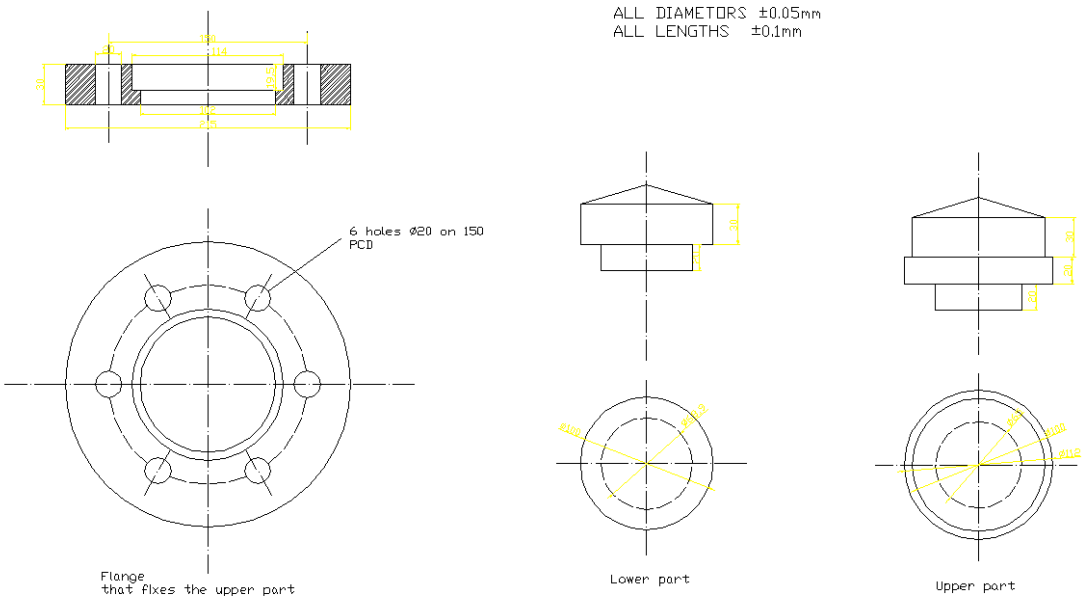


Fig.5.6 The design of experiment tooling

Fig.5.6 shows the design of the experiment tooling. The lower part of the cone is designed to sit on the machine, and the upper part has to be fixed with a flange shown on the very left of Fig.5.6.

The real experiment setup is shown below in Fig.36:

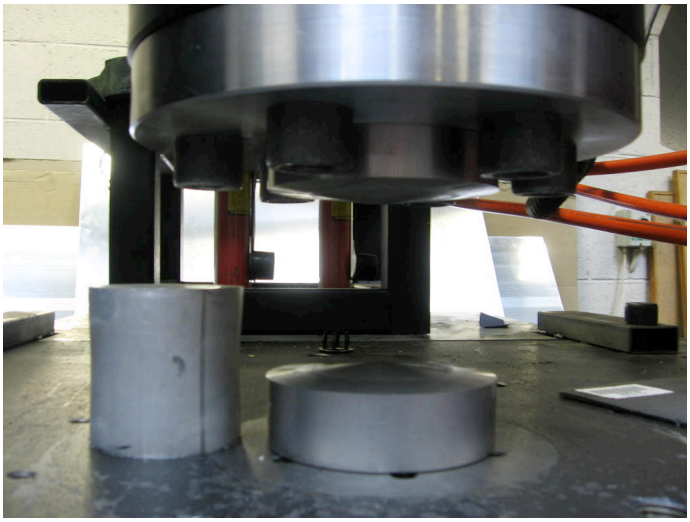

Fig.5.7 Machine for upsetting

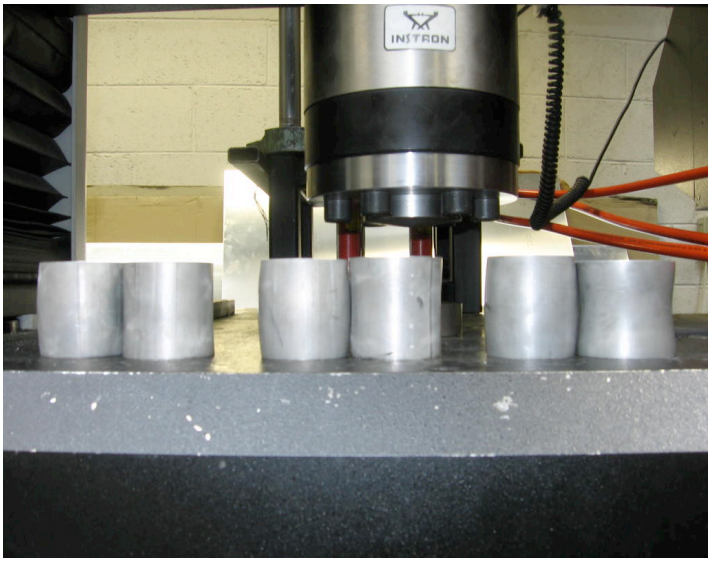


Fig.5.8 $3^0, 7^0, 12^0$ Workpiece after upsetting

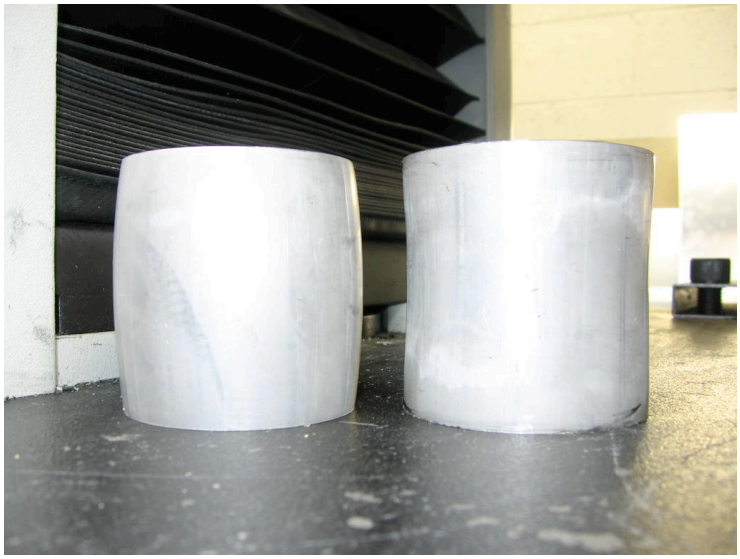

Fig.5.9 The deformation of $7^0$ workpiece (left: frictional. Right: with grease)

### 5.1.2 The experimental results and discussion

The experiments with $3^0$, $7^0$ and $12^0$ cone angles were conducted. Within each cone angle, two identical workpieces were made so that they could be subjected to dry friction and frictionless condition. The frictionless condition is simulated by applying grease on the interface. The experimental measurements are put in Table 5.1:

| Cone angle | Terms | Tool course | Top diameter after forging | Middle diameter after forging |
|---|---|---|---|---|
| $7^0$ | Without grease | 13.2 | 62.8 | 67.6 |
| | With Grease | 15.4 | 67.6 | 64.7 |
| $12^0$ | Without grease | 12.3 | 62.5 | 67.8 |
| | With Grease | 16.5 | 71 | 64.8 |
| $3^0$ | Without grease | 13.7 | 63.3 | 67.8 |
| | With grease | 14.1 | 66.3 | 66 |

Table 5.1

All the results were obtained under the same loading: 550kN. It is noticeable that the ones with grease applied at the interface allow a longer vertical course than the ones with dry friction under the same loading. In frictional model, a portion of the vertical force from the tool is balanced out by the friction force, that's to say the 550kN force is sustained by the sum of frictional force at the interface and the resistance force from the material. Whereas in the frictionless model, the 550kN force is purely supported by the resistance force of the material, so the material has to deform more to meet the equilibrium.

The results in the table are the reference for the simulation.

## 5.2 Simulation

### 5.2.1 Choosing between implicit and explicit analysis for upsetting

For implicit methods, the equilibrium equations need to be solved simultaneously to obtain the displacement of all nodes at the end of each increment. This requirement is usually achieved by matrix techniques. Nonlinear problems with implicit solver could lead to large

amount of iterations and converging difficulties. Due to this reason, disk space and memory usage by implicit solver can be large.

In contrast to implicit method, an explicit method does not require the solving of a simultaneous system of equations or the calculation of a global stiffness matrix. Instead, the solution is advanced kinematically from one increment to the next.

For those problems that can be solved with either implicit or explicit method, the efficiency with which the problem can be solved can determine which method to use.

For many analyses it is clear whether implicit or explicit should be used. Implicit is more efficient for solving smooth nonlinear problems; on the other hand, Explicit is the clear choice for a wave propagation analysis. There are, however, certain static or quasi-static problems that can be simulated well with either method, such as our upsetting problem.

Our final objective in this chapter is to model Pair 3 with its real size. So it is necessary to choose an appropriate and economical method so that not only the task could be finished, but also it will be finished with less cost of computer memory and calculation time. Notice that in previous discussions the scaled-down models are used, but not the real-size model.

One of the major substantial difficulties in modelling the real-size model is the time cost. Mesh has to be very fine to capture the microscopic behaviour of the material under the asperity. Multiplied by the big size of the problem, the number of elements turns out to be huge. In the explicit model, the computational cost is simply proportional to the number of degrees of freedom and roughly inversely proportional to the smallest element dimension.

Whereas in the implicit model, no such straightforward prediction exists, the cost is estimated to be in proportional to the square of the number of degrees of freedom.

The explicit method shows great cost savings over the implicit method as the model size increases, as long as the mesh is relatively uniform. Fig.5.10 illustrates the comparison of cost versus model size using the explicit and implicit methods. Normally the number of degrees of freedom scales with the number of elements.

Though the explicit analysis requires a large number of time increments, it is more efficient when the same analysis with implicit solver requires many iterations due to the contact complexities.

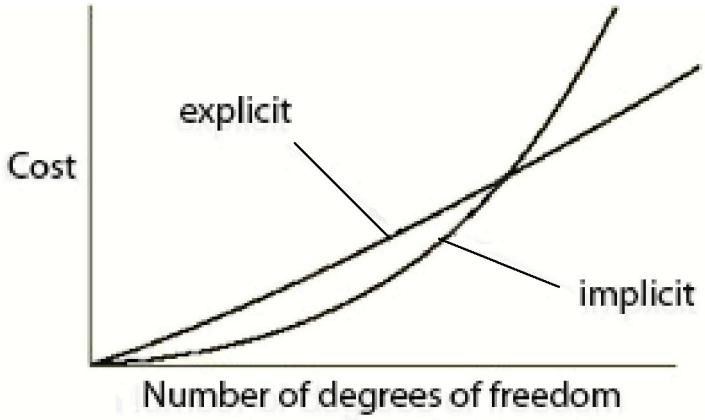


Fig.5.10 Cost versus model size in using the explicit and implicit methods.

In model pair No.3 the number of element is 500,020, and the degrees of freedom is twice as much: 1,000,040. A rough estimate of the time cost from the first few steps time is that the implicit model can take more than 1 month to finish while the explicit model only takes around 10 days if proper mass scaling is used.

### 5.2.2 The explicit model:

| Model description | |
|---|---|
| Size of workpiece (height×width) | 3×4mm |
| Asperity parameters | R=21um AR=360um |
| Tool material | Hard steel |
| Workpiece material | Rigid plastic, Aluminum |
| Stroke speed | Changing |
| Step time | Changing according to stroke speed. |
| Contact properties | Frictionless |
| Element type | Explicit, CAX4R (4-node bilinear axisymmetric quadrilateral, reduced integration, hourglass control) |
| Element size (height×width) | 0.030×0.015mm |
| Number of element | 7650 |
| Total number of variables | 15890 |
| Solver | ABAQUS Explicit |

Table 5.2

For the metal forming problems such as upsetting, artificially increasing the speed of stroke is necessary to obtain an economical solution. The difficulty lies on how large a speedup can be imposed and still obtains an acceptable quasi-static solution. A general recommendation is to run a series of analysis at various punch speeds in a certain range. Perform the analyses in the order of fastest to slowest since the solution time is inversely proportional to the stroke velocity. As the speed is decreased, at some point the solutions will become similar from one stroke speed to the next – an indication that the solutions are converging on a quasi-static solution.

As the loading rate is increased artificially, it becomes more and more important to apply the load in gradual and smooth manner. The simplest way to load the tool is to impose a constant velocity throughout the forming step. Such a loading causes a sudden impact load onto the workpiece metal at the start of the analysis and may produce undesired results. Even if the kinetic energy is fairly small, if it continues large oscillations, the model would be experiencing significant plasticity. See the kinematic energy oscillation from the constant speed loading at Fig.5.11. The effect of any impact load on the results becomes more pronounced as the loading rate is increased. Ramping up the punch velocity from zero using a smooth step amplitude curve minimizes these adverse effects.

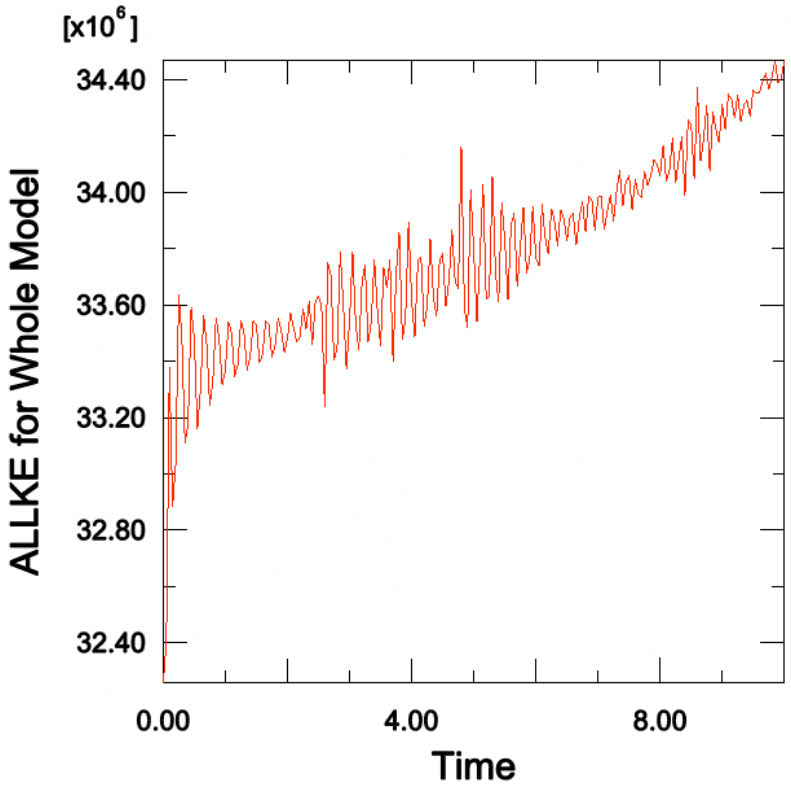


Fig.5.11 Kinematic energy oscillation resulted from the constant speed boundary condition

In order to eliminate sudden, jerky movements which can cause stress waves and induce noisy or inaccurate solutions, the ABAQUS built-in smooth amplitude curves are applied. It automatically connects each of the data pairs with curves whose first and second derivatives

are smooth and whose values are zero at each of the data point. An example of a smooth step amplitude curve is shown in Fig.5.12. Since both of the derivatives are smooth, a displacement loading will be gradual and the intervening motion will be smooth.

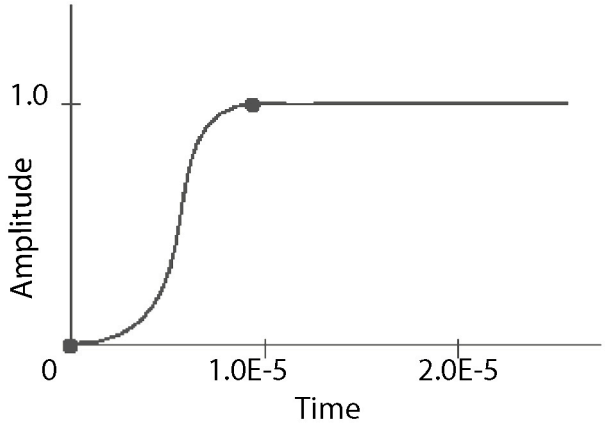


Fig.5.12 Amplitude definition using a smooth step amplitude curve.

### 5.2.3 the results

A group of explicit models varying in step time is executed to approach the quasi-static process. The kinetic energy history and the internal energy history of each model are plotting in the same diagram. To determine whether an acceptable quasi-static solution has been obtained, the kinetic energy of the blank should be no greater than a few percent of its internal energy due to the plastic deformation.

Rather than Fig.5.11, the kinetic energy in Fig 5.13(b) and Fig 5.14 (b) is smoother because of the way the loading is applied. The value of the kinetic energy peaks in the middle of the time history, corresponding to the time when the tool velocity is the greatest. Thus, the kinetic energy is appropriate and reasonable.

However, in Fig 5.13(b) the kinetic energy is too big comparing to the internal energy. The dynamic effects become more dominant. The corresponding deformed model is shown in

Fig.5.13 (a). This obviously does not meet the criteria of the quasi-static process. In Fig.5.14 (b) the step time is increased by a factor of 10, which means the corresponding speed is 1/10 of its original value. Kinetic energy is seen to be small compared to internal energy and the stress/ strain/ displacement distribution of the explicit model is almost identical to the implicit model, as shown in Fig.5.14(a).

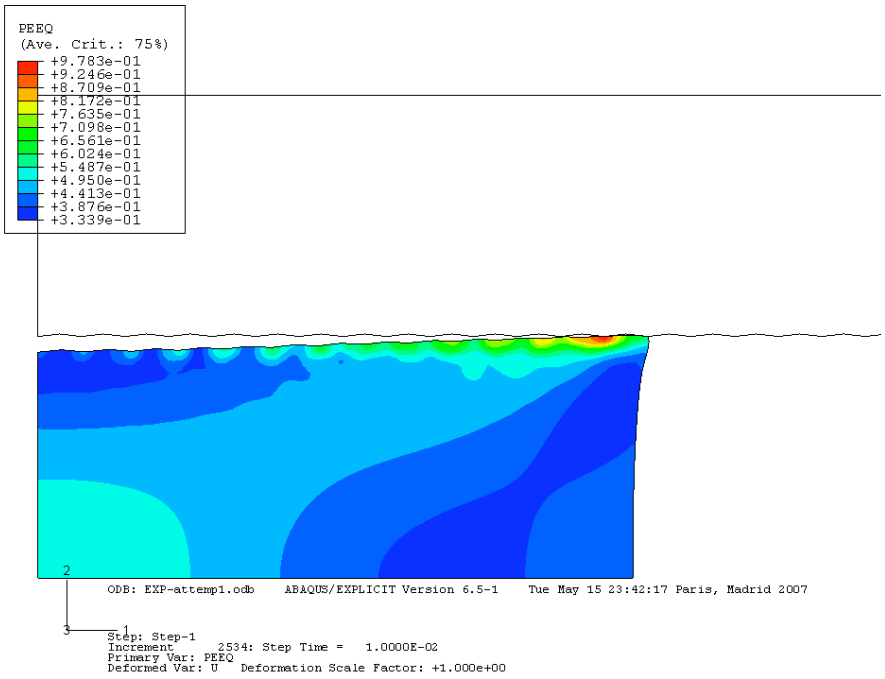


(a)

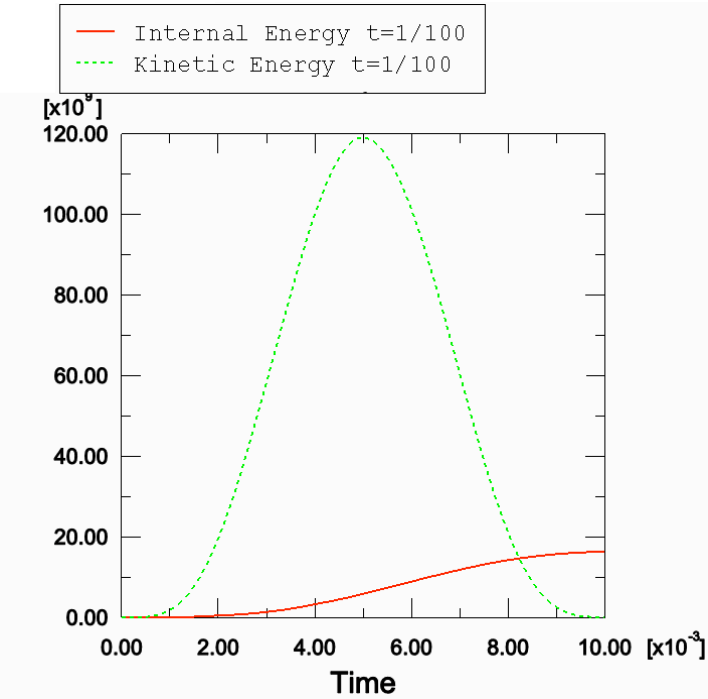


(b)

Fig 5.13 Explicit model: step time=0.01 f=0 average velocity= 1mm/0.01s = 100mm/s (a) the PEEQ at last increment (b) the plot of Internal energy and kinetic energy against time

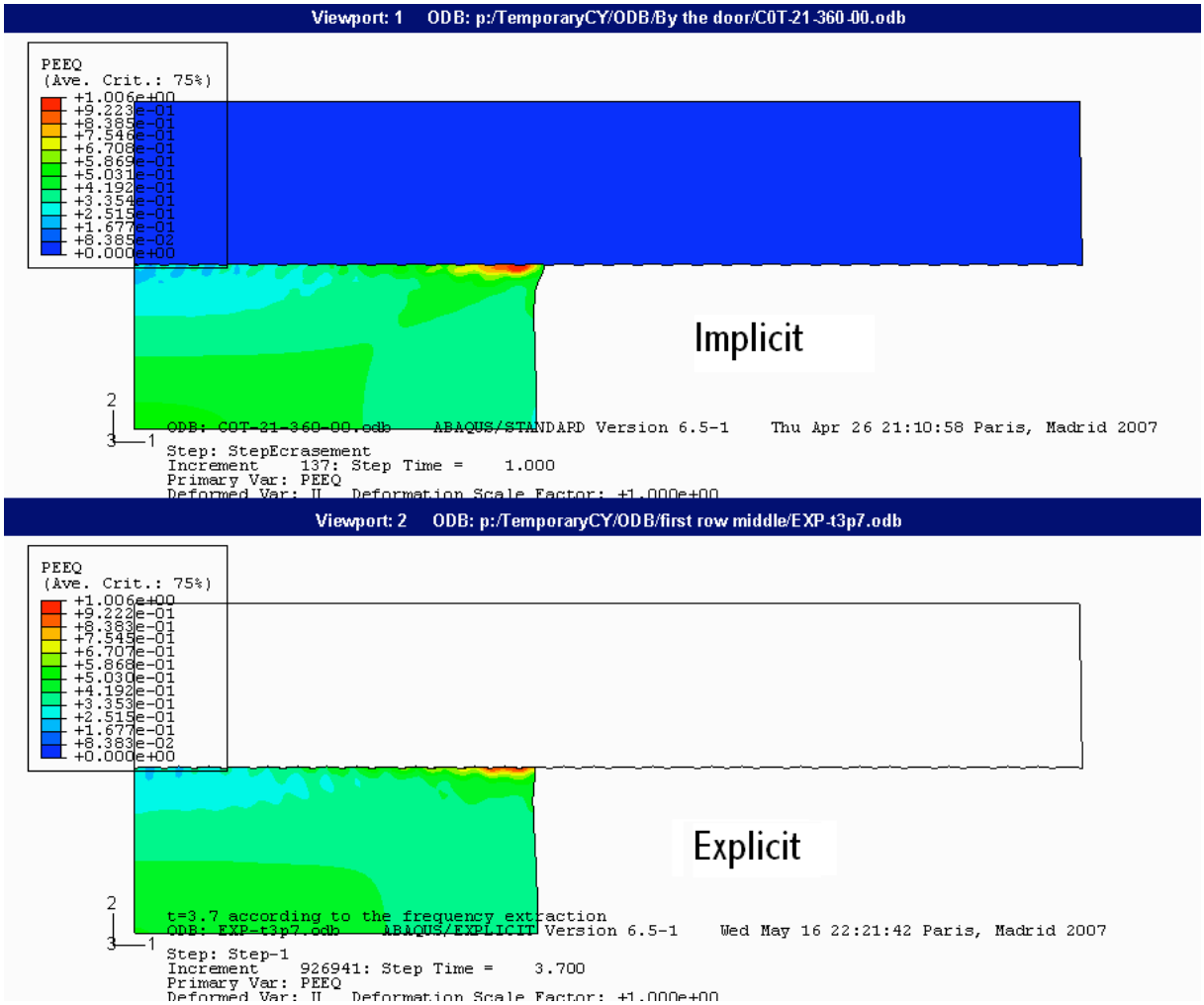
Viewport: 1 ODB: p:/TemporaryCY/ODB/By the door/C0T-21-360-00.odb
PEEQ
(Ave. Crit.: 75%)
+1.006e+00
+9.223e-01
+8.385e-01
+7.546e-01
+6.708e-01
+5.869e-01
+5.031e-01
+4.192e-01
+3.354e-01
+2.515e-01
+1.677e-01
+8.385e-02
+0.000e+00
Implicit
ODB: C0T-21-360-00.odb ABAQUS/STANDARD Version 6.5-1 Thu Apr 26 21:10:58 Paris, Madrid 2007
Step: StepEcrasement
Increment 137: Step Time = 1.000
Primary Var: PEEQ
Viewport: 2 ODB: p:/TemporaryCY/ODB/first row middle/EXP-t3p7.odb
PEEQ
(Ave. Crit.: 75%)
+1.006e+00
+9.222e-01
+8.383e-01
+7.545e-01
+6.707e-01
+5.868e-01
+5.030e-01
+4.192e-01
+3.353e-01
+2.515e-01
+1.677e-01
+8.383e-02
+0.000e+00
Explicit
t=3.7 according to the frequency extraction
ODB: EXP-t3p7.odb ABAQUS/EXPLICIT Version 6.5-1 Wed May 16 22:21:42 Paris, Madrid 2007
Step: Step-1
Increment 926941: Step Time = 3.700
Primary Var: PEEQ

(a)

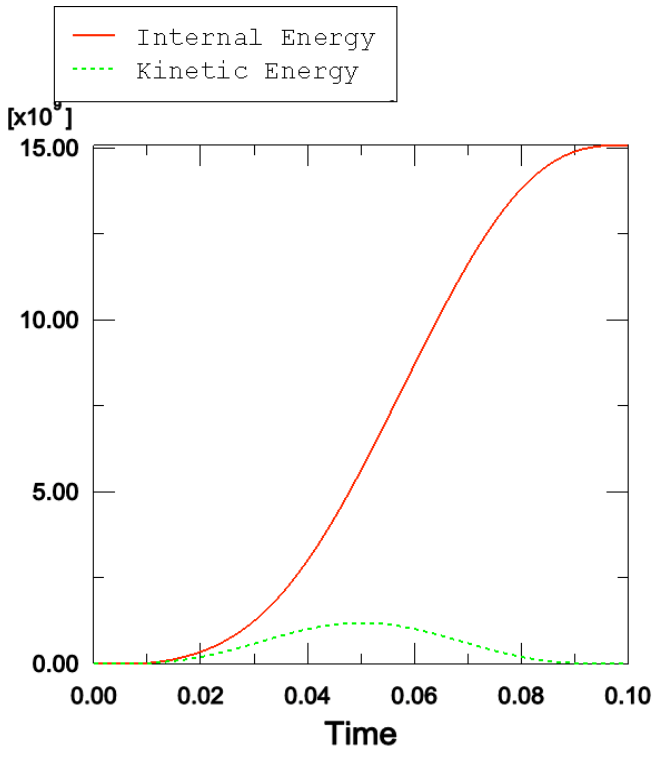
Internal Energy
Kinetic Energy
[x10⁹]
15.00
10.00
5.00
0.00
0.00
0.02
0.04
0.06
0.08
0.10
Time

(b)

Fig 5.14 Explicit model: step time=0.1  f=0 average velocity= 1mm/0.1s = 10mm/s
(a) the PEEQ contour plot of explicit and the corresponding implicit model (b) the plot of Internal energy and kinetic energy against time.

| Point | Deformed coordinate (Explicit) | Deformed coordinate (Implicit) |
|---|---|---|
| Top right | 4.91442, 1.99725 | 4.97847, 2.00771 |
| Bottom right | 4.90872, 0.00000 | 4.89000, 5.57591 |

Table 5.3

### 5.2.4 the real size model

Some real size models are executed to model Pair No. 3 in this section. First he Coulomb model is used to see if the displacement of the simulation matches that of the experiment.

| Model description (Pair No.3) | |
|---|---|
| Size of workpiece (2D-axisymmetric: height×width) | Real size, 80×60mm |
| Asperity parameters | R=38μm AR=360μm Asperity angle= $12^0$ |
| Tool material | Hard steel |
| Workpiece material | Aluminum, rigid plastic |
| Stroke course | 16.5mm |
| Contact properties | Frictionless (grease) |
| Element type | Implicit, CAX4R (4-node bilinear axisymmetric quadrilateral, reduced integration, hourglass control) |
| Element size (height×width) | 1×1.5mm |
| Number of element | 1000 |
| Total number of variables | 2000 |
| Solver | ABAQUS Implicit |

Table 5.4

As usual, the Coulomb model predicts the displacement really well. See Table 7. A close look is taken on the asperity of the tool. As the cone angle equals to the asperity angle, the right side of the asperity is actually parallel to horizontal. This allows a free expansion of the workpiece material in the sense that the right side is not hindering the outflow.

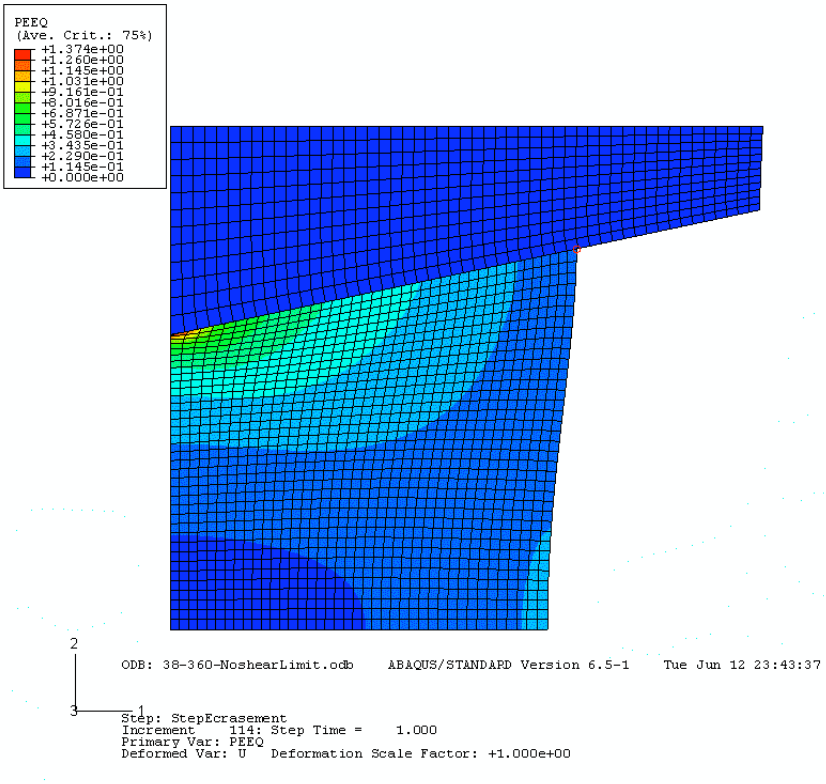


Fig 5.15 the Coulomb model

| Displacement Results | Stroke course (mm) | Deformed surface diameter (mm) | Deformed equatorial diameter (mm) |
|---|---|---|---|
| Experiment | 16.5 | 71 | 64.8 |
| Simulation | 16.5 | 69.96 | 64.94 |

Table 5.5

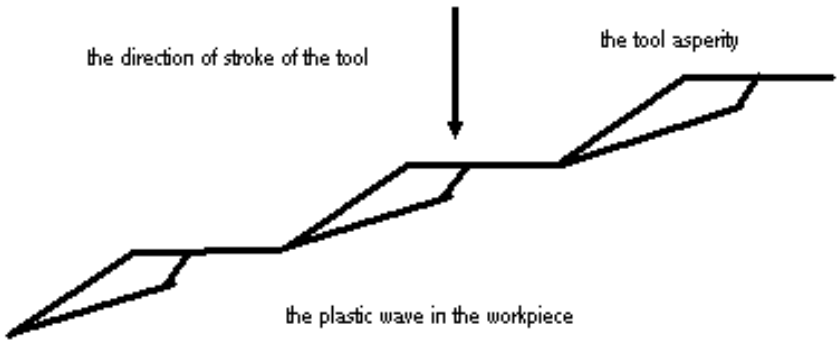


Fig 5.16 the asperity of Pair No.3

If we introduce roughness at the interface, the mesh has to be fine so that the microscopic detail could be captured. Taking into consideration of the contact complexities, the explicit model is the best choice.

| Model description (Pair No.3) | |
|---|---|
| Size of workpiece (2D-axisymmetric: height×width) | Real size, 80×60mm |
| Asperity parameters | R=38μm AR=360μm Asperity angle= $12^0$ |
| Tool material | Hard steel |
| Workpiece material | Aluminum, rigid plastic |
| Stroke course | 16.5mm |
| Contact properties | Frictionless (grease) |
| Element type | Explicit, CAX4R (4-node bilinear axisymmetric quadrilateral, reduced integration, hourglass control) |
| Element size (height×width) | 0.015×0.035mm |
| Number of element | 500020 |
| Total number of variables | 1003708 |
| Solver | ABAQUS Explicit |

Table 5.6

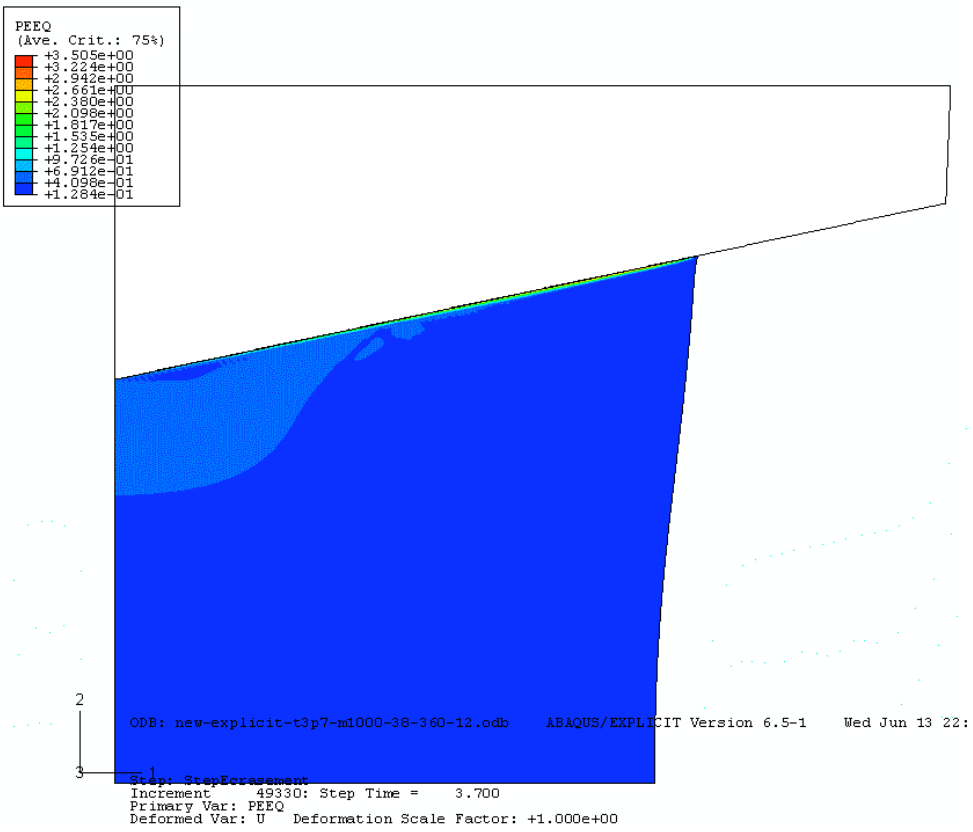


Fig 5.17 the explicit model

From the displacement results, the explicit model is a good match to the experiment. In terms of plastic strain, the model gives out a fairly big value: 3.505. This value is to be verified by further simulation.

| Displacement Results | Stroke course (mm) | Deformed surface diameter (mm) | Deformed equatorial diameter (mm) |
|---|---|---|---|
| Experiment | 16.5 | 71 | 64.8 |
| Explicit Simulation | 16.5 | 72.2 | 65.8 |

Table 5.7

# CONCLUSIONS

## Conclusions

1) Surface roughness is important in friction-sensitive process such as upsetting or free forging. Surface roughness parameters are defined in a way that real surface characteristics can be reflected. The real geometric surface roughness is usually assumed as simplified geometry in the friction law and how the law integrates the factor of surface roughness is crucial.
2) In the upsetting process, a thin layer of local material outflow of the workpiece takes form at the interface because of the microscopic interaction between tool asperity and plastic wave. The analysis of the evolution of this squeezed layer contributes to the understanding of macroscopic friction at the interface.
3) Coulomb's law has a good performance against all the displacement criteria. While plastic wave model is very suitable for stress/strain prediction
4) When dealing with large-scale simulation or highly non-linear contact problems such as axisymmeric upsetting, the explicit method shows great cost savings over the implicit method.

## Recommendations for further work

The investigation of the friction law for the axisymmetric upsetting is very sophisticated because of the complexities of surface roughness. To find a proper friction law on the macroscopic scale which takes into account of all the surface roughness features requires the analysis of various numerical simulations and experiments facts.

a) Coulomb-Orowan's model is an extension of Coulomb's model, and it imposes the shear yield strength thus it is more reasonable in the situation where contact pressure

is high. It is worth looking into Coulomb-Orowan's model and comparing its performance with Coulomb's model and plastic wave model.

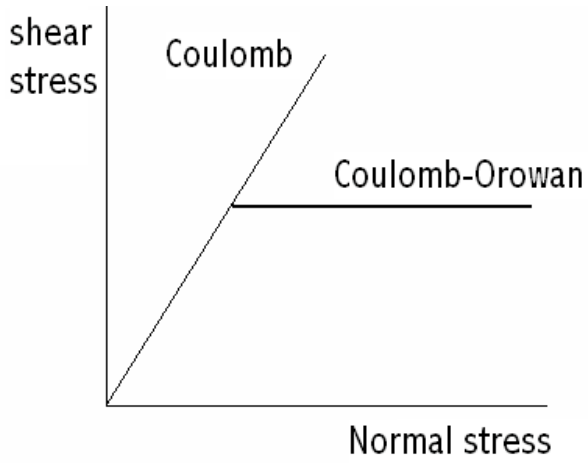


b) The microscopic observation of the Finite Element model in Chapter 2 indicates that the evolution of plastic wave is different than it is stated in plastic wave theory. Whether this difference could contribute to the improvement of plastic wave model should be considered.

c) There are a few other factors, such as the slip velocity and local temperature, need to be taken into consideration. However, to avoid overcomplicating the problem, only the major factors of surface roughness should be extracted.

d) Plastic wave theory and its performance on mixed lubricating conditions are to be investigated.

# CONCLUSIONS

La rugosité de surface est un paramètre essentiel dans les procédés sensibles au frottement tels que “l’écrasement” ou “le forgeage libre”. Les paramètres de rugosité de surface sont définis de façon à ce que les caractéristiques réelles de surface soient reflétées. La rugosité géométrique réelle de surface est habituellement prise comme étant une géométrie simplifiée dans la loi de frottements. Ainsi, la manière avec laquelle la loi intègre le facteur de rugosité de surface est décisif.

Dans le procédé d’écrasement, on observe la formation locale d’une couche mince de matériau s’écoulant à l’interface à cause des interactions microscopiques entre les aspérités de l’outil et le matériau massif du lopin.
L'analyse de l'évolution de cette couche mince contribue à la compréhension des frottements macroscopiques à l'interface.

La loi de Coulomb prédit correctement les déplacements globaux, tandis que le modèle de vague plastique est lui très intéressant pour la prédiction des contraintes et déformations à proximité de l’interface

Quand il s’agit de faire des simulations à grande échelle ou des problèmes de contact fortement non linéaires, comme “”, la méthode explicite permet de réaliser des économies de temps et de coût importantes par rapport à la méthode implicite.

## References


[1] Vidal-Sallé E., Baillet L., Boyer J.-C.**,** *Friction law and parameter identification*, 2nd ESAFORM Conference on Material Forming, Guimarães (Portugal), 13-16/04/1999, p. 603-606.

[2] Vidal-Sallé E., Boyer J.-C.**,** *Thermo-mechanical constitutive laws for a semi-transparent viscous lubricant*. 5th ESAFORM Conference on Material Forming, Krakow (Poland), 14-17/04/2002 (to be published).

[3] N. Bay, T. Wanheim*, Real area of contact and friction stress at high pressure sliding contact*. Wear, Vol.38 (1976), 201-209.

[4] J.M. Challen, P.L.B. Oxley, *An explanation of the different regimes of friction and wear using asperity deformation models*. Wear, Vol.53 (1979), 229-243.

[5] J.F. Schmit, *Elaboration et caractérisation de verres lubrifiants haute température pour le matriçage d'alliages de titane*. PhD of University of Montpellier. 1996. 297 pages.

[6] P.Lacey, A.A.Torrance, J.A.Fitzpatrick, *The relation between the friction of lubricated rough surfaces and apparent normal pressure.*

[7] H.Moalic, J.A.Fizpatrick, A.A.Torrance, a spectral approach to the analysis of rough surfaces. Journal of Tribology, Vol.111(1989),359-363

[8] CHEN, C.C. and KOBAYASHI, S., Rigid-Plastic Finite Element Analysis of Ring Compression, Appl. Num. Method. Form. Proc.,(1978), Vol. 28,p. 163.

[9] N. BAY and T. WANHEIM, Real area of contact and friction stress at high pressure sliding contact, Wear, (1976), Vol. 38, pp. 201-209.

[10] J.M. CHALLEN and P.L.B. OXLEY, An explanation of the different regimes of friction and wear using asperity deformation models, Wear, (1979), Vol. 53, pp. 229-243.

[11] B. AVITZUR, C.K. HUANG, Y.D. ZHU, A friction model based on the upper bound approach to the ridge and sub-layer deformations, Wear, (1984), Vol. 95, pp. 59-77.

[12] B. AVITZUR, Boundary and hydrodynamic lubrication. Wear, 1990, Vol. 139, p. 49-76.

[13] A.T. MALE and M.G. COCKCROFT, J. Inst. Met., Vol. 93, 1964, p.38

[14] K. P. RAO and K. SIVARAM, A review of ring-compression testing and applicability of the calibration curves, Journal of Materials Processing Technology, Vol. 37, 1993, pp. 295-318

[15] D.M. PETTY, Friction models for finite element modelling, Journal of Materials Processing Technology, Vol. 45, 1994, pp. 7-12.

[16] E.SALLE, L. BAILLET and J.C. BOYER

[17] S.B. PETERSEN, P.A.F. MARTINS and N. BAY, Friction in bulk metal forming : a general friction model vs the law of constant friction, Journal of Materials Processing Technology, Vol. 66, 1997, pp. 186-194

[18] X. TAN, P.A.F. MARTINS, N. BAY and W. ZHANG, Friction studies at different normal pressures with alternative ring-compression tests, Journal of Materials Processing Technology, Vol. 80-81, 1998, pp. 292-297

[19] Laurent BAILLET, MODELISATION DU FROTTEMENT POUR LES OPERATIONS DE MATRICAGE, THESE pour obtenir LE GRADE DE DOCTEUR

[20] M. KUNOGI, J. Sci. Res. Inst., Vol. 2, 1954, p. 63

# APPENDIX

## 1.Some numerical test using POLLUX

Cylinder
Radius = 4
Heigth = 3

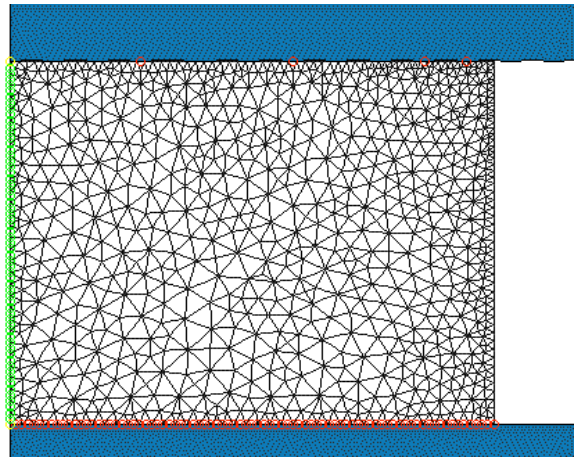

Tool with asperities
R= 0.021 AR=0.360

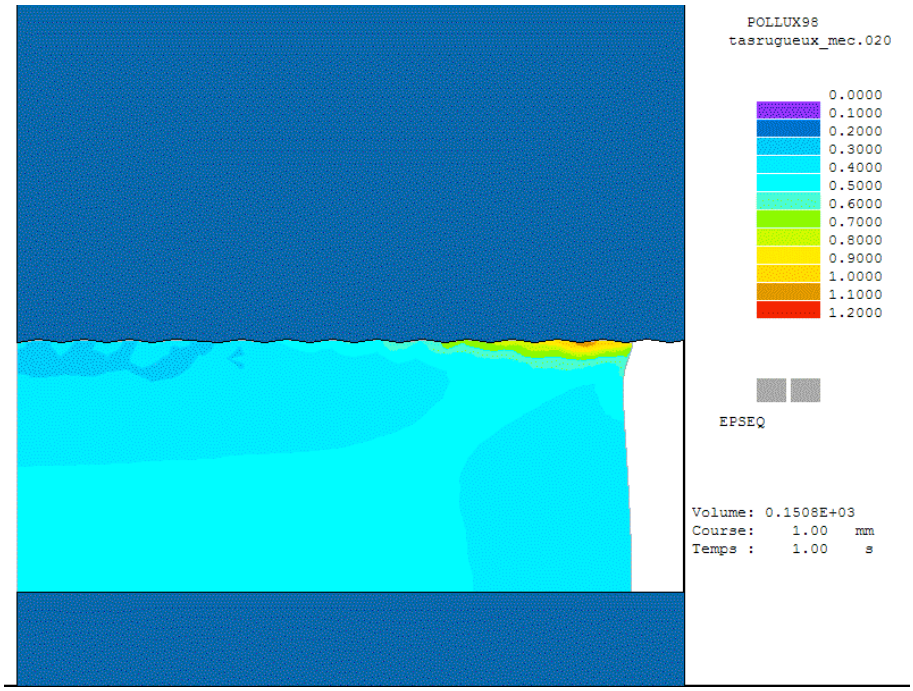

Tool with asperities
R= 0.021 AR=0.360

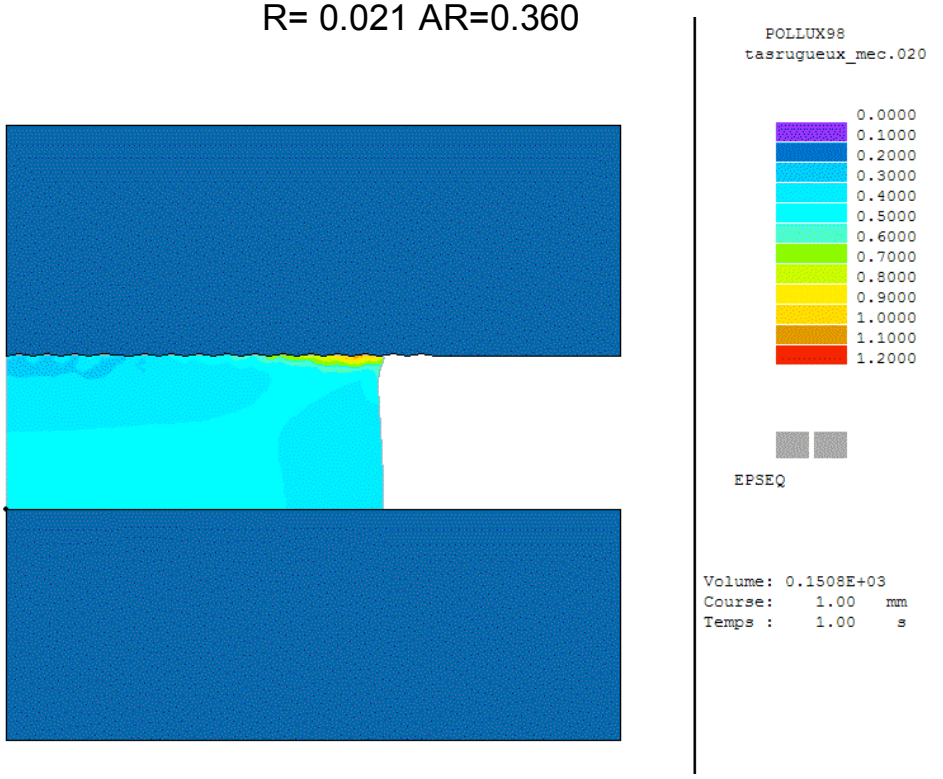


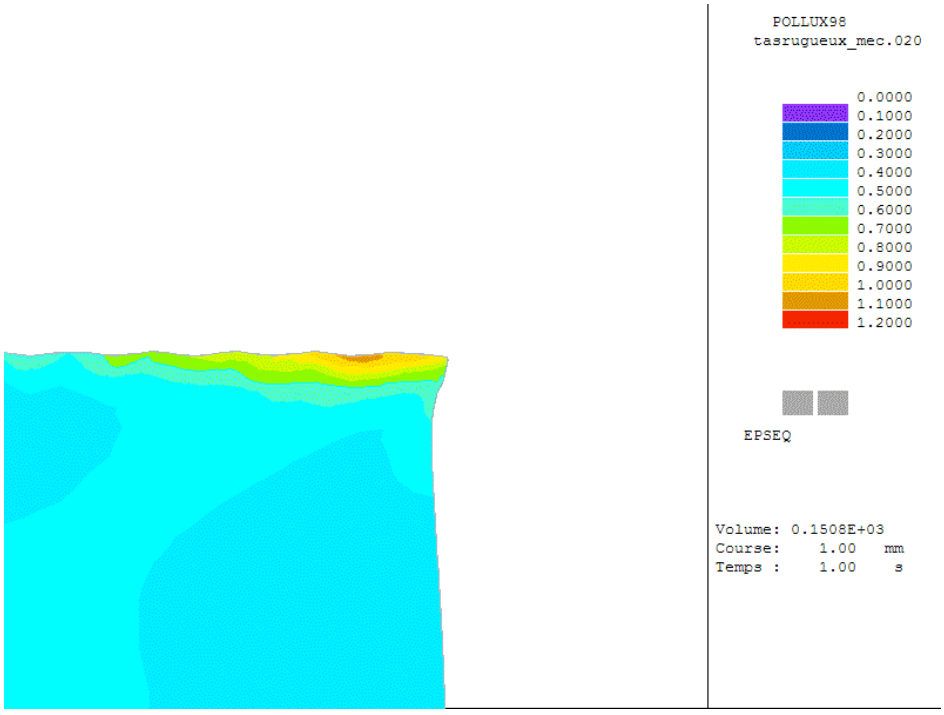

Tool with asperities
R= 0.021 AR=0.360

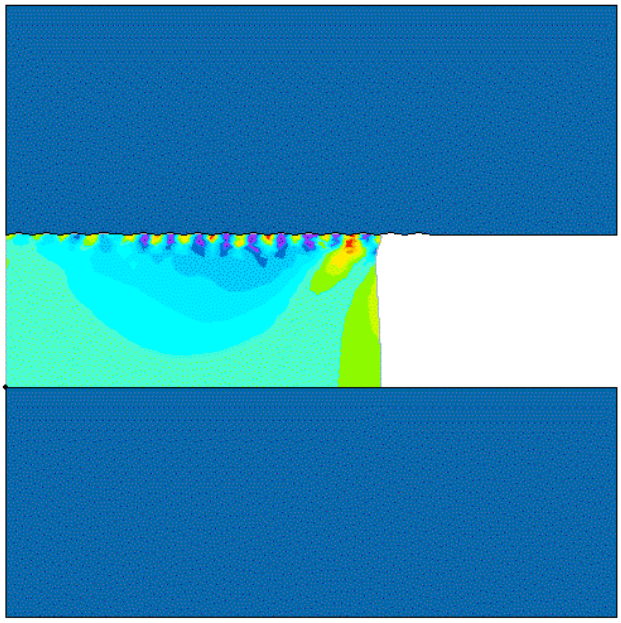

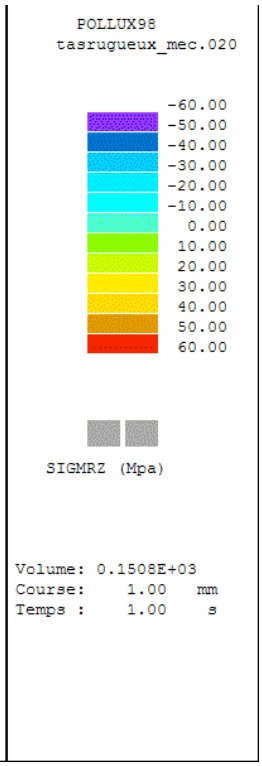


Tool with asperities
R= 0.021 AR=0.360

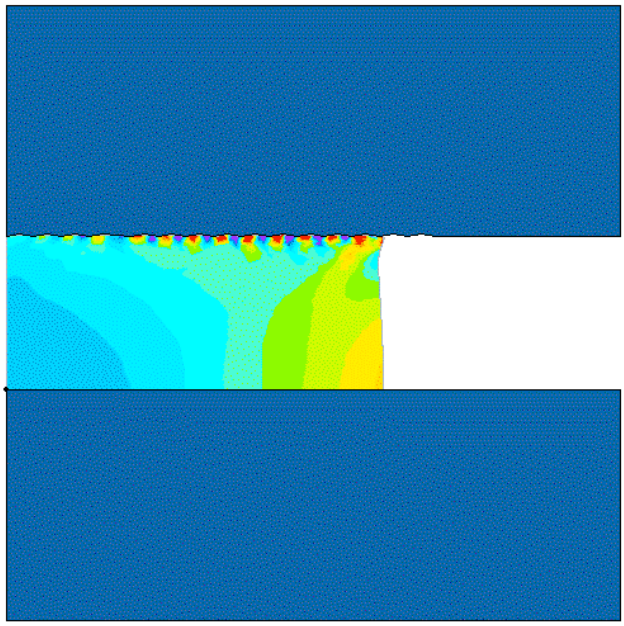

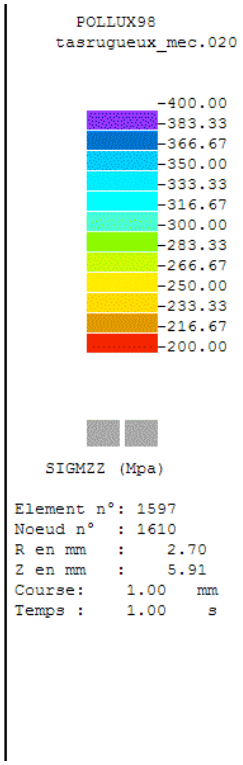

Tool with standard
plastic wave model
R= 0.021 AR=0.360

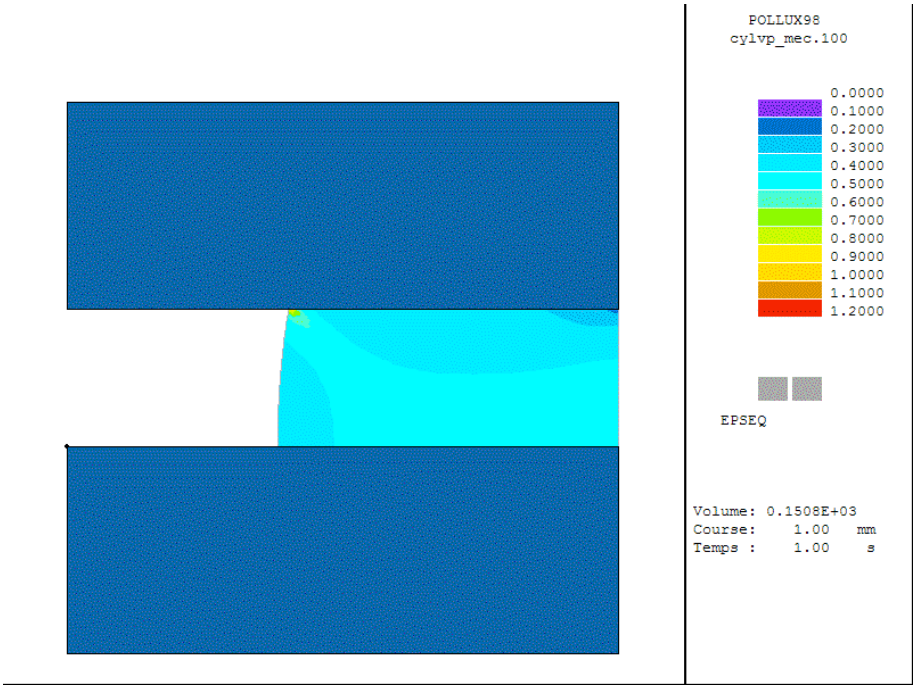

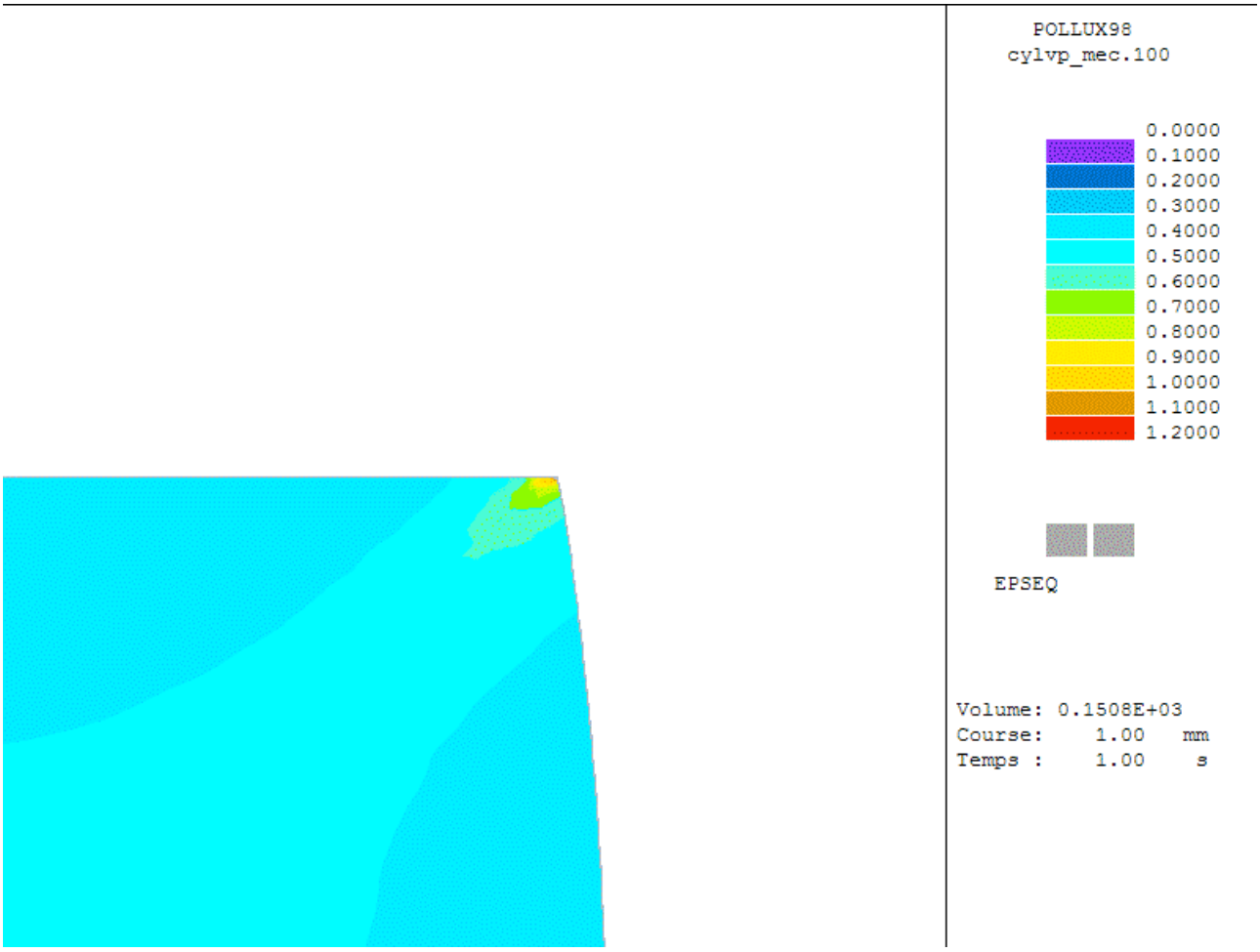


Tool with standard
plastic wave model
R= 0.021 AR=0.360

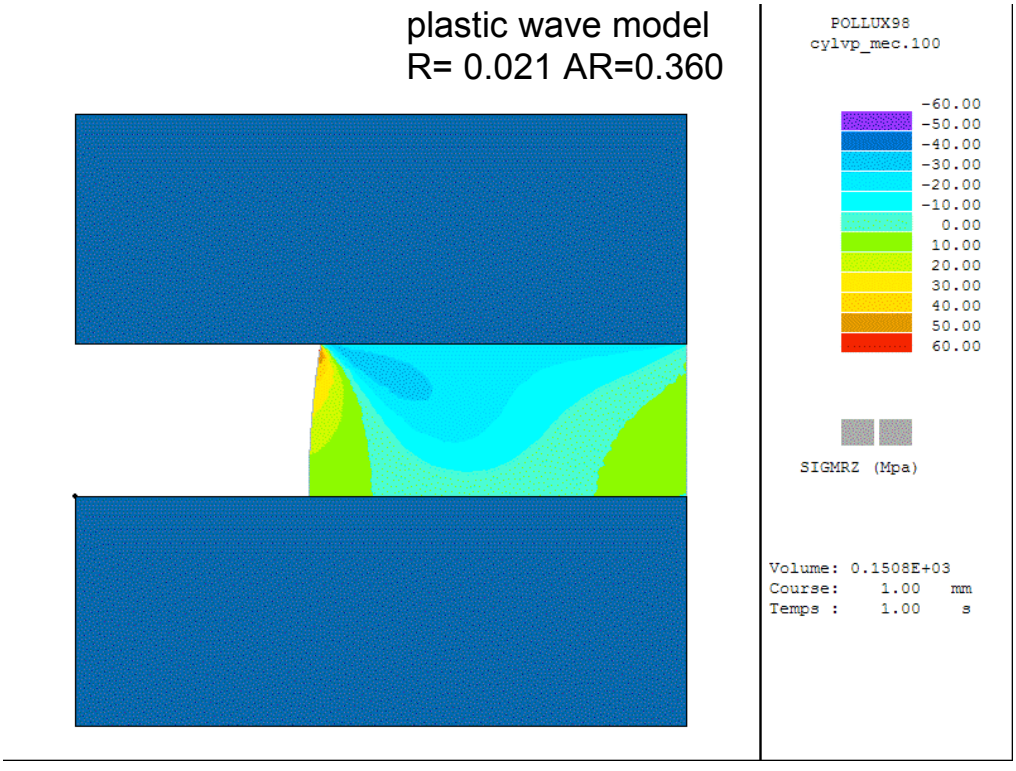

Tool with standard
plastic wave model
R= 0.021 AR=0.360

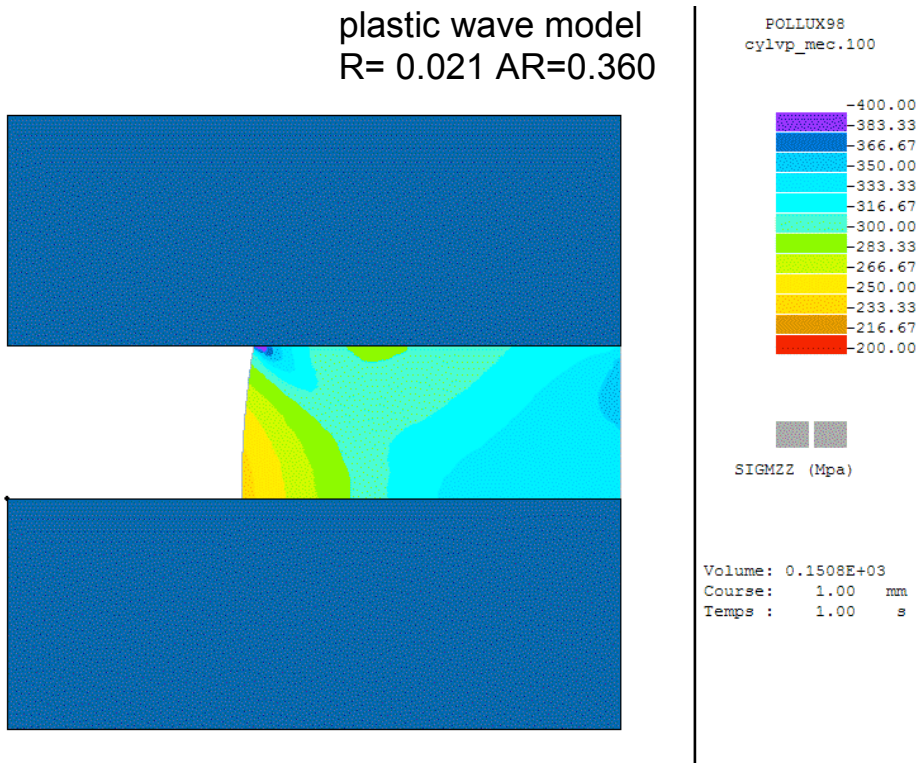


Tool with improved
plastic wave model
R= 0.021 AR=0.360

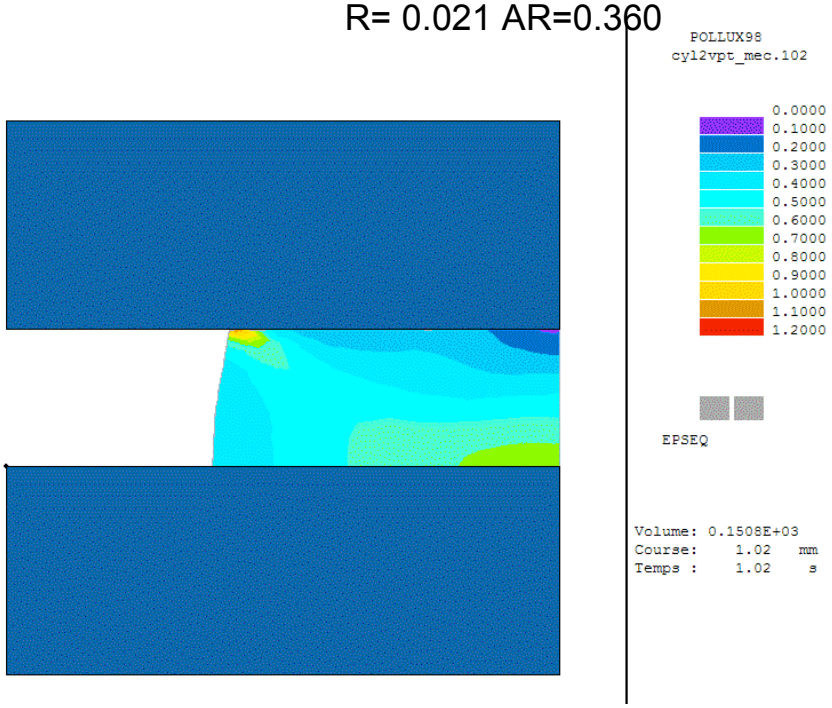

Tool with improved
plastic wave model
R= 0.021 AR=0.360

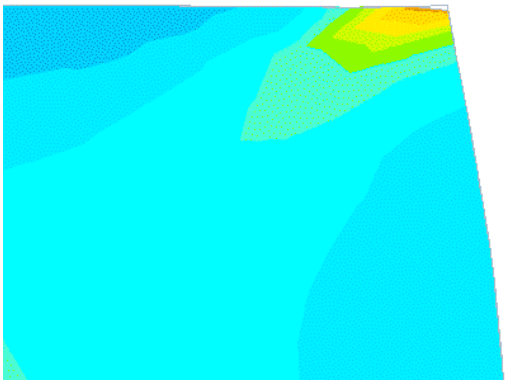

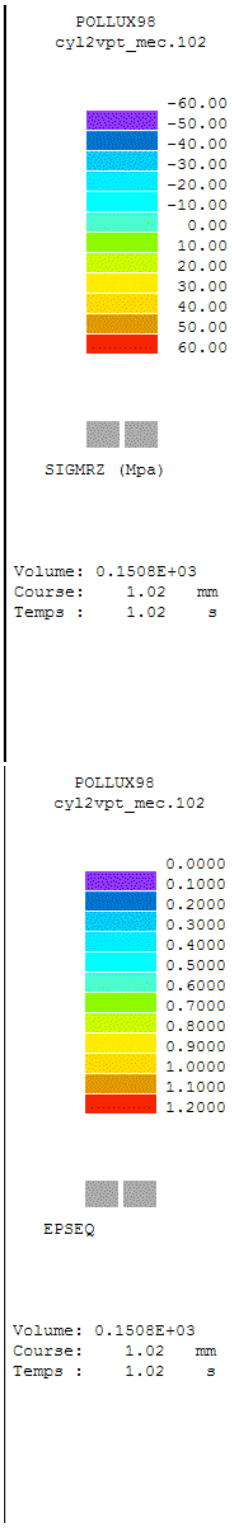

**2. The User Subroutine file Ufric.for**

```
C
      SUBROUTINE FRIC(LM,TAU,DDTDDG,DDTDDP,DSLIP,SED,SPD,
     1 DDTDDT,PNEWDT,STATEV,DGAM,TAULM,PRESS,DPRESS,DDPDDH,SLIP,
     2 KSTEP,KINC,TIME,DTIME,NOEL,CINAME,SLNAME,MSNAME,NPT,NODE,
     3 NPATCH,COORDS,RCOORD,DROT,TEMP,PREDEF,NFDIR,MCRD,NPRED,
     4 NSTATV,CHRLNGTH,PROPS,NPROPS)
C
      INCLUDE 'ABA_PARAM.INC'
C
      CHARACTER*80 CINAME,SLNAME,MSNAME
      DIMENSION TAU(NFDIR),DDTDDG(NFDIR,NFDIR),DDTDDP(NFDIR),
     1         DSLIP(NFDIR),DDTDDT(NFDIR,2),STATEV(*),
     2         DGAM(NFDIR),TAULM(NFDIR),SLIP(NFDIR),TIME(2),
     3         COORDS(MCRD),RCOORD(MCRD),DROT(2,2),TEMP(2),
     4         PREDEF(*),PROPS(NPROPS)
C
C
       PARAMETER(PI=3.141592654)
       IF (LM .EQ. 2) RETURN

C
C   Angle des aspérités et COEFFICIENT de Tresca
C
      A1DEG=PROPS(1)
      F0=PROPS(2)
      A1=A1DEG*PI/180.D+00
      SIG0=PROPS(3)
```

```
      SIGN=PRESS

c                                        colonne 72   *
c     Cree le 17/02/94
c     ***************************************************
c     SOUS-PROGRAMME DE FROTTEMENT A SEC
c     DROITE TYPE COULOMB jusqu a X2,Y2 puis COURBE en ARCTANGENTE
c     DISCONTINUITE lors du passage des 2 courbes
c     COURBE TOTALE CONTINUE MAIS NON CONTINUEMENT DERIVABLE
c     ***************************************************

c     ENTREES
c     *******
c      A1:angle de l asperite de l outil en RADIAN
c      A1DEG:angle de l asperite de l outil en DEGRES
c      F0:coefficient de frottement local de type TRESCA a l interface
c        outil/lopin
c      SIG0:contrainte locale d ecoulement du materiau en MPa
c      SIGN=contrainte normale en MPa

c     SORTIE
c     ******
c      SIGT=contrainte tangentielle en MPa

      VB=(3.3171428E-4*A1DEG**2-1.87829E-2*A1DEG+5.5377E-2)*F0**2
     &    +(-2.53893E-4*A1DEG**2-1.85264E-3*A1DEG+0.52955)*F0
     &    +(-2.77867E-4*A1DEG**2+2.51337E-2*A1DEG+4.07653E-3)

c     La courbe passe par le point x(2),Y(2)
      PHI=0.5*ACOS(F0)-A1
      ETA=ASIN((1.-F0)**(-0.5)*SIN(A1))
      X2=1./(2.*SQRT(3.)*COS(A1))
     &       *( (1.+2.*(PI/4.+PHI-ETA))*COS(A1)+SIN(A1+2.*PHI) )
      Y2=1./(2.*SQRT(3.)*COS(A1))
     &       *( (1.+2.*(PI/4.+PHI-ETA))*SIN(A1)+COS(A1+2.*PHI) )
      VA=X2/TAN(Y2*PI/2./VB)

      IF(SIGN.LE.X2*SIG0) THEN
c ******DROITE SIGT=Y2/X2*SIGN
        SIGT=Y2/X2*SIGN
        DDTDDP(1)=Y2/X2
C       IF (ABS(DGAM(1)) .GE. CHRLNGTH/10.D+00) THEN
C         TAU(1)=-SIGT * (DGAM(1)/ABS(DGAM(1)))
C     ELSE
C         TAU(1)=0
C     END IF
        TAU(1)=-SIGT
        TAU(2)=0.D+00
      ELSE
c ******COURBE SIGT=VB*2/PI*ATAN(SIGN/VA)
        SIGT=(VB*2./PI*ATAN((SIGN/SIG0)/VA))*SIG0
        SIGNP=0.95*SIGN
        SIGTP=(VB*2./PI*ATAN((SIGNP/SIG0)/VA))*SIG0
C       IF (ABS(DGAM(1)) .GE. CHRLNGTH/10.D+00) THEN
C         TAU(1)=-SIGT * (DGAM(1)/ABS(DGAM(1)))
```

```
C    ELSE
C        TAU(1)=0
C    END IF
       TAU(1)=-SIGT
       DDTDDP(1)=(SIGT-SIGTP)/(SIGN-SIGNP)
       TAU(2)=0
     ENDIF

C
C  PLASTIC DISSIPATION
C
     SPD=TAU(1)*DSLIP(1)
     LM=0
     DDTDDG(1,1)=0.
     DDTDDT(1,1)=0.
C
     RETURN
     END
```

**3. Material properties in simulation Work hardening material and rigid plastic material**

**Rigid plastic, Aluminium**

Elastic:
Young's Modulus: 70 Gpa , Poisson's Ratio: 0.33

Plastic:

| Yield stress (Mpa) | Plastic strain |
|---|---|
| 120 | 0 |
| 140 | 0.022 |
| 160 | 0.116 |
| 170 | 0.36 |

Density (Explicit):
2700kg/$m^3$

**Work hardening, Aluminium**

Elastic:
Young's Modulus: 70 Gpa , Poisson's Ratio: 0.33

Plastic:

| Yield stress (Mpa) | Plastic strain |
|---|---|
| 120 | 0 |
| 140 | 0.022 |
| 160 | 0.116 |
| 180 | 0.37 |
| 360 | 2.713 |

Density (Explicit):
2700kg/$m^3$

**4. The roughness parameters of tools**

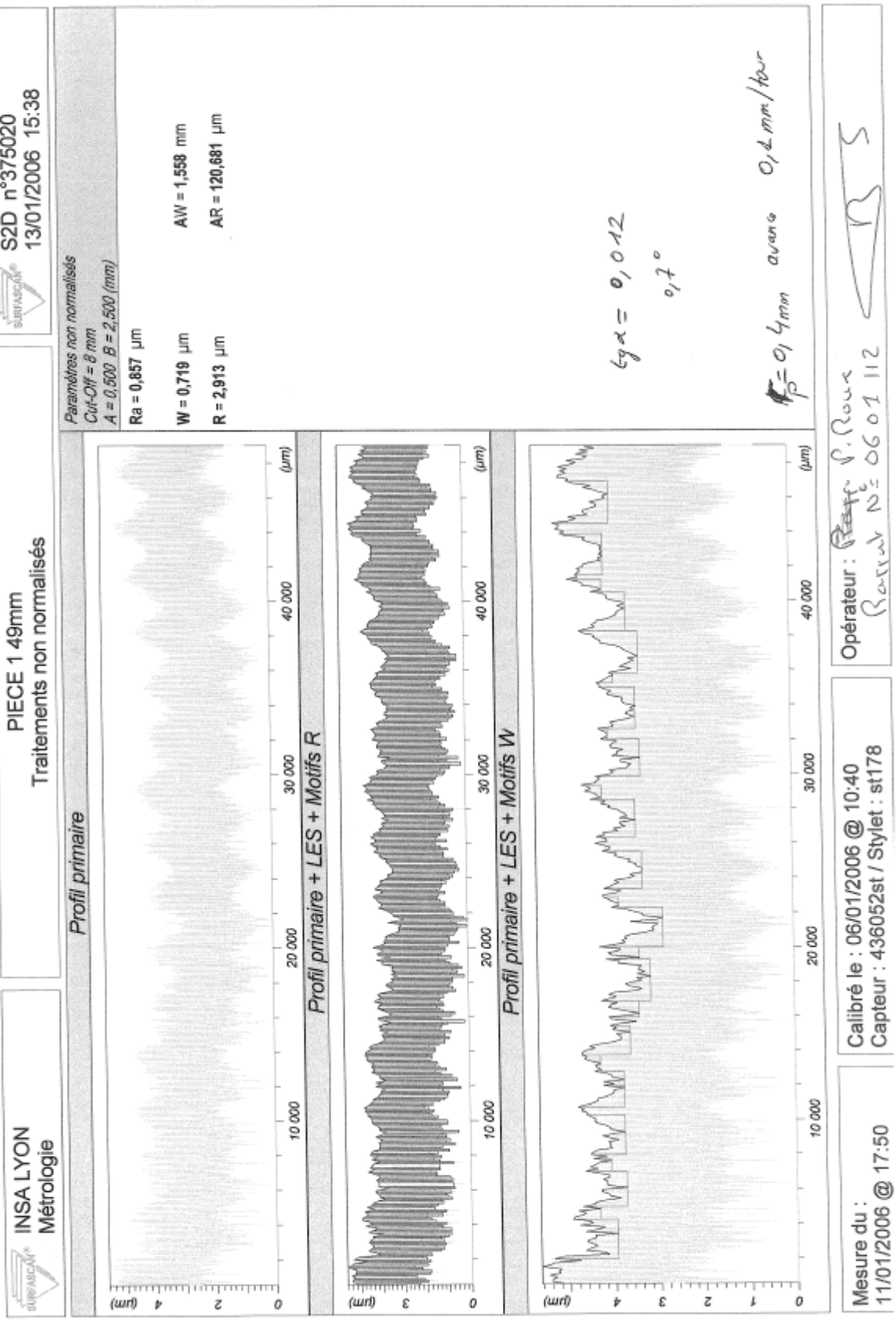

INSA LYON
Métrologie
PIECE 1 49mm
S2D n°375020
13/01/2006 15:45
(µm)
26
25
24
23
22
20 200
20 400
20 600
20 800
(µm)
z = 0,2 µm
x = 50 µm
Mesure du :
11/01/2006 @ 17:50
Calibré le : 06/01/2006 @ 10:40
Capteur : 436052st / Stylet : st178
Opérateur : Q. Rous

INSA LYON
Métrologie

PIECE 2 49mm
Traitements non normalisés

S2D n°375020
13/01/2006 15:40

*Profil primaire*

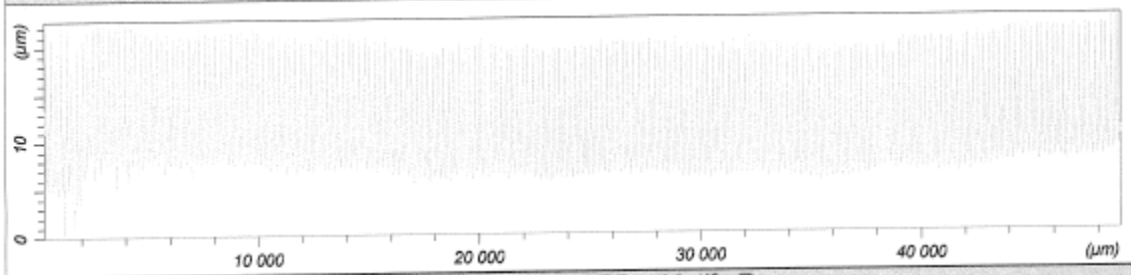


*Profil primaire + LES + Motifs R*

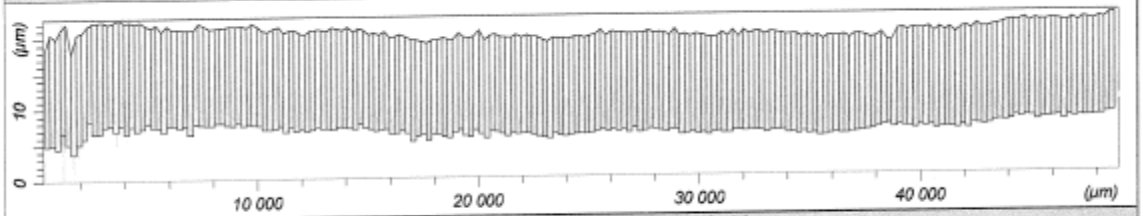


*Profil primaire + LES + Motifs W*

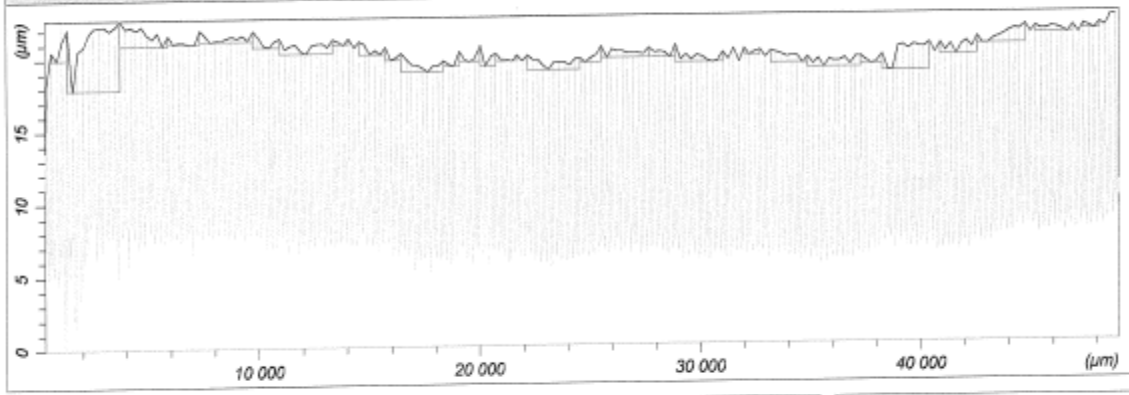


*Paramètres non normalisés*
*Cut-Off = 8 mm*
*A = 0,500 B = 2,500 (mm)*

**Ra = 3,608** µm

**W = 0,954** µm **AW = 1,505** mm

**R = 13,842** µm **AR = 238,970** µm

$tg\alpha = 0,029$

$1,65°$

$r_p = 0,4$ mm avance 0,2 mm/tour

Mesure du :
11/01/2006 @ 17:42

Calibré le : 06/01/2006 @ 10:40
Capteur : 436052st / Stylet : st178

Opérateur : P. Roux
Rapport N° 0601112

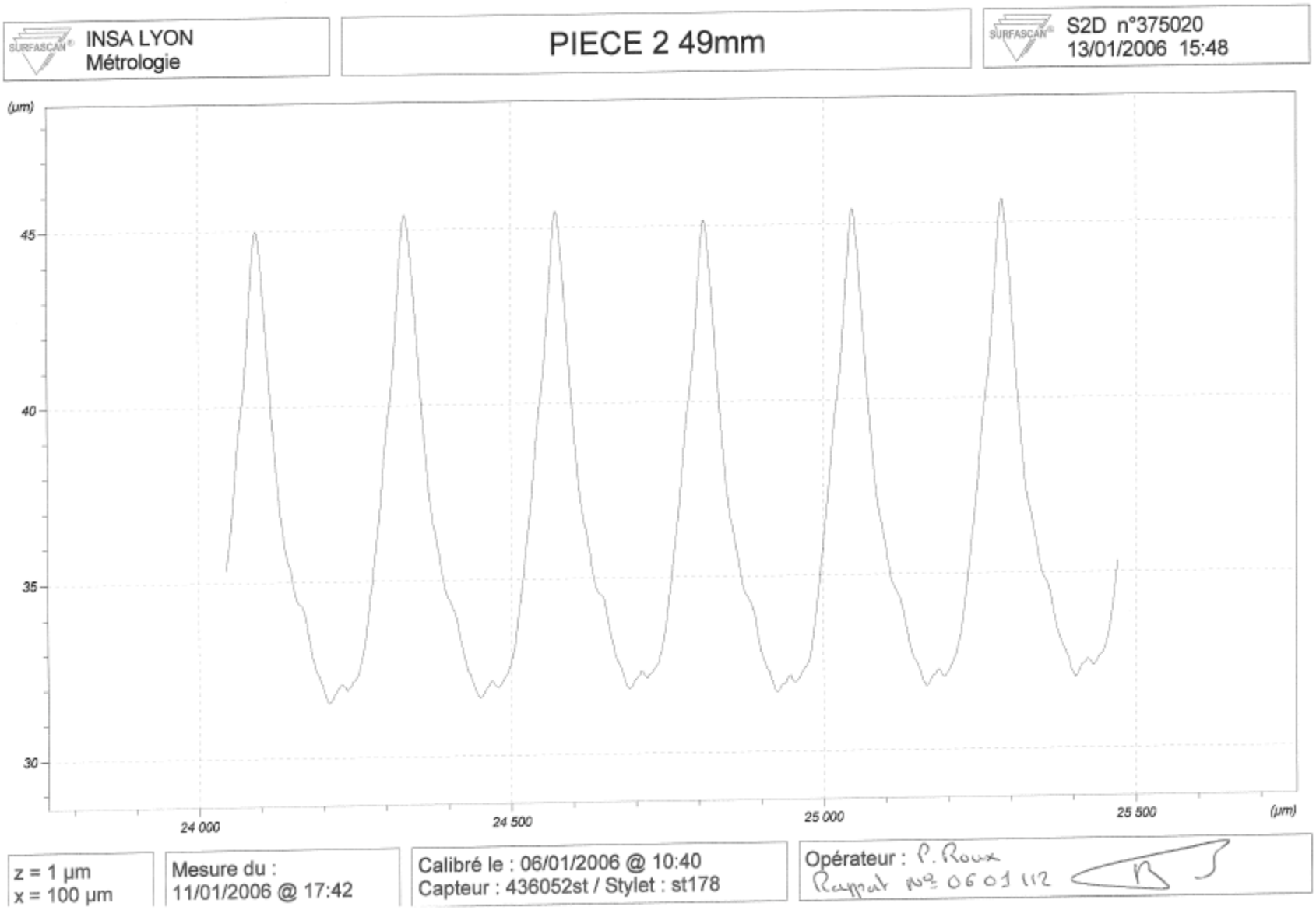
INSA LYON
Métrologie
PIECE 2 49mm
S2D n°375020
13/01/2006 15:48
(µm)
45
40
35
30
24 000
24 500
25 000
25 500
(µm)
z = 1 µm
x = 100 µm
Mesure du :
11/01/2006 @ 17:42
Calibré le : 06/01/2006 @ 10:40
Capteur : 436052st / Stylet : st178
Opérateur : P. Roux
Rapport N° 060112

INSA LYON
Métrologie

PIECE 3 49mm
Traitements non normalisés

S2D n°375020
13/01/2006 15:17

*Profil primaire*

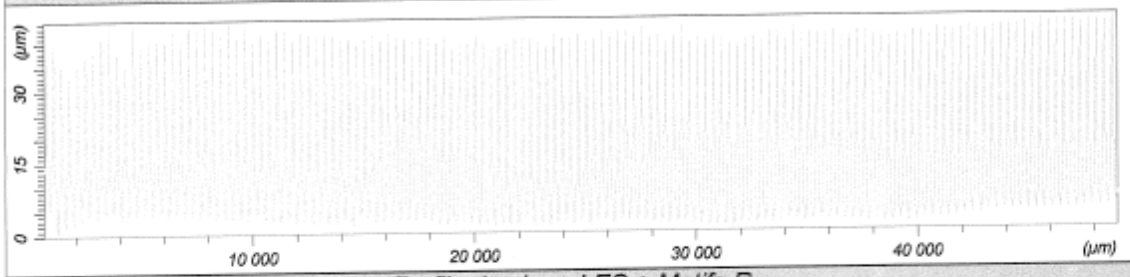


*Profil primaire + LES + Motifs R*

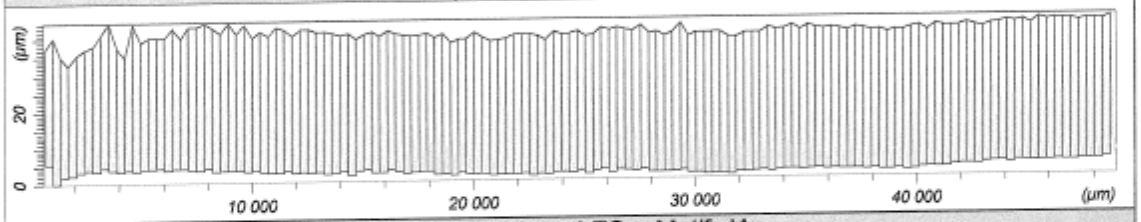


*Profil primaire + LES + Motifs W*

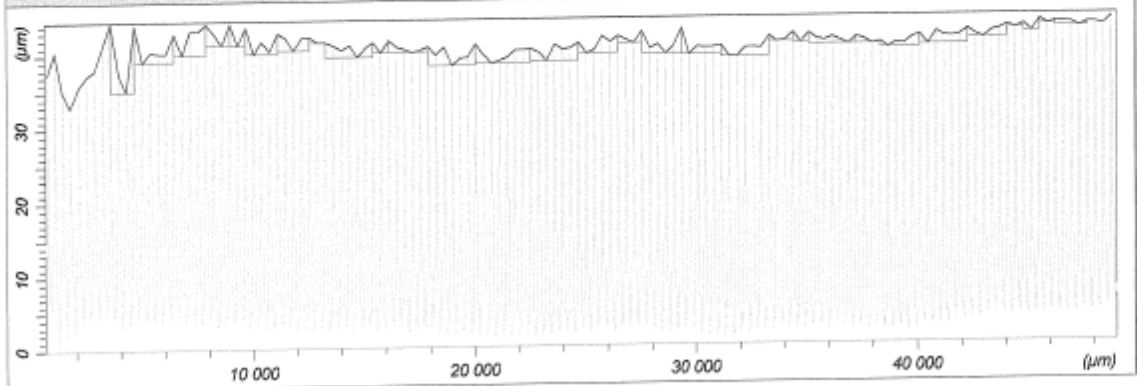


*Paramétres non normalisés*
*Cut-Off = 8 mm*
*A = 0,500 B = 2,500 (mm)*

**Ra = 9,935** µm

**W = 2,087** µm **AW = 1,472** mm

**R = 38,310** µm **AR = 358,978** µm

$tg\,\alpha = 0,053$

$3,05°$

$rp = 0,4$ mm avance 0,3mm/tour

Mesure du :
11/01/2006 @ 17:39

Calibré le : 06/01/2006 @ 10:40
Capteur : 436052st / Stylet : st178

Opérateur : P. Roux
Rapport N° 0601 112

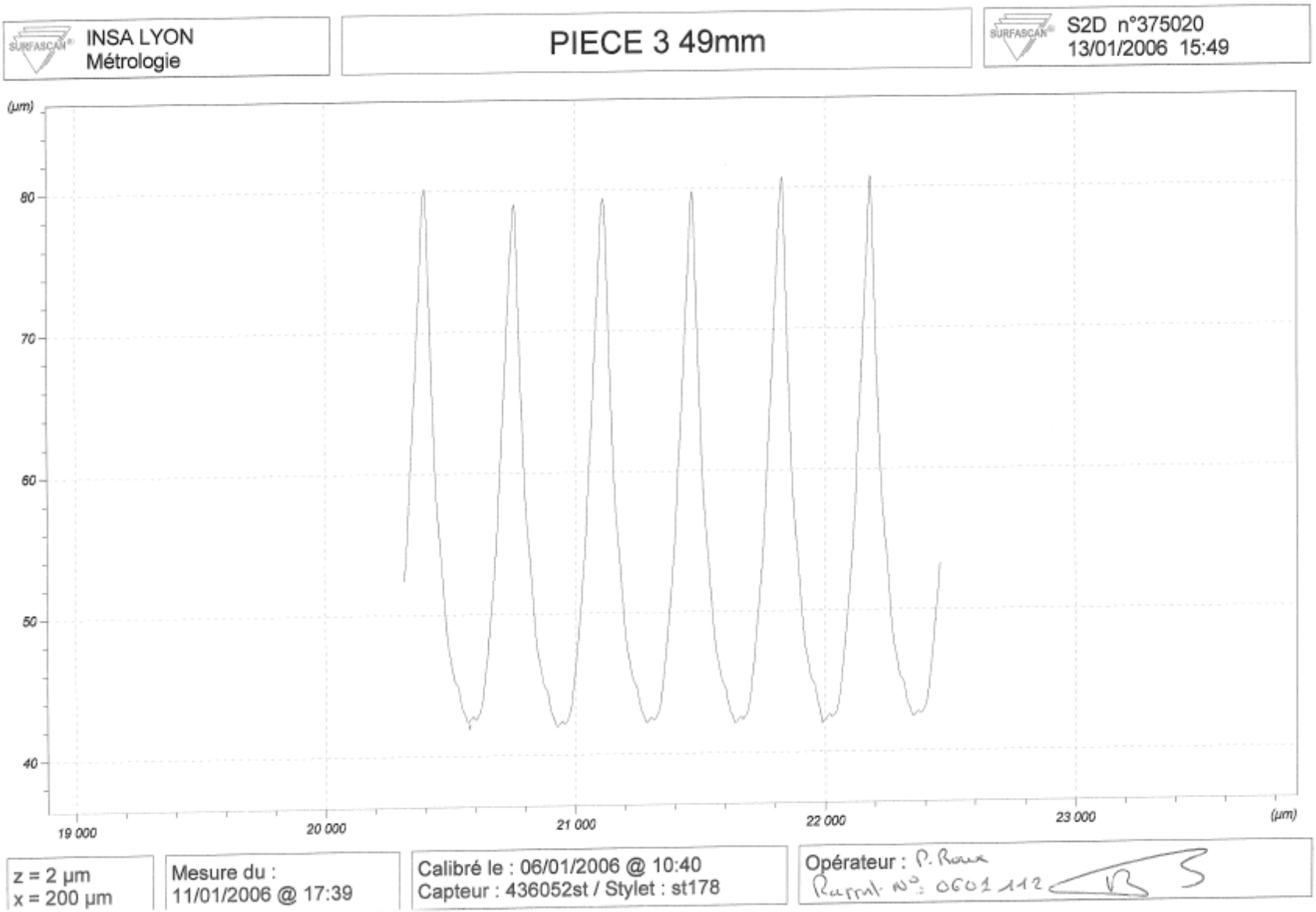
INSA LYON
Métrologie
PIECE 3 49mm
S2D n°375020
13/01/2006 15:49
(µm)
80
70
60
50
40
19 000
20 000
21 000
22 000
23 000
(µm)
z = 2 µm
x = 200 µm
Mesure du :
11/01/2006 @ 17:39
Calibré le : 06/01/2006 @ 10:40
Capteur : 436052st / Stylet : st178
Opérateur : P. Roux
Rapport N° : 0601112

INSA LYON
Métrologie

PIECE 4 49mm
Traitements non normalisés

S2D n°375020
13/01/2006 15:42

*Profil primaire*

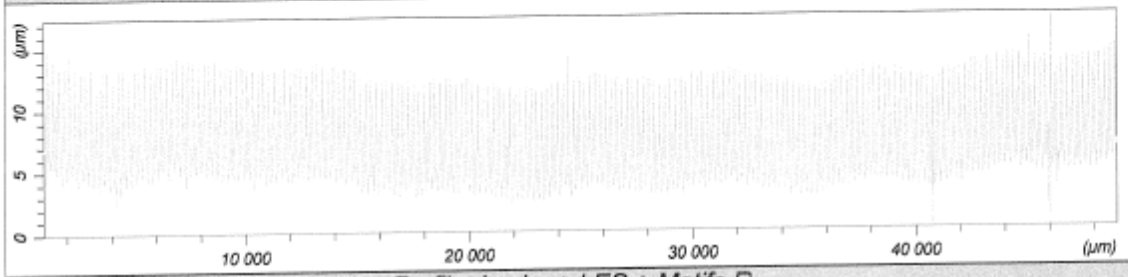


*Profil primaire + LES + Motifs R*

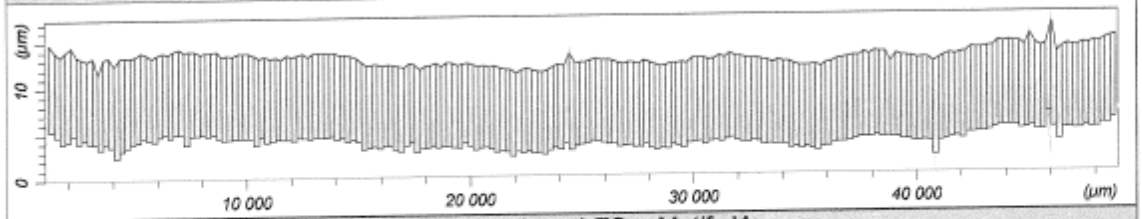


*Profil primaire + LES + Motifs W*

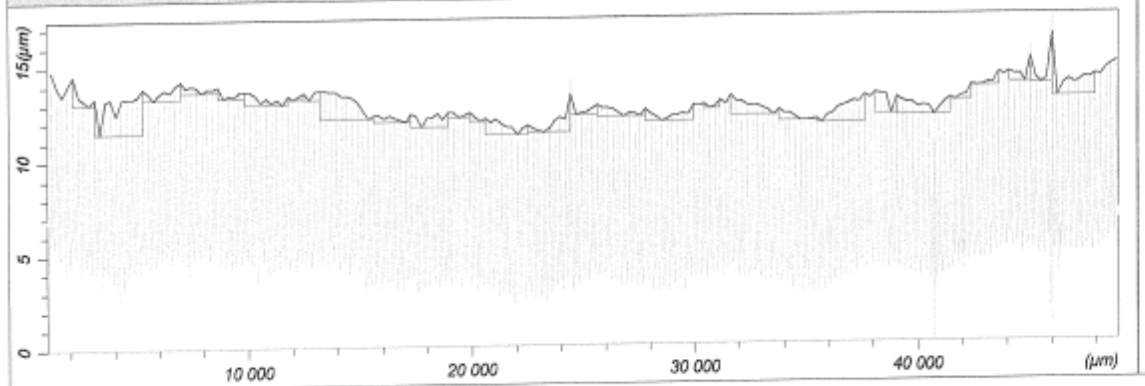


*Paramètres non normalisés*
*Cut-Off = 8 mm*
*A = 0,500 B = 2,500 (mm)*

**Ra = 2,431** µm

**W = 0,794** µm **AW = 1,514** mm

**R = 9,164** µm **AR = 240,131** µm

$tg\alpha = 0,019$

$1,09°$

$rp = 0,8mm$ aucun 0,2 mm /tour

Mesure du :
11/01/2006 @ 17:35

Calibré le : 06/01/2006 @ 10:40
Capteur : 436052st / Stylet : st178

Opérateur : P. Roux
Rapport n° : 0601 112

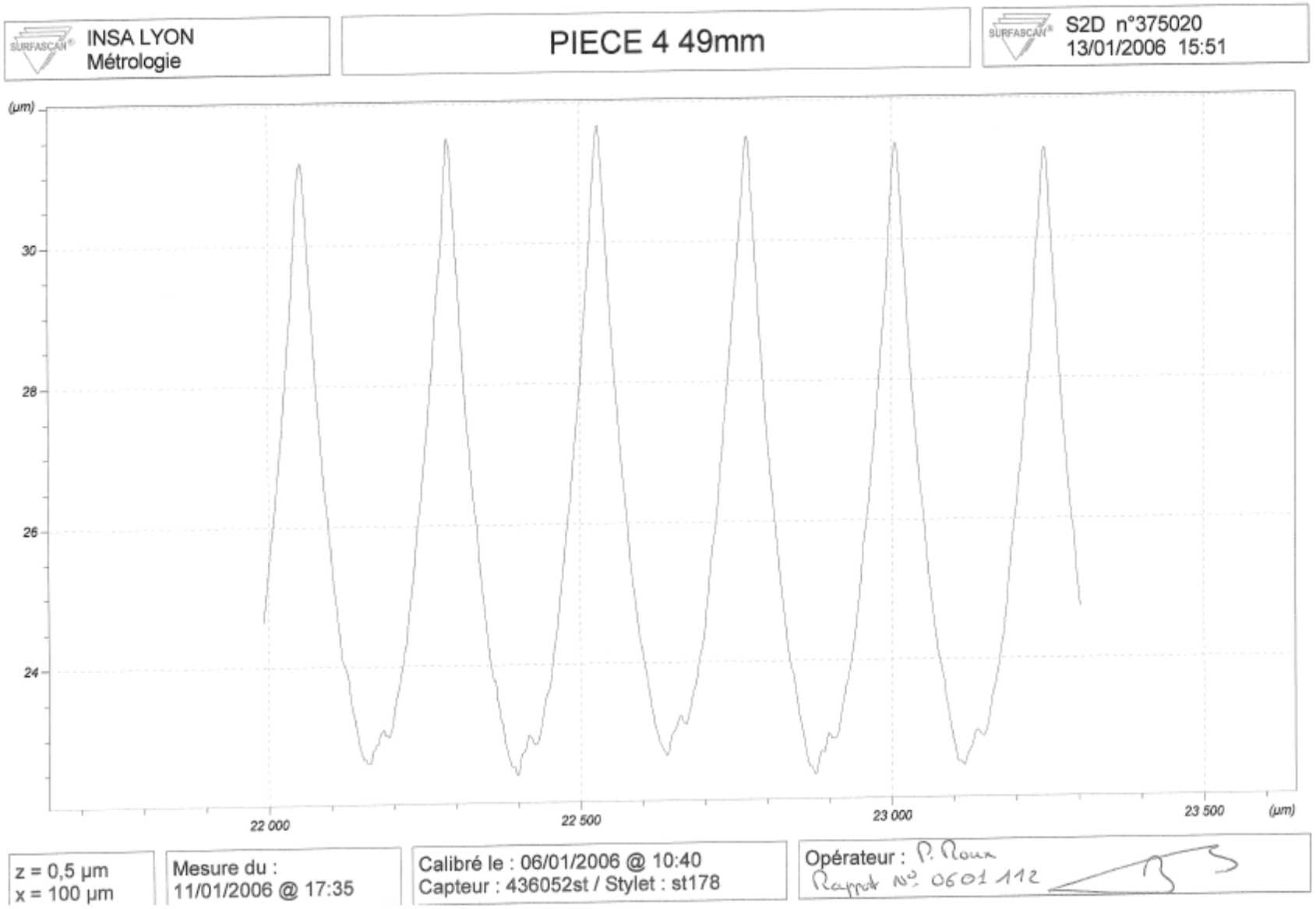
INSA LYON
Métrologie
PIECE 4 49mm
S2D n°375020
13/01/2006 15:51
(µm)
30
28
26
24
22 000
22 500
23 000
23 500
(µm)
z = 0,5 µm
x = 100 µm
Mesure du :
11/01/2006 @ 17:35
Calibré le : 06/01/2006 @ 10:40
Capteur : 436052st / Stylet : st178
Opérateur : P. Roux
Rapport N° 0601 112

INSA LYON
Métrologie

PIECE 5 49mm
Traitements non normalisés

S2D n°375020
13/01/2006 15:43

*Profil primaire*

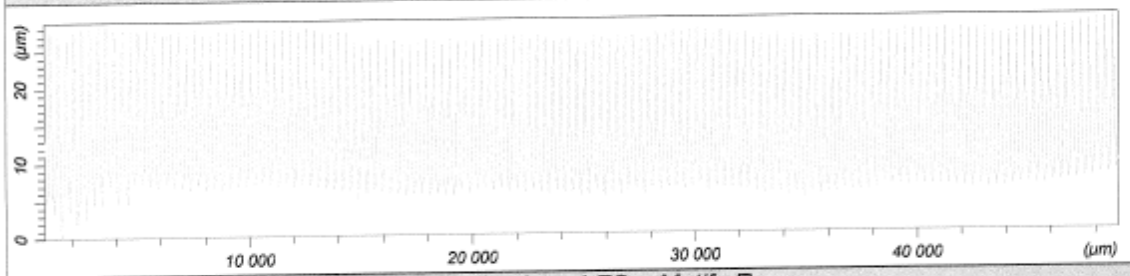


*Profil primaire + LES + Motifs R*

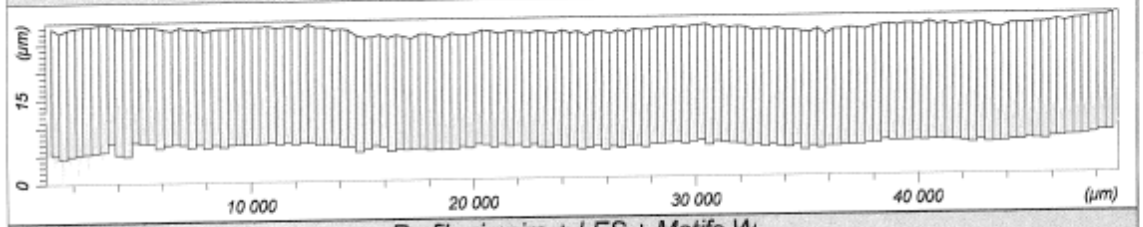


*Profil primaire + LES + Motifs W*

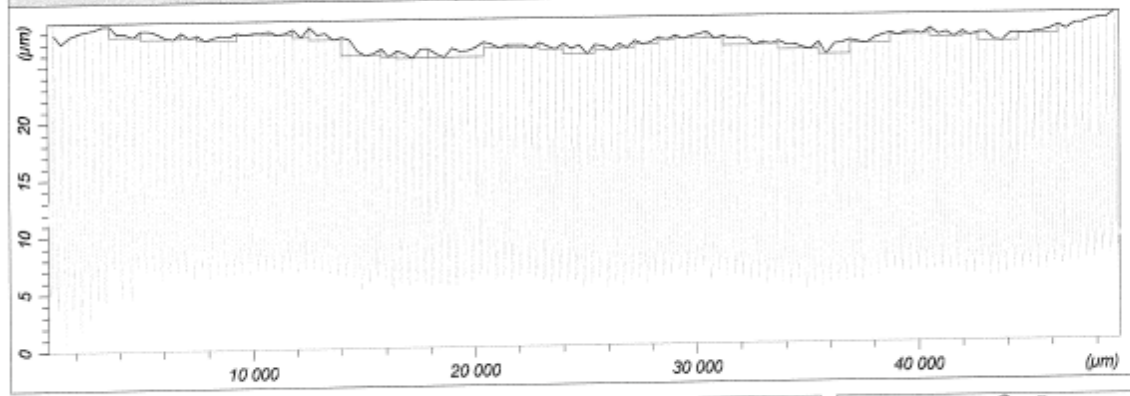


*Paramètres non normalisés*
*Cut-Off = 8 mm*
*A = 0,500 B = 2,500 (mm)*

**Ra = 5,576** µm

**W = 0,577** µm **AW = 1,294** mm

**R = 20,985** µm **AR = 359,060** µm

$tg\alpha = 0,029$

$1,67°$

$r = 0,8mm$ dans 0,3mm/div

Mesure du :
11/01/2006 @ 16:33

Calibré le : 06/01/2006 @ 10:40
Capteur : 436052st / Stylet : st178

Opérateur : P. Roux
Rapport N°: 0601 112

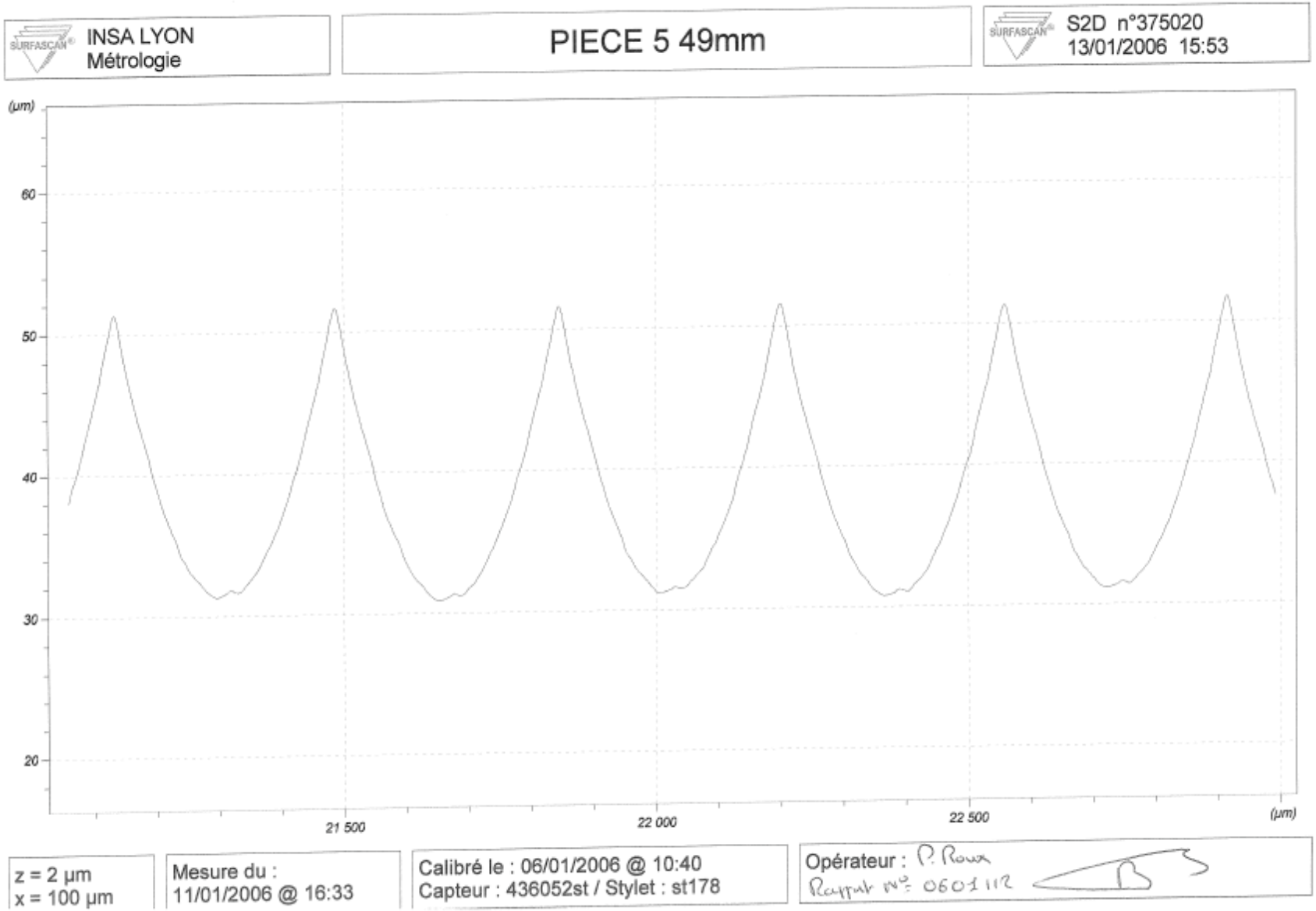
INSA LYON
Métrologie
PIECE 5 49mm
S2D n°375020
13/01/2006 15:53
(µm)
60
50
40
30
20
21 500
22 000
22 500
(µm)
z = 2 µm
x = 100 µm
Mesure du :
11/01/2006 @ 16:33
Calibré le : 06/01/2006 @ 10:40
Capteur : 436052st / Stylet : st178
Opérateur : P. Roux
Rapport N° : 060112

INSA LYON
Métrologie

PIECE 6 49mm
Traitements non normalisés

S2D n°375020
13/01/2006 15:44

*Profil primaire*

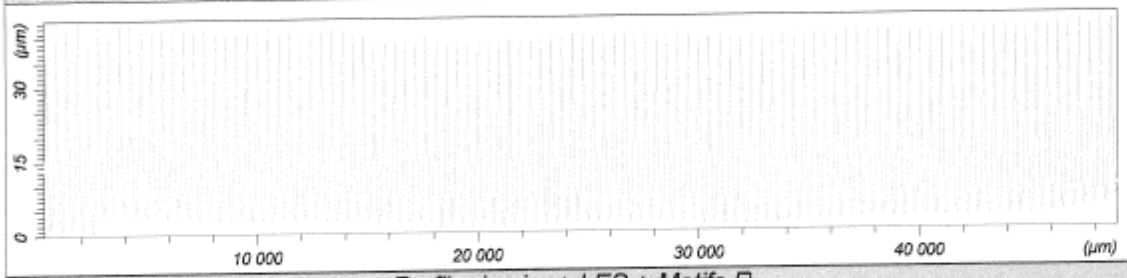


*Profil primaire + LES + Motifs R*

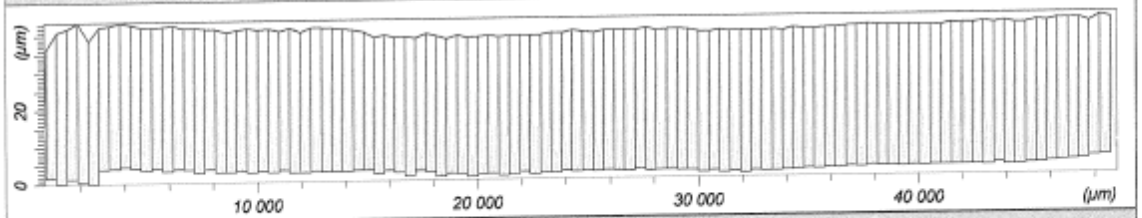


*Profil primaire + LES + Motifs W*

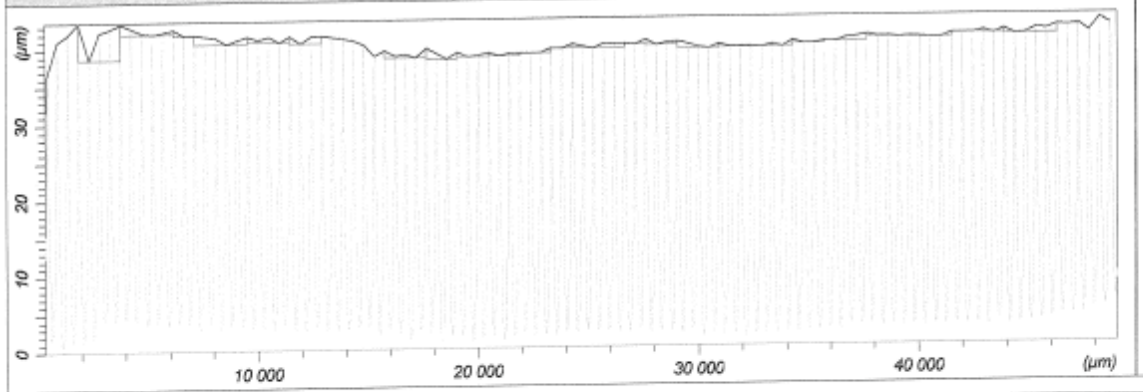


*Paramètres non normalisés*
*Cut-Off = 8 mm*
*A = 0,500 B = 2,500 (mm)*

**Ra = 9,907** µm

**W = 0,782** µm **AW = 1,636** mm

**R = 37,878** µm **AR = 473,755** µm

$tg\alpha = 0,0399$

$2,29°$

$r = 0,8$ avance $0,4$ mm/tour

Mesure du :
11/01/2006 @ 17:46

Calibré le : 06/01/2006 @ 10:40
Capteur : 436052st / Stylet : st178

Opérateur : P. Roux
Rapport N°: 0601 112

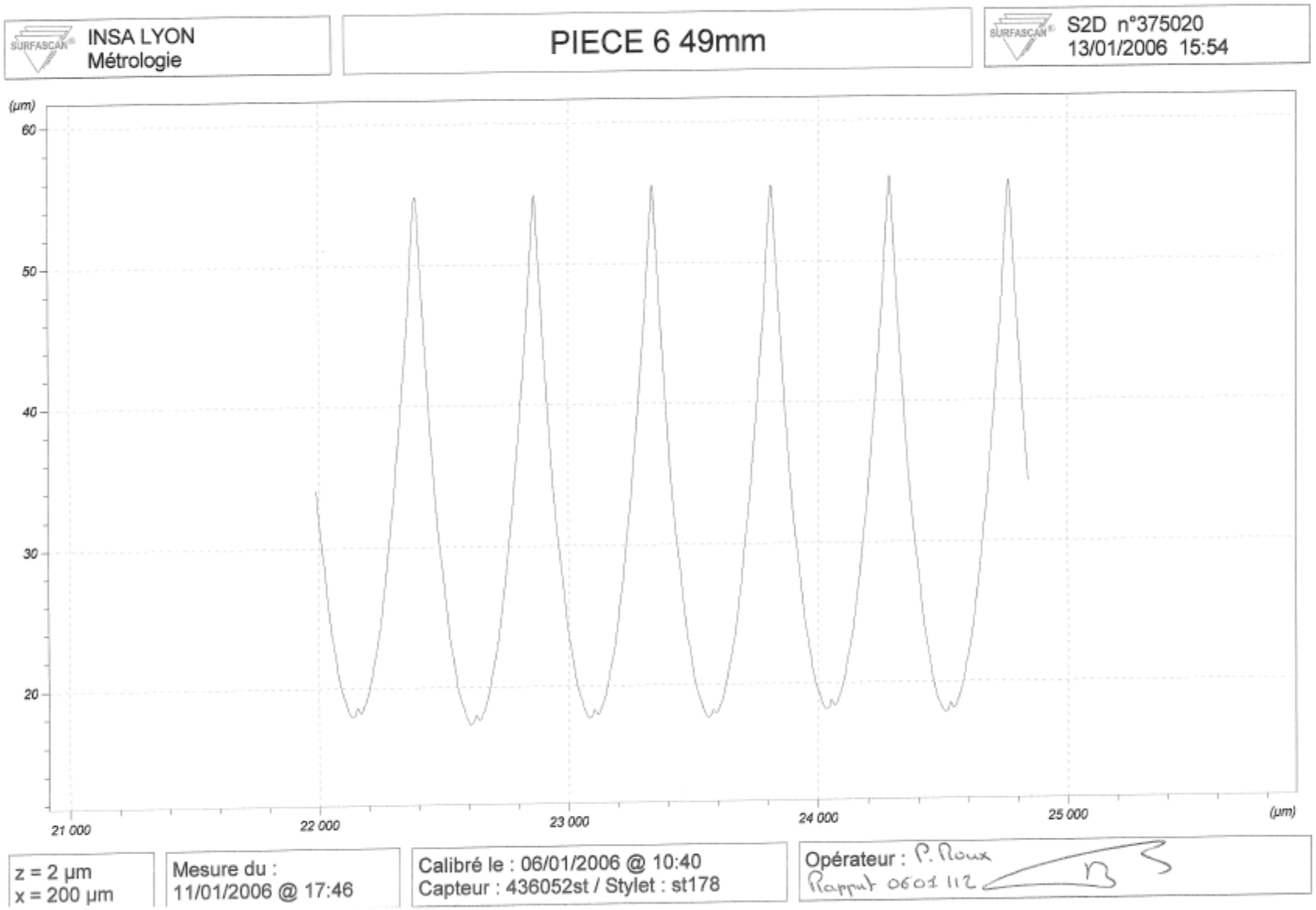
INSA LYON
Métrologie
PIECE 6 49mm
S2D n°375020
13/01/2006 15:54
(µm)
60
50
40
30
20
21 000
22 000
23 000
24 000
25 000
(µm)
z = 2 µm
x = 200 µm
Mesure du :
11/01/2006 @ 17:46
Calibré le : 06/01/2006 @ 10:40
Capteur : 436052st / Stylet : st178
Opérateur : P. Roux
Rapport 0601 112